THE INFLUENCE OF HEAT INPUT ON THE MICROSTRUCTURE AND MECHANICAL PROPERTIES OF A HIGH STRENGTH FLUX CORED WELD METAL

by

Gregory Ross Redden

B.E. Mech. (Hons)

Thesis Submitted for the Degree of

Master of Engineering Science

in

The University of Adelaide

(Department of Mechanical Engineering)

August 1995

ABSTRACT

Relationships between microstructure and mechanical properties for high nickel ferrous weld metals with yield strengths greater than 690 MPa have only recently begun to be investigated. Knowledge of this type of weld metal, with particular reference to gas metal arc processes, has subsequently been found to be incomplete in the literature. This is especially the case for as deposited weld metal in the commonly used heat input range of between 1.0 and 2.5 kJ/mm.

Literature reviewed includes reactions which occur before weld solidification, during solidification and the subsequent solid phase austenite transformations. The effects of shielding gas composition, different alloying elements and factors such as prior austenite grain size and non-metallic inclusion properties are also discussed. The effects of heat input on all of these variables is then related to previous studies on the effects of heat input in submerged arc welding, manual metal arc welding and gas metal arc welding using metal compositions resulting in weld strengths ranging from 400 MPa to high strength welds of over 690 MPa ultimate tensile strength.

This study is subsequently focussed on as deposited weld metal in the 1.0 to 2.5 kJ/mm heat input range using basic flux cored high strength electrodes and a pulsed power supply. Welding was mechanically controlled in the vertical up position. Heat input was recorded using a digital storage

oscilloscope and the weld cooling rate was monitored by plunging thermocouples into the weld pool.

Light, scanning and transmission electron microscopy were employed to examine microstructures. Mechanical tests performed included Vickers hardness, tensile strength and the use of unique sub-size CTOD specimens to obtain fracture toughness comparisons. Weld chemical compositions were also obtained using ICP analysis.

The results of this study showed a large change in the microstructure over the heat input range examined. These differences in microstructure correlated with changes in the mechanical properties. This has suggested a number of areas which require further study.

DECLARATION

This thesis contains no material which has been accepted for the award of any other degree or diploma in any university or other tertiary institution and, to the best of my knowledge and belief, contains no material previously published or written by another person, except where due reference has been made in the text.

I give consent to this copy of my thesis, when deposited in the university library, being available for loan and photocopying.

GREGORY R. REDDEN

14 August 1995

ACKNOWLEDGMENTS

Most importantly, I must thank the Co-operative Research Centre for Materials Welding and Joining which provided financial support and funding for experimentation and analysis. Without this assistance, this study would not have been possible.

There are also many people who must be thanked for their assistance in the planning, experimentation and analysis of results.

Of particular note, my supervisors, Dr John Bee (The University of Adelaide) must be acknowledged for his assistance with TEM operation and interpretation of metallographic results, Dr M. Wahab (The University of Adelaide) for general guidance and Dr Ian French (CSIRO DMT) for the selection of the welding process, access to CSIRO facilities and for general guidance.

In addition to these people there are numerous others who must also be thanked for their assistance. The most significant of these include Dr Graham Powell (CSIRO) - interpretation of light and SEM microstructures, John Terlet (The University of Adelaide - CEMMSA) - SEM instruction and EDS analysis advice, Dr John Yellup (CSIRO) - mechanical testing assistance, David Viano (CSIRO) and Gunter Herfurth (CSIRO) - advise and assistance on metallographic specimen preparation, Trevor Kenyon (CSIRO) - photographic processing, Ian Brown (Adelaide Uni) - photographic processing and Ron Jaeger and the staff of The University of Adelaide, Mechanical Engineering workshop - mechanical test sample preparation and test rig construction.

TABLE OF CONTENTS

APPENDICES

FIGURES

TABLES

EQUATIONS

ACRONYMS

BHP	Broken Hill Proprietary Ltd
CCT	Continuous Cooling Transformation
CDT	Controlled Drop Transfer
CEMMSA	Centre for Electron Microscopy and Microstructure Analysis
CIG	Commonwealth Industrial Gases
CRC	Co-operative Research Centre
CSIRO	Commonwealth Scientific and Industrial Research Organisation
CTOD	Crack Tip Opening Displacement
CVN	Charpy V Notch
DSO	Digital Storage Oscilloscope
EDS	Energy Dispersion Spectrum
FCAW	Flux Cored Arc Welding
HAZ	Heat Affected Zone
NATA	National Association of Testing Authorities
Q&T	Quenched and Tempered
SAW	Submerged Arc Welding
SEM	Scanning Electron Microscopy
TEM	Transmission Electron Microscopy
WIA	Welding Industries of Australia
WTIA	Welding Technology Institute of Australia

NOMENCLATURE

σ_{UTS}	Ultimate tensile strength
a	Effective crack length
a_0	Initial crack length
B	Test piece thickness
b_0	Initial uncracked ligament
E	Young's modulus of elasticity
K	Stress intensity factor
P_f	Fatigue pre-cracking force
S	Specimen span
V	Clip gauge displacement
W	Test piece width
Y	Stress intensity coefficient
z	Distance of clip gauge location from test piece surface

CHAPTER 1. INTRODUCTION

The increased usage of high strength steels in recent years has seen a corresponding increase in the development of welding processes and consumables capable of meeting the mechanical properties of these high performance steels. This increased usage, combined with continuing developments in technology, has resulted in a pressure to improve productivity and production processes to meet the requirements of increasingly demanding applications. High productivity and versatility can only be achieved if the processes employed are also of high quality and reliability. This in turn is only possible if the processes are fully understood, thus allowing proper process control and design. For these reasons, high strength welds categorised as having a strength level of 690 MPa and above are of particular interest as the metallurgy of these welds is far from understood and these are now commonly used in the construction of structures as diverse and demanding as ships, pressure vessels and armoured vehicles.

To improve productivity, flux cored welding consumables have been employed in Australia since the 1960's but it is only in recent times that they have been used for high strength applications. This recent introduction, combined with the limited knowledge base on high strength weld metal metallurgy, dictates the need for research into the effects of factors influencing mechanical properties.

Factors which have a bearing on the final weld mechanical properties are the chemical and physical properties of the consumables and base plate, the joint geometry, preheat and inter-pass temperatures and the welding parameters of speed, current and voltage.

The parameters of speed, current and voltage can be collectively grouped together in a relationship representing the electrical heat input. This is important because this is the parameter which the welder has quoted as a value to adhere to, and on which acceptable mechanical properties often depend. Even so, a study on the effects of heat input is really a study concerned with the weld cooling profile while in the molten state, during solidification and then through the various solid phase transformations. In these stages of weld development, factors such as weld chemistry, which may itself be influenced by heat input, have a highly significant role to play in the complex interactions taking place.

In response to this lack of fundamental knowledge in the literature, the present study discusses known theory and experimental work on high strength welding metallurgy and relates it to the flux cored pulsed welding technique through an experimental study of high strength weld metal deposited using an out of position manganese-nickel-molybdenum high strength consumable.

CHAPTER 2. LITERATURE SURVEY

2.1. INTRODUCTION

There are many sources of information discussing microstructure and mechanical property relationships. This is due to the large number of factors which effect the weld deposit combined with the great economic importance of the field. This review has been divided into four sections, each covering a specific stage of weld development.

Firstly the reactions which occur when the weld is still in the molten state, then the effects of solidification are briefly discussed. After this the vitally important austenite to ferrite transformations are reviewed with particular reference to the effects of prior austenite grain size and non-metallic inclusions. Finally, individual studies which have previously focussed on high strength weld metal microstructure and mechanical property relationships are reviewed. In this way an overview of the fundamental metallurgy governing the properties of the weld deposit is first discussed and then specifics of research directly focussed upon heat input effects is described, thus allowing conclusions to be made about the current state of knowledge in this field.

2.2. MOLTEN METAL REACTIONS

Reactions which occur in the molten state can lead to chemical changes in the weld pool through the formation of metal oxides, sulphides and nitrides as well as by evaporation. These chemical changes are known to influence microstructure and mechanical properties. The weld pool is also known to absorb elements from the shielding gas. It follows that the weld metal composition is a function of the cover gas composition, welding wire, slag system, base metal and most importantly, the time allowed for reactions. This reaction time is dependent on the material physical properties, the welding process used, and of particular interest to this study, the heat input. In fact, the time the weld remains in its molten state is directly proportional to the heat input. It follows that the extent of the many chemical reactions which occur in the molten state are also directly proportional to the heat input.

The most dominant reaction to occur while in the molten state is the oxidation of elements such as aluminium and titanium to form particles which have been reported to have a significant effect on the final weld microstructure during solid state transformations as discussed in section 2.4. Of course, other reactions such as the formation of sulphides also occur. These reactions often result in particles of heterogenous compositions. These particles and their effect on the final weld microstructure and mechanical properties are discussed further in section 2.4.6.

Shielding gas composition exerts a significant effect over the handling characteristics and spatter levels and although it does not have an effect on the electrical heat input it does have an effect on arc efficiency. By altering the shielding gas composition the actual heat input can be decreased by an effective decrease in arc efficiency of over 10 percent when using argon rich mixtures, relative to that obtained when using a CO_2 shielding gas [1].

As the shielding gas is one of the consumables in direct contact with the weld, it must be considered to influence the weld deposit microstructure and mechanical properties through chemical reactions.

The most significant shielding gas parameter affecting the weld metal composition is the oxidation potential of the shielding gas. The oxidation potential refers to the ability of the shielding gas to alter the oxygen content of the weld deposit. This study is not focussed on the ability of different shielding gases to alter the weld metal oxygen content, however, further information in this area can be found in work by Vaidya and Ahlblom [2,3]. For reference, the weld oxygen content can also be influenced by the flux composition as discussed by Chai [4].

Effects of changing the oxygen content of the weld are discussed well by Francis [5] where it is stated that the shielding gas composition will influence the amount, size and composition of oxide inclusions formed in the weld metal.

As well as increasing the oxygen content in the weld metal, increasing the oxidation potential of the shielding gas can affect the concentrations of other elements, namely a decrease in the concentration of silicon and manganese. These elements become oxidised in the arc transfer. This decrease, among other findings, has been found to be the case in basic flux-cored electrodes by Vines [1,6].

While many researchers have found changes in weld deposit chemical concentrations due to shielding gas composition variations, these changes are minimal and thus have little effect on mechanical properties [7,8].

2.3. SOLIDIFICATION

Solidification behaviour controls dendrite arm spacing, solute banding, the extent of segregation, the extent of defects such as porosity and hot cracks, the distribution of inclusions, the size and shape of grains, the microstructure, and ultimately the properties of the weld metal itself [9-12].

The solidification of castings is a process that is well understood with usually well behaved and controllable conditions. For welding processes, much of this theory is interchangeable. However, there are a number of features which must be taken into account which make it a fundamentally different process to that of ingot casting and cause it to be more closely related to a continuous casting process [9].

Of the many authors who have discussed the features which make these differences, Easterling [13] has listed the most significant features as:

- The weld pool contains impurities.
- Dilution.
- Considerable turbulence resulting in good weld pool mixing.
- The molten metal volume is small compared with the size of the mould (the base metal).
- The composition of the molten metal and mould are very similar.
- There are large temperature gradients across the melt.

- Since the heat source moves, weld solidification is essentially a dynamic process and the solidification behaviour is thus dependent on the welding speed.
- In high energy welds or in multi-run welds where the base metal is pre-heated, temperature gradients and hence solidification behaviour are affected.

Taking all of these factors into account the complexity of weld solidification processes is evident.

Even though these factors have a great influence, it is still the cooling rate of the weld deposit which has the greatest potential to change the properties of the weld. Cooling rate is therefore one of the most significant variables in determining the final microstructural morphology. It not only has a critical role to play in solid state transformations, but it is also crucial in solidification theory. A number of authors have attempted to determine the cooling rate of different welding processes using experimental or numerical techniques. Some of the better published literature and classical papers are those of Rosenthal, Adams and Blodgett [14-16].

Due to the effect of grain growth from the base metal grains and grain nucleation, the weld pool shape has been found to have a large effect on the weld macro and micro-structures [17]. The shape of the weld pool is dependent upon numerous factors such as the thermal properties of the base

metal, the surfactant effect of impurities and the heat input. The effects of heat input on the spacing of the solidification microstructure of a high strength weld metal is clearly shown in figure 2-1.

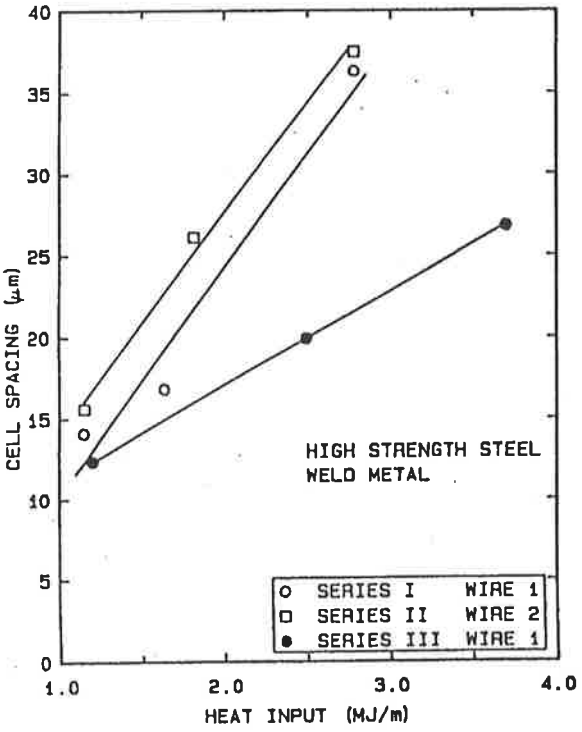

Figure 2-1 Cell Spacing as a Function of Heat Input

Figure 2-1 from Oldland [18] represents the cell spacing in three series of high strength welds.

For low alloy weld metals this has significance as austenite grains form by the transformation of δ ferrite through nucleation at the δ ferrite grain boundaries. Their higher rate of growth along the δ ferrite grain boundaries leads to the formation of columnar austenite grains whose shape resembles that of the original solidification microstructure [19,20]. For higher alloy weld metals however, it is found that the weld metal will solidify directly as austenite, thus the cell spacing shown in figure 2-1 is the prior austenite grain size. This is also discussed by Sudgen [21] and has a great effect on properties as discussed in section 2.4.

2.4. AUSTENITE TRANSFORMATION

2.4.1. Introduction

While the effects of chemical reactions in the molten state and the subsequent solidification of the weld deposit are important, it is the austenite transformation products which directly determine the final weld mechanical properties.

This section outlines the mechanisms involved in the transformation of austenite to the different forms of ferrite. The athermal shear transformation which forms martensite is also discussed as this microconstituent is of great importance in high strength weld metallurgy.

The ability to describe austenite transformation mechanisms depends on elemental effects, non-metallic particles and the prior austenite grain size. Each of these are discussed in the following sections. At this point it should be noted that while it may seem as though these are not variables of any significance in a heat input study, heat input has an effect on all of these. They must therefore be considered.

2.4.2. Austenite Transformation Products

2.4.2.1. Classification of Weld Metal Microstructures

Microstructures observed in ferrous welding can be highly complex. As a result there is a wide variety of terminology in frequent use by various researchers. This is unfortunate, as it can lead to mis-identification of micro-constituents and confusion when comparing research results in an already complex field. Some of these nomenclatures used for low alloy carbon weld microstructures are interchangeable, others are not. A review of the different terms in common use and their general interchangeability for the microstructures observed in this study is given in table 2-1. The reference used for the IIW Scheme was IIW Doc IX-1533-88 [22] while "Other Terminology" comes from the large amount of literature which has been published in this field over the past fifteen years.

This Document	IIW Scheme	Other Terminology
Grain Boundary Ferrite	Primary Ferrite (PF) Grain Boundary Ferrite (PF[G])	Polygonal Ferrite Proeutectoid Ferrite Grain Boundary Alliotriomorphs
Widmanstätten Ferrite	Ferrite with Second Phase (FS) Ferrite with Aligned Second Phase (FS[A]) Ferrite Side Plates (FS[SP])	Ferrite with Aligned MAC Side Plate Ferrite Lath like ferrite Secondary Ferrite
Acicular Ferrite	Acicular Ferrite (AF)	Fine Bainitic Ferrite Needle like ferrite Fine Grained Ferrite Intra-granular ferrite
Bainite	Ferrite with Second Phase (FS) Bainite (FS[B]) Upper Bainite (FS[UB]) Lower Bainite (FS[LB])	Lath Ferrite
Martensite	Martensite (M) Lath Martensite (M[L])	Martensite Packets
Retained Austenite		Micro Phases

Table 2-1 Microstructural Terminology

2.4.2.2. Grain Boundary Ferrite

This is usually the first phase to form and is nucleated heterogeneously on high energy austenite grain boundaries. In low alloy welds, the austenite grain boundaries often become decorated with ferrite [20]. In higher alloy welds (such as the one used in the present study) little grain boundary ferrite is formed since the austenite to ferrite transformation is suppressed by most alloying elements.

2.4.2.3. Widmanstätten Ferrite

Grain boundary ferrite and Widmanstätten side plate ferrite are often grouped together as primary ferrite. They both form at relatively slow cooling rates but unlike grain boundary ferrite, Widmanstätten ferrite nucleates and grows from grain boundary ferrite as long needle-like laths that protrude into the austenite grains. Widmanstätten ferrite can sometimes be detrimental to mechanical properties because the ferrite plates can grow in parallel formations which permit cleavage cracks to propagate with little deviation [23-25].

2.4.2.4. Acicular Ferrite

At cooling rates faster than those associated with the formation of Widmanstätten ferrite, transformation occurs at a lower temperature and if appropriate and sufficiently well distributed nucleant's are available, the transformation product consists of fine high aspect ratio ferrite laths. These nucleate intra-granularly on inclusions producing a fine microstructure known as acicular ferrite. The term acicular means shaped and pointed like a needle

but it is generally recognised that acicular ferrite has in three dimensions the morphology of thin lenticular plates [20]. Acicular ferrite is the most favourable microstructure with respect to mechanical properties, particularly fracture toughness [26-28].

Acicular ferrite has been claimed by authors such as Ali [29] and Yang [30] to be intra-granularly nucleated bainite. This is supported by later work of Bhadeshia and Sudgen [31,32] where "lower" acicular ferrite was shown to exist where carbide precipitates form between the acicular ferrite laths when the carbon content is sufficiently high. Transformation of austenite to acicular ferrite has also been shown to begin below the bainite start temperature thus adding further weight to this theory [33]. Whatever the mechanism by which acicular ferrite is formed, it has been shown that heat input will affect its development [34] and that microstructures containing acicular ferrite are commonly found in C-Mn-Ni welds [35].

2.4.2.5. Bainite

If the cooling rate is sufficiently rapid, the austenite can transform to bainite in preference to acicular ferrite. At even greater cooling rates, there is insufficient time for carbon diffusion to occur and the austenite transforms directly to martensite as discussed in section 2.4.2.6. Classical ferrous bainite consists of a non-lamellar aggregate of lath or plate shaped ferrite grains with carbide precipitation within the grains or in inter-lath regions. In some steels however (for example, steels containing significant silicon

content), carbide precipitation can be suppressed completely, although a lath-like ferritic product still forms in a manner identical in morphology and kinetics to the formation of classical upper bainitic ferrite. Such special carbide-free structures are also generally referred to as bainitic [36] and are commonly encountered in high strength weld metals due to low carbon contents. The start temperature of bainite is below that of acicular ferrite and above that of martensite. Alloying elements do have an effect on the temperature at which bainite begins to form. This is described by Honeycombe [37] using equation 2-1 where the relative importance of different alloying elements are shown.

$$B_S\ (°C) = 830 - 270\%C - 90\%Mn - 37\%Ni - 70\%Cr - 83\%Mo$$

Equation 2-1 Bainite Start Temperature

As with other microstructural constituents, the formation of bainite is recognised to be dependent on the cooling rate, the prior austenite grain size and the inclusion content and composition [30]. A study by Yang et al [38] concluded that at low temperatures bainite cannot provide superior toughness to acicular ferrite even if the weld deposit contains an extremely low carbon content thus avoiding inter-plate cementite in the bainite-ferrite matrix. This was said to be because the plane of the cleavage crack was frequently deflected in acicular ferrite while the bainite allowed cracks to propagate with less deflection.

2.4.2.6. Martensite

Unlike other microstructural constituents found in low carbon steels which form by means of isothermal kinetics that characterise thermally-activated diffusion-controlled transformations, martensite forms by an athermal reaction. If the cooling of the weld deposit is uninterrupted and rapid enough to prevent the decomposition of austenite by nucleation and growth processes then a shear mechanism will occur resulting in the near instantaneous formation of martensite. Martensite, once nucleated, propagates at the velocity of an elastic wave. The resulting martensite units that form in the shape of laths are grouped into larger sheaves or packets. This structure is generally called lath or packet martensite. When the martensite units form as individual lenticular plate-shaped units the structure is called plate martensite as discussed by Speich [39].

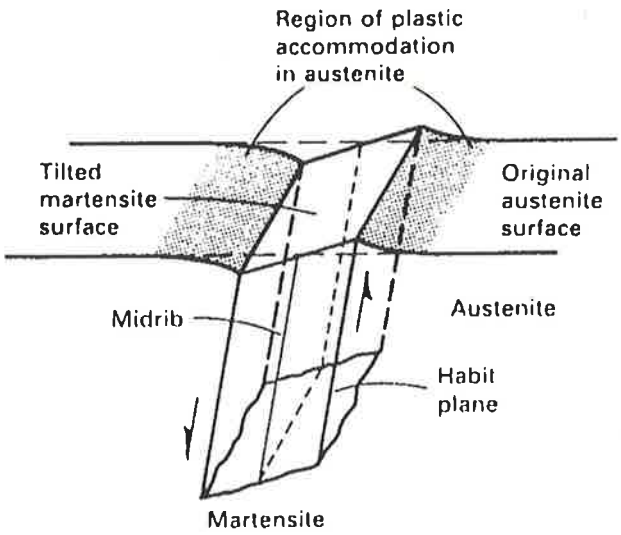

Figure 2-2 Formation of Martensite

Figure 2-2 from Bilby [40] shows a schematic of shear and surface tilt associated with formation of a martensite plate.

In low carbon steels lath martensite is the expected form as also discussed in Speich [39].

In general, martensite has high strength due to it being a supersaturated solid solution of carbon in a tetragonal iron matrix which is highly stressed. While much of this strength increase can be directly contributed to increased interstitial solid solution hardening there is also a contribution from the high dislocation density which is characteristic of martensitic transformations in iron-carbon alloys [37].

While the tensile strength of martensite is very high, the fracture or impact strength of this micro-constituent is poor. There are however exceptions to this rule, for example, where retained austenite films between the laths can increase the toughness. This can sometimes be found in weld deposits with low carbon levels.

Like all micro-constituents found in weld metals, there is a temperature above which the phase under consideration will not begin to form. This temperature is determined by the alloy composition of the weld metal. For martensite the effects of different alloying elements on this start temperature is shown below in equation 2-2 from Honeycombe [37].

$$M_S(°C) = 539 - 423\%C - 30.4\%Mn - 17.7\%Ni - 12.1\%Cr - 7.5\%Mo$$

Equation 2-2 Martensite Start Temperature

2.4.2.7. Retained Austenite

In low carbon alloys retained austenite usually represents only a small percentage of the micro-constituents. This retained austenite exists because when ferrite is formed, carbon must diffuse into the remaining austenite. This remaining austenite, which can be enriched with up to 7at% carbon, may transform into a large variety of microstructural constituents such as pearlite, upper and lower bainite and martensite or it can remain as intra-granular islands of retained austenite within an acicular ferrite structure. Alternatively it can remain between the laths of martensite [41-43].

2.4.2.8. CCT Diagrams

A means of characterising the solid state transformation behaviour of austenite to other phases is by the use of a continuous cooling transformation diagram (CCT diagram). These are generated using techniques such as dilatometry which examine the volume changes associated with different phases as they transform. The resultant diagram can be used as an aid to predict the expected weld microstructure based on the profile of the cooling rate. Examples of CCT diagrams, and their applications, can be found in a number of papers [44-48].

Figure 2-3 is an example of a CCT diagram in which the cooling rate curves for three different heat input welds are shown. In the low heat input weld the cooling rate curve avoids all high temperature transformation products and forms 100% martensite. The medium heat input weld would result in a final microstructure consisting of a mixture of bainite and martensite and the high heat input weld has the slowest cooling rate resulting in a microstructure consisting of ferrite, bainite and martensite.

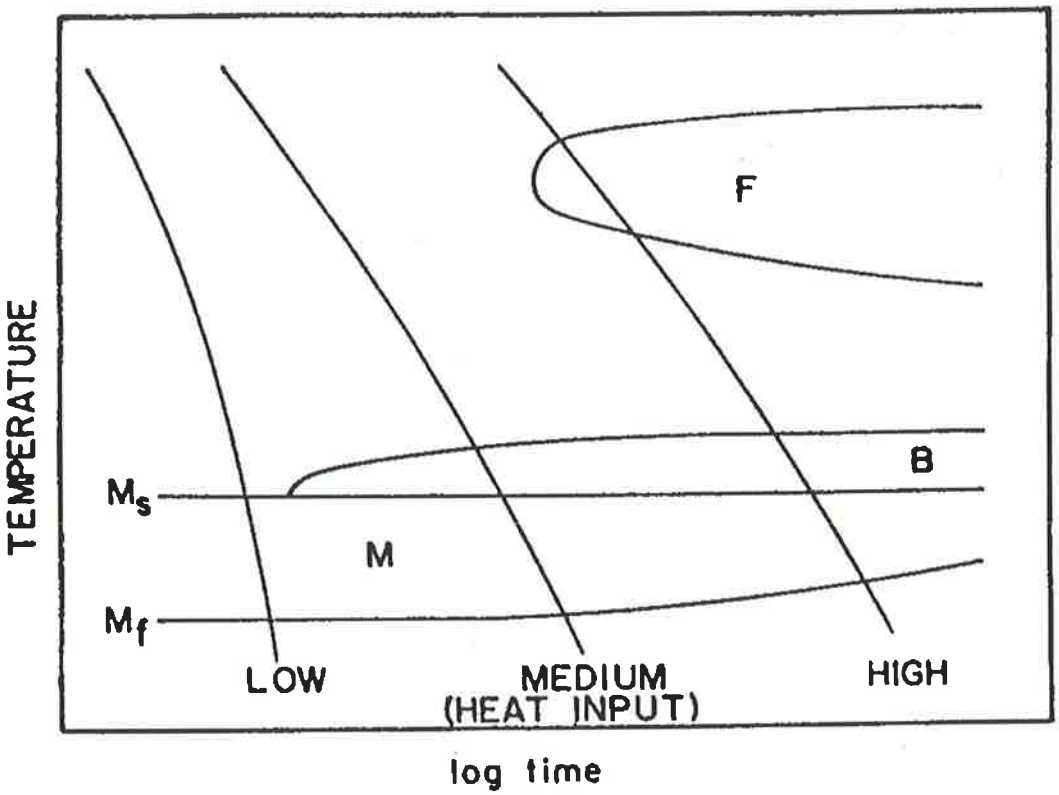

Figure 2-3 Continuous Cooling Transformation Diagram

Figure 2-3 from Oldland et al [18] is a schematic of a continuous cooling transformation diagram for a high strength weld metal.

2.4.3. Effects of Alloying Elements

2.4.3.1. Introduction

Due to the possibility that the heat input may have an effect on the concentration of elements in the weld deposit the effects of different elements, relevant to the present study, on the microstructure and mechanical properties are briefly reviewed in this section.

The weld deposit composition is influenced by numerous factors. Base metal dilution, shielding gas absorption and flux additions are the predominant sources of foreign elements in the weld deposit. Some of these elements are intentionally included while others are undesirable impurities or contaminants.

The effect of different alloying elements on the hardenability of the resultant weld deposit is often difficult to assess as there are many interactions occurring between the different elements in an already complex thermodynamic and kinetic environment.

There has been a great deal of study in this field by numerous researchers. Many researchers have published work not only in the field of welding, but have also published in related areas such as steel production and casting. The review conducted in this section is therefore a discussion of known effects of different elements on low carbon steel metallurgy, with particular emphasis on GMA welding.

2.4.3.2. Carbon, Manganese and Silicon

Carbon is the most powerful alloying element in ferrous metallurgy. This element has a great effect on hardenability but its concentration is usually kept low to prevent brittle fracture initiation in the weld region and also to safeguard against the effects of hydrogen-assisted cold cracking in the HAZ. The yield strength, tensile strength and weld metal hardness in the as-welded condition is influenced by small changes in the carbon concentration. Studies by Surian and Evans [49,50] where the carbon content was varied in the range of 0.05% to 0.15% strongly support this. The effect of carbon concentration on CTOD toughness is shown in figure 2-4.

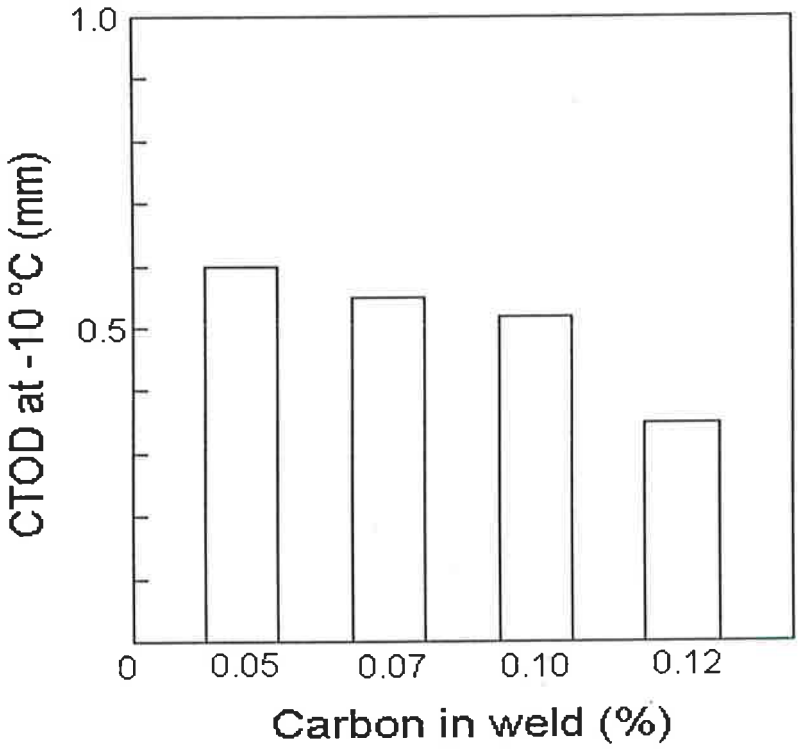

Figure 2-4 Effect of Carbon Concentration on CTOD Values

It should be noted that the data presented in figure 2-4 by Surian et al [49] is of special relevance as the specimens were in the as welded condition.

Unfortunately figure 2-4 cannot be relied on to predict mechanical properties. One reason is because carbon acts differently in the presence of other alloying elements [51].

Manganese is a commonly employed and effective alloying element to increase the strength and hardenability of steel. Manganese has also been found to decrease the transformation temperature of austenite to ferrite [52]. In addition to this, it is now widely accepted that the addition of manganese to the weld deposit increases the toughness by promoting the formation of acicular ferrite. It has been determined that the optimum amount of manganese in the weld deposit is approximately 1.4% [53,54], although it must be remembered that this optimum level is influenced by the welding process used and the extent of other alloying additions. Manganese also strongly combines with sulphur [37]. This often results in a population of manganese sulphide-rich inclusions in the weld deposit.

Unlike manganese, silicon is considered detrimental to the weld deposit toughness even in small concentrations. This is due to its encouraging effect on the formation of martensite and retained austenite micro-phases. The detrimental effects of silicon can be reduced by the addition of an appropriate amount of manganese to balance. Mn and Si concentration has been shown to be influenced by heat input [34].

2.4.3.3. Nickel, Copper, Molybdenum and Chromium

As discussed by Grong [55], improved weld metal toughness may be obtained by additions of nickel, copper, molybdenum or chromium. Copper and nickel are believed to have effects on the steel transformation temperature similar to those of manganese, while molybdenum and chromium suppress the austenite transformation and therefore lower the transformation temperature [52]. The role of molybdenum and chromium in the weld metal transformation kinetics is not fully understood but it has been claimed that precipitation of molybdenum or chromium carbides can restrict the formation of grain boundary ferrite on the prior austenite grain boundaries by either pinning or dragging effects. It has also been shown that increasing chromium concentration promotes the formation of acicular ferrite [56].

Increasing levels of nickel increase the amount of acicular ferrite, and also reduce the importance of manganese on weld metal toughness [57].

2.4.3.4. Vanadium, Niobium and Aluminium

The influence of vanadium and niobium on weld metal microstructure and toughness was reviewed by Dolby [58]. The influence of these elements produces varied results which are often unpredictable in nature. However, vanadium (in the absence of niobium) is considered to reduced the development of ferrite side plates at the prior austenite grain boundaries, while niobium restricts the formation of grain boundary ferrite [59]. Niobium is known to be detrimental, however, resulting in reduced fracture toughness [60]. Upon stress relief, vanadium can have a progressively deleterious effect on toughness but levels up to 200 ppm can be tolerated [61]

Aluminium has been shown to have a significant effect on the microstructure with increased levels of acicular ferrite reported [62].

2.4.3.5. Boron and Titanium

The effect of boron on the weld deposit is not yet fully understood. However, boron is known to segregate to prior austenite boundaries where it suppresses the growth of pro-eutectoid ferrite by lowering the free energy of the grain boundary. This effect hinders the nucleation and growth of grain boundary and side plate ferrite [63]. This is also consistent with the model of Mori et al [64].

The role of titanium in relation to boron is to preferentially combine with nitrogen and oxygen thus protecting the boron [63,41]. Titanium is also required to combine with excess nitrogen after available oxygen has been depleted. This prevents the formation of boron nitrides [19]. In addition to this, titanium has recently been examined more closely as its nitrides and oxides are believed to act as nucleation sites for intra-granular ferrite growth thus promoting the formation of acicular ferrite [65]. The importance of this effect, with reference to titanium, is discussed further in section 2.4.6.

While there is currently debate over the mechanisms by which these elements affect austenite transformation, the all important effects of different combinations of these elements on the volume fraction of different microstructures is well described in figures 2-5 and 2-6 for a 0.1C-1.4Mn-0.5Si-0.06Ni-0.005Nb multi-pass weld deposit with heat inputs ranging between 1.0 and 2.2 kJ/mm.

Titanium in very high concentrations (typically > 0.05 - 0.1%) can however lead to a deterioration in toughness [66]. Optimum mechanical properties are achieved using titanium at concentrations of 30 and 200 ppm [63,67,68].

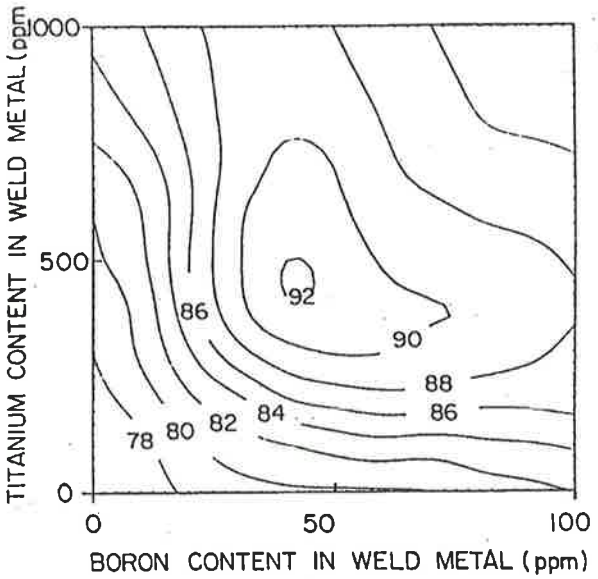

Figure 2-5 Effects of Boron and Titanium on Acicular Ferrite

Figure 2-5 from Oh [63] represents the effect of weld metal boron and titanium content ratios on the volume fraction of acicular ferrite.

Figure 2-6 Effects of Boron and Titanium on Grain Boundary Ferrite

Figure 2-6 from Oh [63] represents the effect of weld metal boron and titanium content ratios on the volume fraction of grain boundary ferrite.

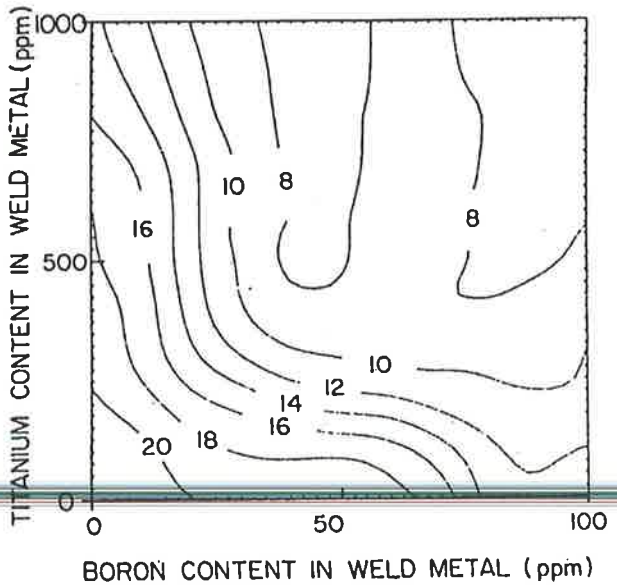

2.4.4. Carbon Equivalents

As a means of comparing different weld metals, the concept of a carbon equivalent was introduced so the given alloy contents of a weld could be expressed as a carbon level that is equivalent in hardenability. Many different expressions for carbon equivalent have been developed from different weldability criteria such as the HAZ hardness, toughness and transformation temperatures.

Today there are two carbon equivalent formulae in common usage. Equation 2-3 was originally developed for C-Mn steels with carbon contents above 0.18% and is usually referred to as the IIW formula.

$$CE_{IIW} \quad C_{eq} = C + \frac{Mn}{6} + \frac{(Cr + Mo + V)}{5} + \frac{(Ni + Cu)}{15}$$

Equation 2-3 IIW Carbon Equivalent

For steels with less that 0.18% carbon, equation 2-4, known as the Ito-Besseyo formula is more appropriate for the assessment of low carbon steels.

$$P_{cm} = C + \frac{(Mn + Cr + Cu)}{20} + \frac{Si}{30} + \frac{V}{10} + \frac{Mo}{15} + \frac{Ni}{60} + 5B$$

Equation 2-4 Ito-Besseyo Carbon Equivalent

Equation 2-3 has a much smaller tolerance to substitutional alloying elements than equation 2-4 because at low carbon concentrations the kinetics of transformation become sufficiently rapid to permit increased alloying, without unduly increasing the hardenability, as discussed by Bhadeshia [20].

2.4.5. Effect of Prior Austenite Grain Size

As heat input has a great effect on the solidification microstructure, it follows that the prior austenite grain size is also affected by the heat input. Unfortunately it is not yet possible to predict the austenite grain size based on heat input alone. At present, the factors controlling the austenite grain size continue to be unclear, and the best techniques involve the use of regression equations to make crude estimates of the columnar austenite grain size as a function of chemistry and heat input [20].

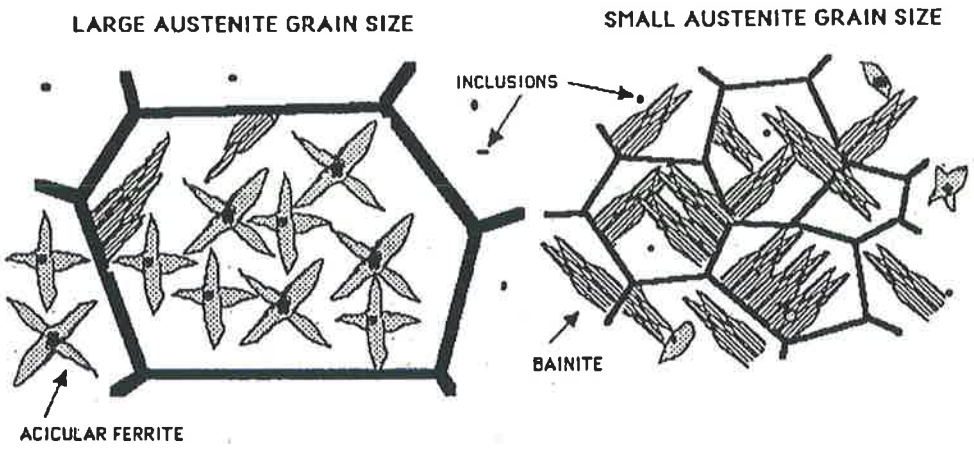

Figure 2-7 Effect of Prior Austenite Grain Size on Microstructure

Figure 2-7 is from Bhadeshia [20].

In recent times, prominent work relating to prior austenite grain size effects has been published [20,30,38,69-71]. In these studies prior austenite grain size was shown to affect the composition of the resultant microstructure. This was especially the case in a paper by Yang [30] where a high strength Si-Mn-Ni-Mo weld was examined to explain the co-existence of acicular ferrite and bainite and in a paper by Dallam [71] where the prior austenite grain size and

applied stress was examined. However, these studies were not the first as a decade earlier other studies also suggested that a factor affecting the formation of acicular ferrite was the prior austenite grain size [72].

Figure 2-7 illustrates how small prior austenite grain sizes result in a bainitic microstructure while large prior austenite grain sizes result in an acicular ferrite microstructure. In large prior austenite grains, ferrite has the opportunity to nucleate on the intra-granular inclusions before all the austenite has transformed into grain boundary nucleated products. This is consistent with the theory that acicular ferrite is simply intra-granularly nucleated ferritic bainite [73].

Of course factors other than just the prior austenite grain size and inclusion characteristics determine the resultant microstructure. The cooling rate of the weld is still of great significance. For this reason, varying factors such as prior austenite grain size can only affect the transformation temperatures for different micro-constituents. This was in fact the result obtained by Farrar et al who found that increasing the grain size depressed the start temperature of grain boundary ferrite and slightly increased the acicular ferrite start temperature [74]. Farrar also noted that microstructural products changed from a grain boundary dominated effect to an intra-granular dominated effect in the large grain sizes and at the same time the morphology of the acicular ferrite was seen to change to a larger aspect ratio. In Farrar's study, dilatometric techniques on C-Mn-Ni weld metal were used to produce CCT

diagrams for different prior austenite grain sizes. The fractions of different transformation products were assessed and the change in morphology of the microstructures was observed.

Farrar's explanation of the effects of austenite grain size were that accompanying the grain boundary transformation, the diffusion of alloying elements, mainly carbon, will occur from the grain boundary regions toward the intra-granular regions.

Therefore, the yet to be transformed austenite in the smaller grained metal will be enriched by carbon to a greater extent than in the larger grained metal. This process is illustrated in figure 2-8 where C_0 is the original carbon content and C_0^+ is the enriched level. This enrichment of carbon in figure 2-8(b) will depress the acicular ferrite start temperature to a lower value compared with the coarse-grained material illustrated in figure 2-8(a).

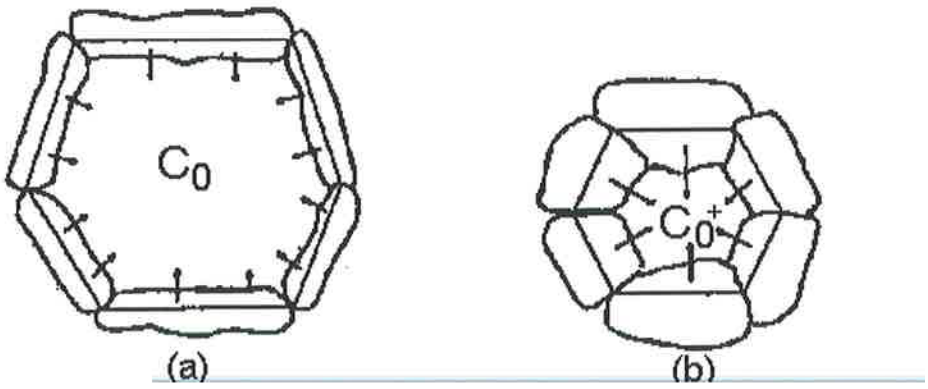

Figure 2-8 Carbon Diffusion in Large and Small Austenite Grain

While investigating the effect of grain size it was also found that although smaller austenite grain sizes favoured the formation of grain boundary nucleated products it also promoted martensite to form at lower cooling rates. This effect is also thought to be the result of local enrichment of carbon in the centre of the transforming austenite grains. Another important microstructural change was the variation in the acicular ferrite morphology. The results indicate that with increasing prior austenite grain size, the acicular ferrite constituent became larger and its aspect ratio increased as well, whereas with smaller grain size, intra-granular products were refined. Similarly, Barrite found that weld metals with a larger amount of acicular ferrite are found to exhibit coarser prior austenite grains [72]. Farrar's conclusions were:

- Prior austenite grain size has a profound effect on the transformation behaviour of C-Mn-Ni weld metal.
- The reasons are thought to be the availability of grain boundary nucleation sites and the elemental redistribution into the intra-granular areas of the retained austenite.
- A large grain size will suppress grain boundary ferrite formation and increase the percentage of acicular ferrite at lower cooling rates but would increase the amount of martensite when the cooling rate is sufficiently high.

The decomposition of austenite is a competitive process between the grain boundary and the intra-granular transformations. Controlling the prior austenite grain structure is therefore important in terms of both microstructure and toughness of low alloy weld metals [74].

2.4.6. Effect of Non-Metallic Inclusions

The origin of inclusions in the weld metal can be from either of two sources. Firstly, external contaminants such as entrapped welding slag, surface corrosion and external coatings applied to the pre-welded surface and secondly, due to chemical reactions forming precipitates within the weld metal.

Even though large amounts of oxygen can be removed from the weld metal through chemical reactions with de-oxidising elements, the removal of oxides is seldom complete and entrapment of solid oxide particles in the form of inclusions occurs [55].

Oxides are formed in the molten state and precipitation of nitrides and carbides occur in the solid phase thus introducing even more particles into the weld deposit. Predominantly the effect of these inclusions, depending upon their composition, is to alter the microstructure and to adversely affect the ductile fracture strength of the metal [75-77].

There have been numerous studies on the effects of non-metallic particles in the weld deposit and to discuss the results of each of these papers is beyond the scope of this review. However, in 1989 Abson published a comprehensive literature review on non-metallic inclusions in ferritic weld metals [78]. His conclusions were:

1. Weld metal inclusions are primarily a mixture of oxides of manganese and silicon and other strong de-oxidants, including Al and Ti, when these are present in the weld. Inclusions are often heterogeneous, with particles at their surface of different composition and crystal structure, including sulphides of Cu and Mn. The number density of inclusions is of the order of 10^8 mm^{-3}, their shapes are roughly spherical and their diameters are commonly in the range 0.2 to 1.0μm.

2. An important role of inclusions is to act as sites for nucleation of fine-grained intra-granular ferrite, a high proportion of which is generally associated with high toughness. Thus a sufficient inclusion content is required in order to provide an adequate number of these nucleants. However, increasing weld oxygen content reduces the prior austenite grain size giving an increase in the proportion of grain boundary ferrite, both indirectly through the increased grain boundary surface area and directly because inclusions facilitate the nucleation of ferrite.

3. Inclusion composition is important in influencing ferrite nucleation. With increasing recovery of Al in the inclusions, the proportion of acicular ferrite has been reported to increase. However, an excess of Al yields inclusions of Al_2O_3 which are poor ferrite nucleants. An approximate balance of aluminium and oxygen in the weld is desirable with limited data suggesting the optimum ratio may be ~0.84. Additions of Ti to the weld are generally

beneficial, with limited data suggesting that >2% Ti in the inclusions (implying a ratio of Ti/(O+S) roughly) >1/15 is desirable.

4. The mechanism by which the more effective nucleants facilitate the nucleation of acicular ferrite is not certain. Both Ti additions and the achievement of the correct Al/O balance have been shown to raise the temperature for the maximum rate of transformation, indicating that the changes in composition improve the efficacy of inclusions as ferrite nucleants. Epitaxial growth of ferrite on crystalline patches of the spinel galaxite ($MnO.Al_2O_3$) or of TiO appears to be a likely mechanism. Inclusion size may also be important, but stresses arising from the difference in thermal expansion coefficient between the inclusions and ferrite are unlikely to make a significant contribution.

5. The efficacy of inclusions for nucleating acicular ferrite is reduced by the presence of patches or shells of MnS on their surface.

More recently, in agreement with Abson, further work by Barbaro [79] has found that the formation of intra-granular or acicular ferrite is dependent on inclusions being over 0.4μm in size and a number of other authors have also found similar results [80,81]. Court found nucleation events frequently occurred on the surface of Mn or Cu-rich inclusions >0.2μm in size [80].

Other work on structural steel microstructural refinement using x-ray and electron diffraction of individual inclusions has also found that Ti_2O_3 particles are responsible for nucleation of acicular ferrite [82], while other studies are continuing to characterise the heterogenous nature of inclusions and their effect on nucleation [83,84].

In addition to the findings relating Ti_2O_3 to ferrite nucleation above, Thewlis et al found that calcium diluted in the weld pool also has a significant effect on acicular ferrite nucleation by changing the weld metal inclusion volume and size distribution [85].

Abson's study, and more recent work by others [80] is however primarily based on lower strength weld metal. Unfortunately there has been little work published on high strength weld metals where the deposits are frequently of a bainitic microstructure, interspersed with martensite and retained austenite.

Of these few studies, Ramsay [86] examined microstructures consisting of auto-tempered lath martensite, bainite and retained austenite. Limited particle-nucleated ferrite laths were also examined. The conclusions of his research were:

1. Intra-granular nucleation of ferrite will occur in high strength steel weld metal when a suitable proportion of non-metallic inclusions are present.

2. Intra-granular nucleation of ferrite laths segments the prior austenite grains. On subsequent transformation the effective martensite packet size is refined.

3. Non-metallic inclusions in high strength weld metal can effectively pin austenite grain boundaries resulting in smaller austenite grains and a finer martensite packet size.

Further work by Oldland et al [18] found that there are a number of different types of inclusions found in these types of weld metals. Using SEM and energy dispersive x-ray spectrometry, qualitative chemical compositions of inclusions were found. These inclusions were found to contain differing amounts of aluminium, manganese, titanium, sulphur and iron. No discussion was made on the effects of these different particles on the nucleation of ferrite except that it was found that some particles would nucleate ferrite while others would not. However, it is not only the chemical compositions of the inclusions which are significant in affecting the weld microstructure but also the size distribution. This was made apparent by Ramsay [86] in other work which he referred to [87] in which it is stated that "a population of $\approx$0.5μm inclusions are required to act as nucleation sites for ferrite and a population of smaller inclusions are required to pin prior austenite boundaries."

Even though many of the effects of particles in the weld deposit are understood it is clear there is still further work required to determine the effects of different particle types on the weld microstructure. This is especially the case for particles found in high strength weld microstructures where considerably less research has been focussed and the effect of different particles having different propensities to nucleate ferrite is found.

The factors influencing inclusion size are not understood in detail and although inclusions are sometimes regarded as a means to obtain improved weld microstructure their ability to nucleate cleavage and ductile failure must also be appreciated [19].

2.5. PREVIOUS HEAT INPUT EFFECT STUDIES

2.5.1. Overview

The majority of studies focussed specifically on heat input have been on submerged arc welds with a view to validating the use of very high heat inputs to achieve greater productivity. Significant research has also been on low strength C-Mn welds made using a variety of processes. However, little work has been published on high strength welds of strength greater that 690 MPa. This is especially the case for welds made using flux cored consumables.

2.5.2. Low Strength Weld Metal Studies

Of the studies done on heat input effects on welds with strength levels below 690 MPa there have been some studies which are relevant to heat input effects regardless of the weld strength level.

A study by Evans [34] on C-Mn manual metal arc welds in the heat input range of 0.6 to 4.3 kJ/mm for Mn contents of 0.6 to 1.8 % wt in the down hand position, found that increasing the heat input increased the bead size and increased the size of the HAZ (as would be expected of a higher heat input). The higher heat input also decreased the amount of acicular ferrite formed, resulting in a general coarsening of the weld metal microstructure. This corresponded with a reduction in tensile strength and hardness. Optimum impact properties were achieved at 2 kJ/mm heat input. Similar results were also found by Gonzalez [88] in a study of self-shielded flux-cored wires in the heat input range of 1.0 to 2.4 kJ/mm.

Evans [34] found the chemical compositions of the weld deposit changed only marginally with changes in heat input. There were only minimal decreases in the contents of C, Mn and Si as the heat input increased.

Overall, as heat input was increased, Evans found that for the as deposited weld:

- Mn and Si contents were marginally reduced.
- Hardness of as-deposited weld metal decreased.
- Average width of the columnar grains increased.
- Pro-eutectoid ferrite increased at the expense of acicular ferrite.
- Lath size of acicular ferrite increased.
- Grain size of equiaxed fine grained regions increased.
- Yield and ultimate tensile strength decreased; and
- The strengthening effect of Mn decreased.

2.5.3. High Strength Weld Metal Studies

As stated in section 2.5.1., more high strength weld metal research has been on the submerged arc welding process (SAW) to gain productivity increases. The SAW process has thus been the topic of much recent research [18,86,89-94].

Oldland [18] included heat input as part of a more general study on high strength weld metal microstructures and Rorvik [90] was mainly interested in high heat input welding in the range 3 - 7 kJ/mm.

Gianetto's study [89] was on the influence of heat input on the microstructure and mechanical properties of high strength submerged arc welds in HY-80 and HSLA-80 steels using a basic flux. A significant part of the study was to determine the influence of the resultant dilution (which is proportional to the heat input) on the weld characteristics. As expected, when welding HY-80 steel a major decrease in the yield strength and microhardness was observed with increasing heat input. The heat input range was 1 - 4 kJ/mm.

When welding HY-80 steel the observed microstructure ranged between that of lath martensite at the lower heat input to that of fine bainite at intermediate heat inputs of around 2 kJ/mm and finally to increased packet sizes of bainite at 4 kJ/mm heat input. This increased bainite packet size was said to be the cause of a decrease in the transition temperature at that heat input and the hard lath martensite at 1 kJ/mm was considered to be the cause of poor notch toughness.

HSLA steels, however, only showed a small decrease in yield strength with increasing energy input. Notch toughness was shown to be independent of heat input. The microstructural constituent of the HSLA welds was shown to

be ≈80% acicular ferrite which probably accounted for the better notch toughness performance.

Additional work by Gianetto used radial dilatometry to find the CCT diagrams for different welds. To do this, weld metal samples were machined from the weld deposits and subjected to thermal cycles estimated to approximate the cooling rate of welds deposited under different heat inputs.

The findings of Rorvik's study, which was focussed on determining the effect on weld properties by increasing the heat input to high levels in the range 3 - 7 kJ/mm, were much the same as those of Gianetto in that CVN and CTOD results obtained were excellent, however a slight degradation in properties was seen with increasing heat inputs.

Oldland's study was the most general and covered the greatest number of parameters associated with weld characteristics. His study dealt with SAW in a high strength low carbon steel with a 5Ni-Cr-Mo weld. He found that as the heat input was increased the tensile strength was reduced, the ductility increased and the fracture toughness increased. This was considered to be due to the change in microstructure from auto-tempered martensite to a mixture of martensite, bainite and retained austenite as the heat input increased.

Inclusion characteristics in high strength weld metal were also examined by Oldland and it was shown that weld metal inclusions (which are known to nucleate ferrite in lower strength weld metal) were shown to have a mixed effect on the development of microstructures in high strength weld metal. Inclusions in bainite appeared to have little effect while some nucleated ferrite laths.

In Ramsay [86], two different heat inputs were used in a study of microstructures and properties of a high strength steel weld metal. His results were similar to those of Oldland.

The effects of heat input due to cooling rate for a generic weld metal are summarised well by Francis [5] where he states that two primary changes occur in the weld metal microstructure due to alteration of the cooling rate. First a decreased cooling rate will produce generally coarser microstructural features. Second, changes in cooling rate will influence the nucleation and growth processes involved in the decomposition of austenite to ferrite and carbides or to martensite.

Francis also notes that an increase in heat input represents a longer time to solidify and thus a longer time of exposure to the atmosphere after the welding gun and cover gas envelope have passed. The significance of such observations is yet to be determined.

More recently, was a study by Dixon [95] where increased hardness levels were associated with the formation of martensite and bainite.

Dixon's work was designed to identify the optimum match of welding parameters, notably pre-heat and inter-pass temperatures and the heat input for the welding of a 690 MPa Q&T steel. The weld metal used was a Mn-Ni-Mo composition and the heat inputs examined were 1.3, 2.9 and 4.0 kJ/mm. A variety of pre-heat and inter-pass temperatures were examined using these heat inputs.

The mechanical properties Dixon examined were hardness, tensile strength and Charpy toughness for which full transition curves were generally obtained. The welds were however multi-pass and only minimal microstructural examination was presented. Nonetheless, the mechanical properties obtained showed a general decrease in hardness as the heat input increased as seen in figure 2-9. Dixon explained this increase in hardness as being due to the formation of martensite and bainite at the lower heat input/preheat temperatures.

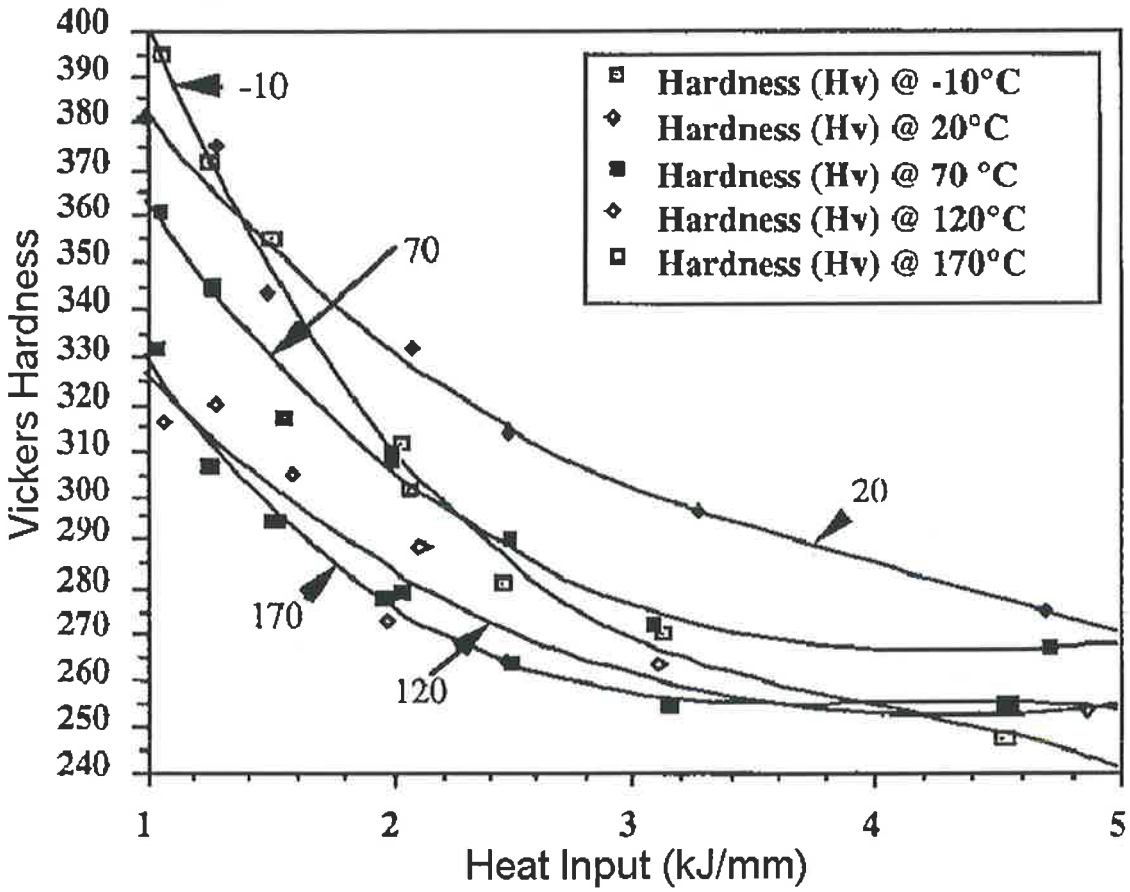

Figure 2-9 Hardness Variation as a Function of Heat Input

Figure 2-9 is from Dixon [95]

2.6. CONCLUSIONS

Much research has already been done in areas which control weld microstructural development. For this reason it has only been possible to discuss the main factors which influence microstructure and mechanical properties. Particular attention was given to individual studies on heat input effects, especially those on high strength weld metals.

The review of molten metal reactions, solidification and austenite transformation has made it evident that there is still much to be learned. This is especially the case for high strength weld metals where microstructures containing bainite and martensite are a common occurrence. There is also a general lack of published research using processes such as pulsed welding with the latest developments in flux cored consumables. This lack of research using recent developments in welding technology may be because researchers are still coming to terms with more fundamental issues such as the effects of welding parameters and chemistry on inclusion characteristics and their propensity to alter the microstructure to be concerned with any, supposedly, minor effects of the individual welding processes.

Available information focussed on the submerged arc welding process with little discussion of other processes employing technologies such as flux-cored-wire or pulsed welding. It therefore follows that an experimental programme focussing on weld metal in this strength range will appropriately

contribute to this shortfall in the literature, especially if the programme was to employ some of the more recent advances in welding technology such as pulsed welding and the new range of flux cored wires now available.

Within such a study many aspects of weld microstructural development could be examined. The most significant of which would be the types of particles found in such weld deposits and their effect on microstructure and mechanical properties.

CHAPTER 3. EXPERIMENTAL PROGRAMME

3.1. INTRODUCTION

Based on the needs discussed in section 2.6., an experimental programme was devised to examine as deposited high strength weld metal using an out of position flux-cored consumable. The welding equipment available was a WIA synchro-pulse power supply. This was not only used due to the availability but also because of the necessity to use pulsed welding when using an out of position consumable.

Using this equipment and consumable, six welds in the heat input range of 1.0 to 2.5 kJ/mm were prepared in the vertical up position and the critical parameters of heat input and cooling rate were monitored during the welding process. The weld microstructure was then examined using light, scanning electron and transmission electron microscopy and mechanical tests employed were Vickers hardness, tensile strength and fracture toughness at two temperatures using specially prepared sub-size CTOD specimens.

Many references including [97-117] were used as guidelines in the development of mechanical tests and inspection techniques. Details of each of these techniques and tests are explained later in this chapter and also in chapters 4, 5 and 6. The remainder of chapter 3 is devoted to detailing the experimental programme and the characteristics of consumables and techniques used prior to the commencement of welding.

3.2. CONSUMABLES AND BASE MATERIAL

3.2.1. Consumables

The consumable selected was a flux cored basic electrode, with designation MIL 690. This specification is primarily used for the welding of high strength steels. At the time of writing one such application under consideration for this consumable was the welding of BIS812EMA Q&T steel plate used in the Collins Class Submarines manufactured by the Australian Submarine Corporation in Adelaide. The electrode had a diameter of 1.2 mm. A cross section of a similar electrode can be seen in figure 3-1.

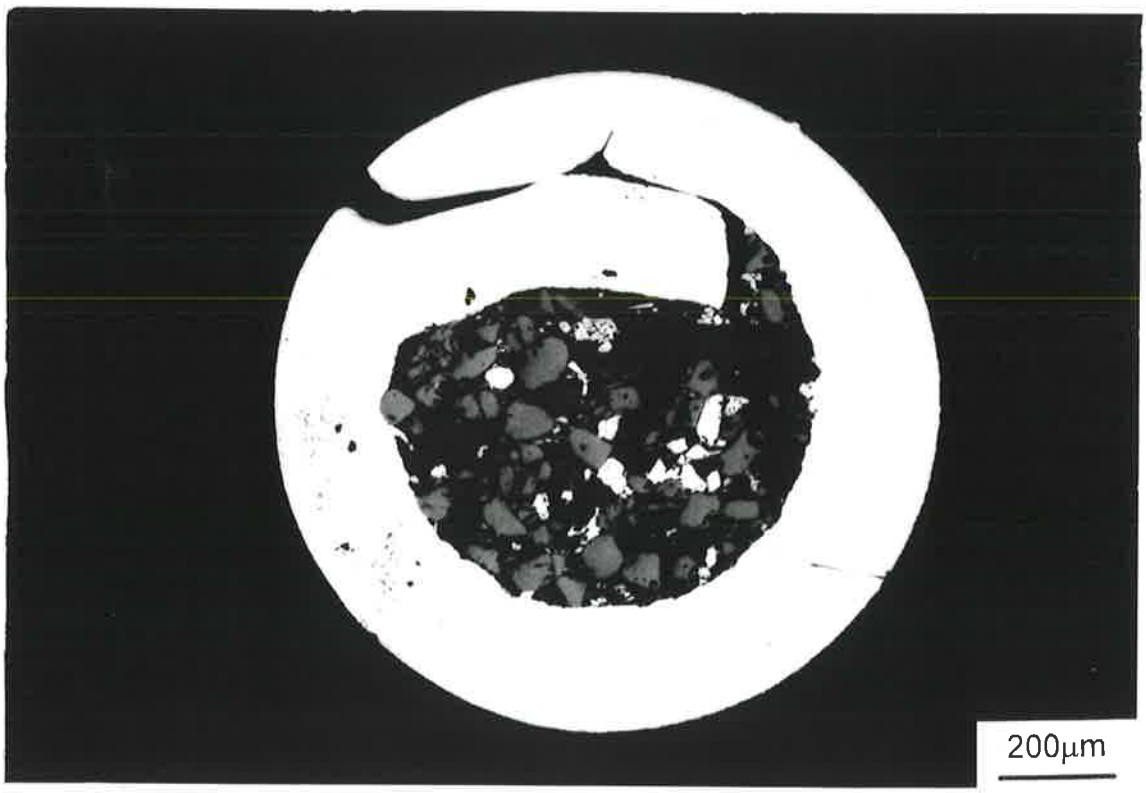

Figure 3-1 Cross Section of Flux Cored Electrode

The elemental analysis of MIL690, as prepared by CSIRO Division of Manufacturing Technology using an in house wire mill, is given in table 3-1. This is nominally the composition used for all experimentation in this study.

Element	*Fe*	*C*	*Mn*	*Si*	*Ni*	*Mo*	*Ti*	*Al*	*B*
Percentage by weight	Bal	0.03	1.13	0.47	2.91	0.27	0.09	0.04	1.08 ppm

Table 3-1 Chemical Composition of MIL690 electrodes

The shielding gas used was a 95% Argon / 5% CO_2 special mixture. This gas was prepared and analysed by CIG.

3.2.2. Base Plate Chemical Composition

The consumable used in this study has been designed for the welding of a number of different high strength steels available on the market. The use of a single high strength steel as the base plate material would include the complicating factors of dilution with various elements of different concentrations found in the base plate. This would be further complicated by having different levels of dilution as the heat input was varied. For these reasons, a base material which was as inert as possible was desired. To satisfy these conditions a low alloy steel was buttered on the surfaces to be welded. As can be seen from figure 3-2, of the commonly available steels listed, AS1204 250 grade BHP mild steel bar is a suitable choice in that it contains no elements known to have a micro-alloying effect on the weld metal. The only effect that may result is a small concentration decrease of the consumable alloys in the weld deposit. Of course the other advantage of this material as a base plate was that it is cheap and readily available.

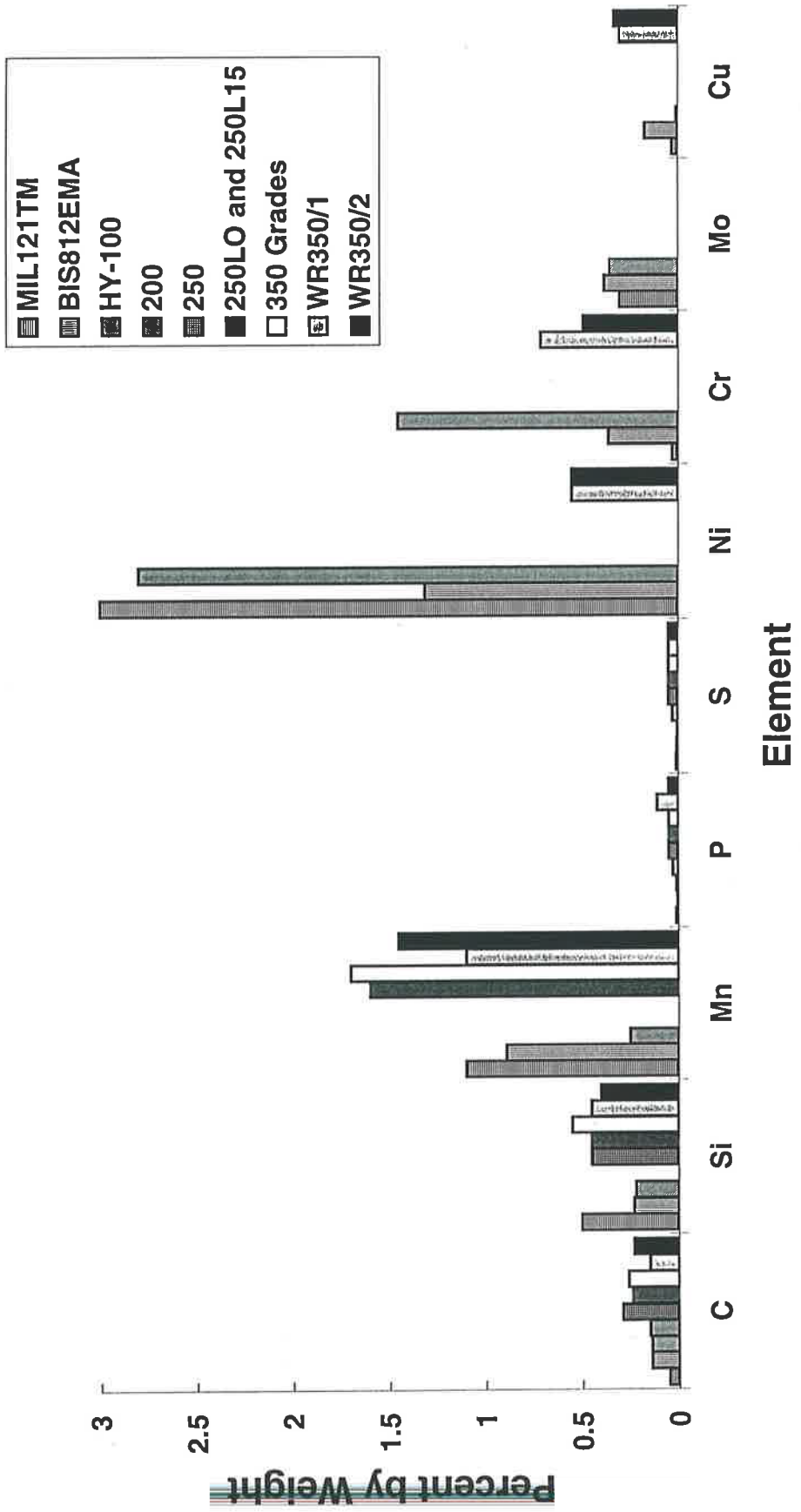

Figure 3-2 Chemical Compositions of Base Plates Considered

3.2.3. Base Plate Dimensions

The base plate dimensions of thickness and width have an influence on the cooling rate of the weld deposit. Ideally the base plate dimensions should be such that no change in cooling rate would occur if the dimensions were increased. In this way the weld deposit sees the base plate as being of infinite dimensions thus eliminating any cooling rate bias due to plate thickness.

To determine the dimensions of base plates required it was necessary to determine the smallest dimensions which may be considered infinite for welds up to 2.5 kJ/mm. Previously, a number of researchers have considered such problems mostly using theory based on the fundamental work of Rosthenthal [14]. Since then, a number of more refined theoretical studies have been done. One of the better analytical studies was by Blodgett [16] where he developed software in which numerical integration techniques were used to develop a non-dimensional curve from which cooling rates could be calculated easily. This theory was also compared to experimental studies on weld cooling rate by Signes [118].

Using the theory discussed by Blodgett [16], the thickness of plate required for which no further increase in thickness will have any effect on weld cooling rate was calculated as being 34mm. If this is compared to data extracted from Signes [118] work where he measured weld cooling rate by implanting thermocouples in the weld pool, it is found that 34mm is the thickness for

which no further increase in cooling rate will result by increasing the plate thickness. However, the thickness can be as low as 20mm before any significant increase in cooling rate will result for welds of up to 2.5 kJ/mm.

The next dimension to take into consideration was the plate width. Again looking at Signes study of weld bead cooling rates it is found that for welds of up to 3.5 kJ/mm heat input and for plates under 25mm thickness a 230mm wide plate was necessary to avoid edge effects for cooling down to as low as 260 °C. As these parameters are in excess of what is required here (as the maximum heat input used is only 2.5 kJ/mm) a plate width of 200mm was considered satisfactory. Dimensions of the base plates on which to deposit the welds were thus selected to be 20mm x 200mm x 400mm.

The length of 400 mm was necessary in order to obtain the required number of samples while still being able to discard 25 mm of weld at either end of the plate before the arc had stabilised and to avoid end effects on cooling. Figure 3-3 shows the location of the samples removed from the base plate.

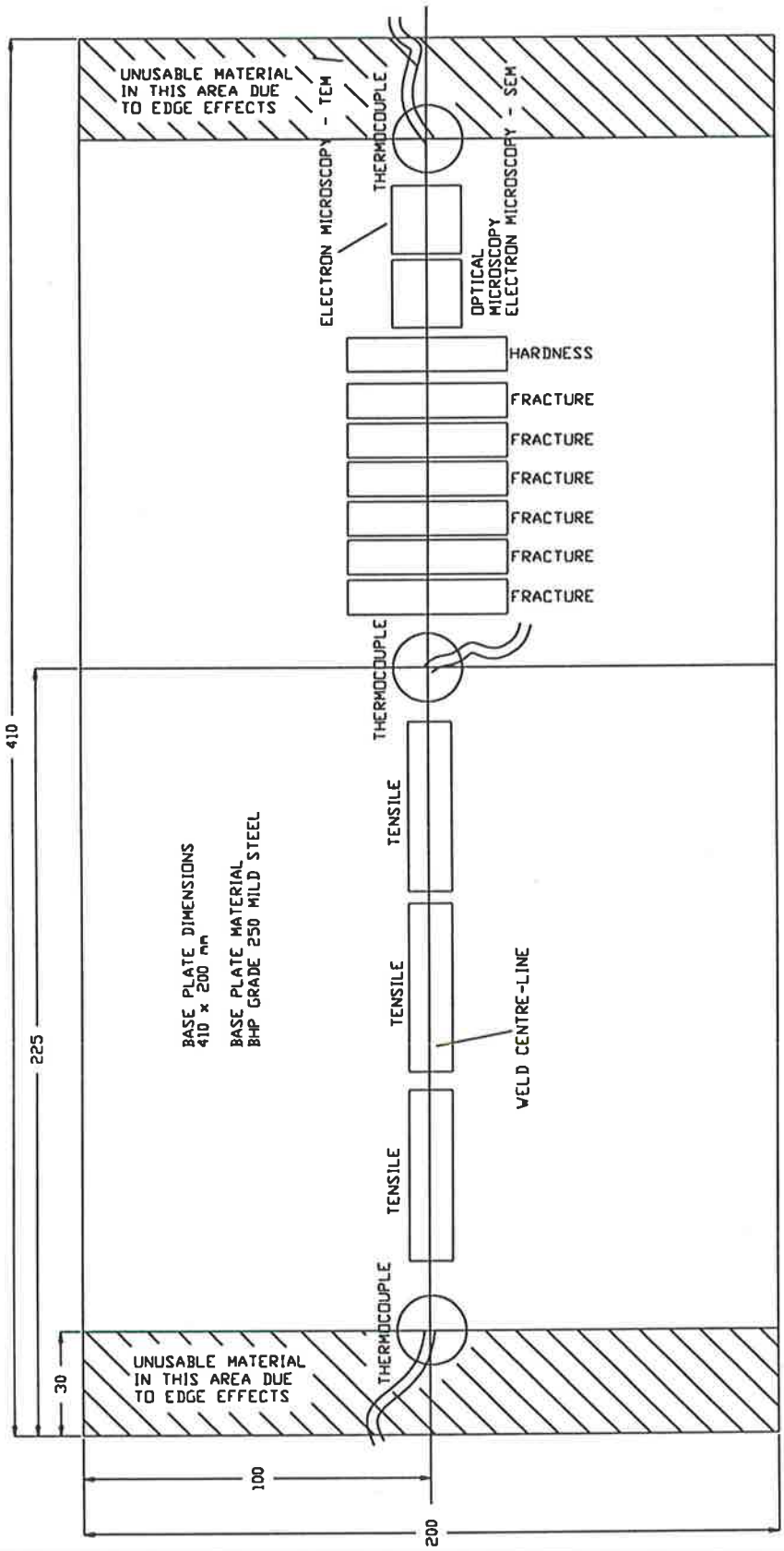

Figure 3-3 Location of Specimens Removed From Welds

CHAPTER 4. WELDING AND INSTRUMENTATION

4.1. INTRODUCTION

This chapter details the specifics of the welding process, equipment and instrumentation used for welding. Process parameters recorded and final welding results are also detailed.

Some of the equipment required to make and monitor the welds was already available. However in many cases, modifications or construction was required. These modifications are also detailed in this chapter. As well as equipment modifications, the development of instrumentation and associated software is discussed.

4.2. WELDING EQUIPMENT

A CDT-450 Synchro pulse power supply manufactured by WIA was used. Typical currents were between 100 and 150 Amps. CDT is an acronym for controlled drop transfer, this metal transfer mode allows out of position welding using consumables which would otherwise be confined to non-positional welding. Metal transfer modes are described well by Kim [119].

Attached to the CDT-450 power supply was a WIA C-21 wire feeder and a Bernard 300 Amp water cooled torch. The water jacket on the 300 Amp torch failed during plate preparation and was subsequently replaced by a 400 Amp non-water cooled unit. The replacement of the torch was not expected to cause differences in the deposited metal characteristics although feed problems were more evident with the non-water cooled unit. The increased occurrence of contact tip friction problems after the failure of the water cooled unit required the use of small quantities of molybdenum disulphide as a wire lubricant. The quantities used were minute and were assumed to have had an insignificant effect.

The torch was supported and guided by a BUG-9660 Speed Weaver. This was set on stringer mode and did not weave during welding. The only purpose of the BUG-9660 was to traverse the welding torch up the work piece at an accurate and constant predetermined velocity. The torch and the BUG-9660 were supported by a metal frame.

4.3. BASE PLATE PREPARATION

Prior to welding, the base plates underwent considerable preparation. This preparation was primarily aimed at buttering weld metal on the base metal so as to prevent different weld deposit dilutions occurring as a function of the heat input. If these weld metal layers were not applied, the weld bead would have been expected to have been diluted with up to 20 percent of the base metal. This would cause significant changes in weld chemical composition, thus biasing the results. Three layers of weld metal were subsequently applied to the base plate surfaces to be welded. This provided a buttered layer of four to five millimetre thickness.

A photo of the "buttering" operation can be seen in figure 4-1 where welding is taking place in the down hand position using the CDT-450 and a tractor to move the plate past the welding torch. A supporting jig was used to hold the plate in position with clamps fastening the base plate to the jig and similarly the jig to the tractor.

After the angled surfaces of the base plate had been fully buttered they were machined back to the dimensions shown in figure 4-2.

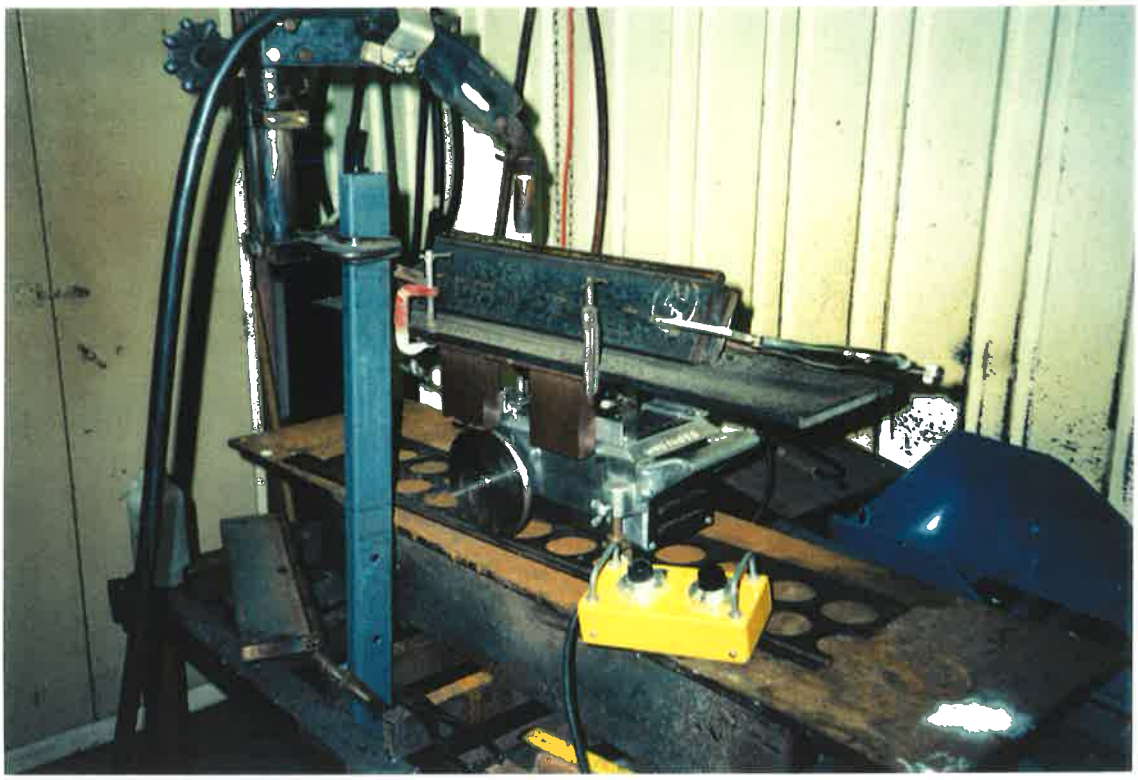

Figure 4-1 Photo of Base Plate Preparation

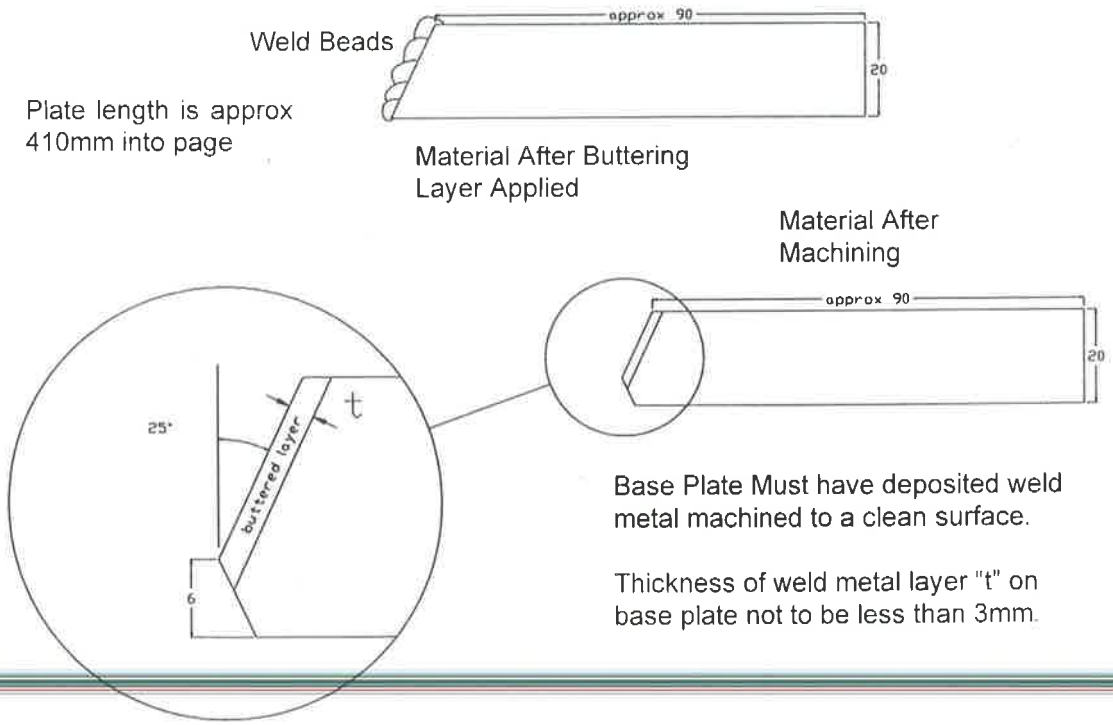

Figure 4-2 Base Plate Preparation

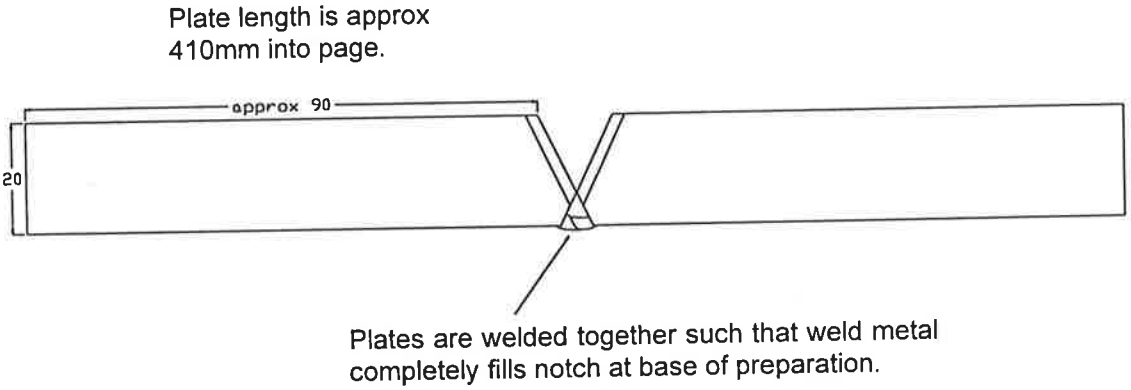

Figure 4-3 Final Base Plate Configuration

The base plates were then welded together at the base to form a rigid preparation. This final base plate configuration is illustrated in figure 4-3.

The angle of the base plate was initially set at a 60 degree included angle with no root gap. No root gap was used so as to maximise the height of available weld metal for mechanical testing. Even so, this configuration still proved to provide insufficient weld metal from which to obtain a fracture specimen, and also presented difficulties in obtaining tensile specimens. This angle was subsequently reduced to 50 degrees and tests on base plates proved this angle to provide a suitable weld bead geometry for removal of test specimens. The use of such a tight angle imposed the danger of minor root gap defects developing. This proved to be the case when the final welds were made.

However, equation 4-2 still does not give high accuracy results. In order to determine the exact heat input for a particular weld, using a unique consumable and gas type, the instantaneous voltage and current wave-forms must be recorded and analysed. This was especially necessary in this project as the range over which heat inputs were varied was small.

4.4.3. Heat Input Measurement Technique and Results

Because of reasons discussed in section 4.4.2. instantaneous voltage and current wave-forms were recorded using an M440 NICOLET digital storage oscilloscope. This was connected to the welder using the arrangement shown in figure 4-4.

The resistor used was a shunt resistor which developed a voltage of 75 mV when 200 amps was passing through it. The DSO then recorded this voltage and was programmed to map it to the corresponding current. Typical wave-forms which were obtained by the DSO are shown in figure 4-5.

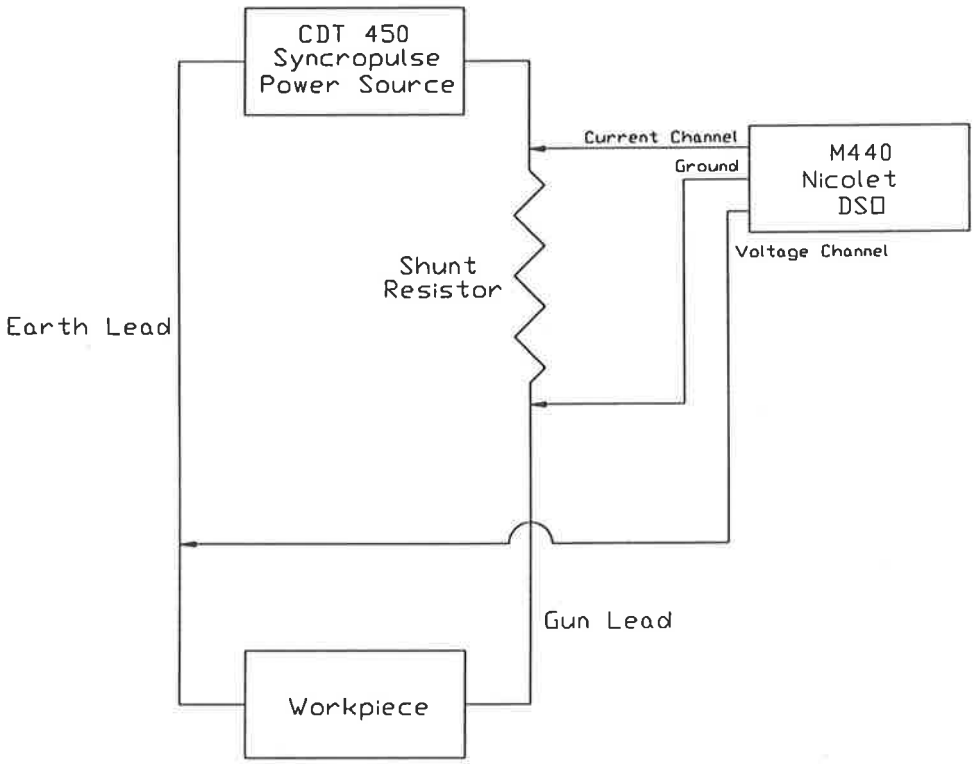

Figure 4-4 Connection of DSO to Welding Equipment

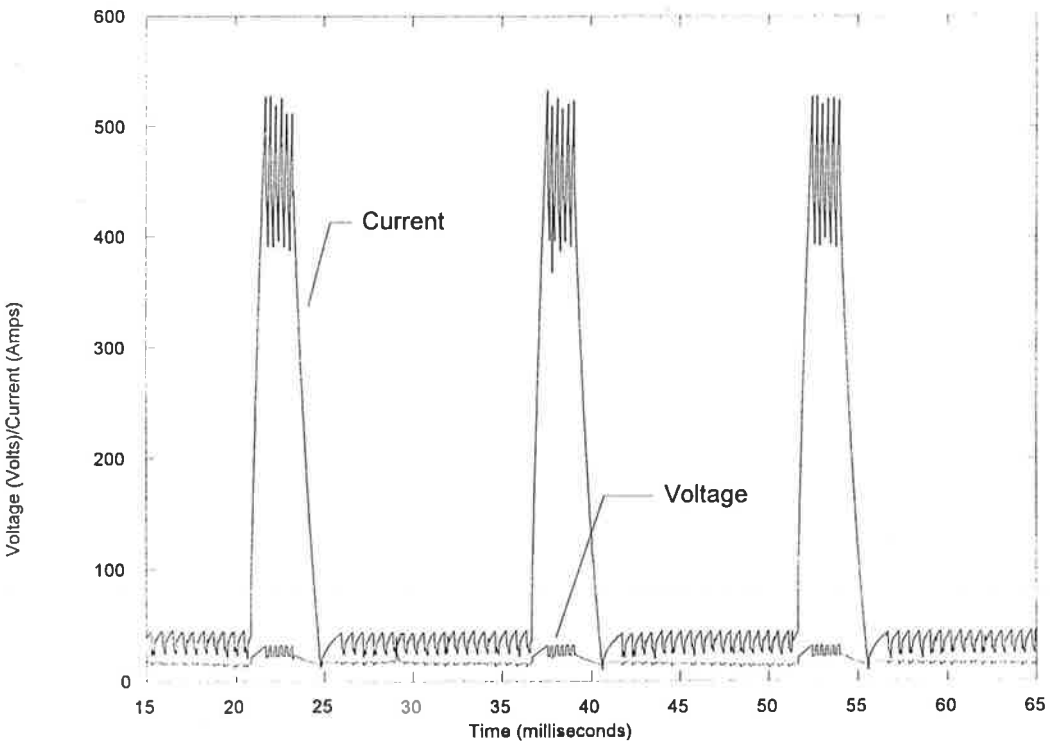

Figure 4-5 Voltage and Current Wave-forms Recorded by DSO

To convert data collected in the form of figure 4-5 into values of heat input, software functions within the M440 DSO were used to process the data to give a mean value of the instantaneous product of voltage and current. The resultant values of heat input, and the target values, are tabulated below in table 4-1. Values of the heat input based on the values read from the welder display panel and then converted to heat input using equations 4-1 and 4-2 are also tabulated in table 4-1 for comparison.

Target	1.00	1.25	1.50	1.75	2.00	2.25	2.50
Welder Display (Eqn 4-1)	0.82	1.02	1.18	1.47	1.58	1.83	2.07
Welder Display (Eqn 4-2)	1.00	1.24	1.50	1.80	2.03	2.23	2.53
Actual (DSO)	1.19	1.12	1.21	1.66	1.74	1.94	1.97

Table 4-1 Heat Inputs Obtained (kJ/mm)

As can be seen in table 4-1, the target heat input values were difficult to achieve, however, reasonable spacings over the heat input range of interest were obtained. This variation from the target values makes the need to use accurate instrumentation when examining heat inputs over a small range apparent.

4.5. MEASUREMENT OF WELD DEPOSIT COOLING RATE

4.5.1. Introduction

The effect of cooling rate is one of the most significant and critical factors in determining the resultant microstructure and mechanical properties of a weld deposit. Previous welding studies aimed at determining this cooling rate, have used either physical measurements or have made predictions based upon such experimental studies, with the assistance of theoretical or computational methods. These methods have not however been able to allow accurate prediction of the weld cooling rate for all situations. This leaves the only sure option to be experimental measurement.

Theoretical examination of heat flow and weld cooling rates has been in progress since the 1930's. The early work in this era can be best summarised by Rosenthal's paper [14] published in 1941. Since that time there have been numerous developments, many of which (through the 1960's) involved the development of mathematical models for the cooling rate and temperature distributions for bead-on-plate welds [15,118,122-128]. These methods were predominantly based on "thick" and "thin" plate models in which two and three dimensional heat flow was examined.

In more recent times, with the advent of powerful computers, researchers such as Blodgett [16] and Kannatey [129] have applied numerical techniques to solving heat flow and cooling rate problems for welding, resulting in greatly improved estimates.

Despite these advances there have been a number of difficulties associated with applying such theoretical models to real situations. These are associated with factors such as the arc efficiency for different processes, the base plate composition and the geometry of the weld preparation. Also, there is no reference source or technique available as an accurate guide to quickly determine the expected cooling rate for a given welding process using a specified set of parameters and preparation geometry. If accuracy is to be guaranteed it would seem experimental methods continue to remain the only option.

Some experimentally determined data has been published on weld cooling rates [1,126,130-133]. This data is limited, but it is sufficient to obtain an approximate figure for the expected cooling rate of the types of welds of interest here. For example, typical cooling rates for a 2.0 kJ/mm heat input flux cored bead on plate weld are in the order of ten seconds from 800°C to 500°C [1]. This cooling rate published by Vines [1] was determined by plunging thermocouples into the weld pool.

In early stages of this study there were a number of experimental techniques considered which employ technologies other than thermocouples for the measurement of weld cooling rates:

- **Optical fibre insertion** - Although not used to a great extent, the use of optical fibres may become more commonplace in the future. The

advantage of optical fibres is they avoid the electrical interference associated with thermocouples and they are not prone to contamination. They do however melt at temperatures lower than those of noble metal thermocouples.

- **Optical pyrometry** - This is a good technique for measuring temperatures in the region of a cooling weld deposit after solidification, however, ambient light radiation from the arc makes such measurement in the weld pool impossible. It would also be potentially dangerous to eyes due to the high levels of ultra violet radiation.

- **Infra red thermography** - This has the advantage of less interference from the arc than optical pyrometry due to the use of filters which exclude radiation with wavelengths shorter than approximately 2mm. It also has no contact with the work piece thus avoiding electrical interference to which thermocouples are prone. Thermocouples are however more accurate than infra red thermography. Thermography equipment availability is also very limited. In addition to this, infra red thermography only measures the surface temperature of the weld, not the temperature near the centre of the weld as discussed by Lukens [134].

Thermocouples were however decided on due to their availability, ease of use and because they require no special equipment to interface with instrumentation [135-137].

With the use of thermocouples, the means for recording data then needed to be addressed. Previous researchers have used analogue amplifiers connected between a thermocouple and a paper chart recorder. In the laboratory at CSIRO the technique previously used for thermocouple measurements has been a signal conditioner connected between a thermocouple and an A/D card in a computer. This technique has a number of advantages in that the data is easy to analysis and if a suitably high data collection rate is employed the time and temperature resolution is superior to that obtained using conventional chart recorders. As equipment of this nature was also available it was selected as the system for data collection.

Thermocouple probes were employed for weld thermal profile measurement. These are discussed in section 4.5.2. Thermocouples were connected to an Analogue Devices 3B-01 signal conditioner which in turn was connected to a PC-30PGL A/D card in a 80486DX-50 PC. The data received through this system was then analysed and recorded using software discussed in section 4.5.4.

4.5.2. Thermocouple Construction

Although thermocouple lances into the weld pool have been used by researchers in the past [132], little literature was found detailing the actual construction of such probes. A design was subsequently made using information in a number of references and through discussion with members of the CSIRO Division of Applied Physics - National Measurement Laboratory.

Factors considered when deciding on the thermocouple construction to employ were:

- Due to the likely high cost of the thermocouple materials the construction needed to be able to be used more than once.
- The thermocouple metal selected needed to be able to withstand the high temperatures expected.
- Construction needed to be easy, using equipment readily available.
- Thermal conduction along the thermocouple wires, if allowed to reach the effective cold junction end of the thermocouple, will reduce the output voltage.
- The thermocouple requires shielding from the hostile environment in the vicinity of the arc.

There are many different types of thermocouples available. Thermocouples commonly used in welding are K and R type. R-type is a noble metal thermocouple and K-type is made from a combination of Nicrosil and Alumel. Although K-type thermocouples are relatively cheap they melt at 1400°C

which makes them unsuitable for insertion into molten ferrous alloys. R-type melt at 1795°C which is about 200°C above the temperature of the molten metal. This combined with their reasonable degree of availability made them an acceptable choice. In retrospect tungsten-rhenium thermocouples may have been a better choice due to their much higher melting point (about 3100°C) despite their lower sensitivity and limited availability.

The thermocouple probe design, illustrated in figure 4-6, was constructed in the following manner:

1. 180mm of 0.25mm diameter pure platinum wire and the same length of 87% platinum, 13% rhodium alloy wire were inserted into a 1.55mm outside diameter, 130mm length of high density twin bore alumina.
2. The hot junction end of the thermocouple was joined by fusing it together using a high temperature hydrogen/oxygen flame torch.
3. The remaining 50mm of wire, extending from the end of the alumina, was sheathed by Teflon tubing. The need for Teflon sheathing is two fold. Firstly the application of heat shrink tubing (in step 6) would melt most PVC type insulating materials and secondly, Teflon is highly resistant to spatter from the arc welding process.
4. The thermocouple wires were then soldered to a three metre length of shielded copper wire.
5. The shielded wire was then terminated with an R-type thermocouple plug.
6. Heat shrink tubing was applied to prevent wire movement and possible short circuiting at the end of the alumina sheath.

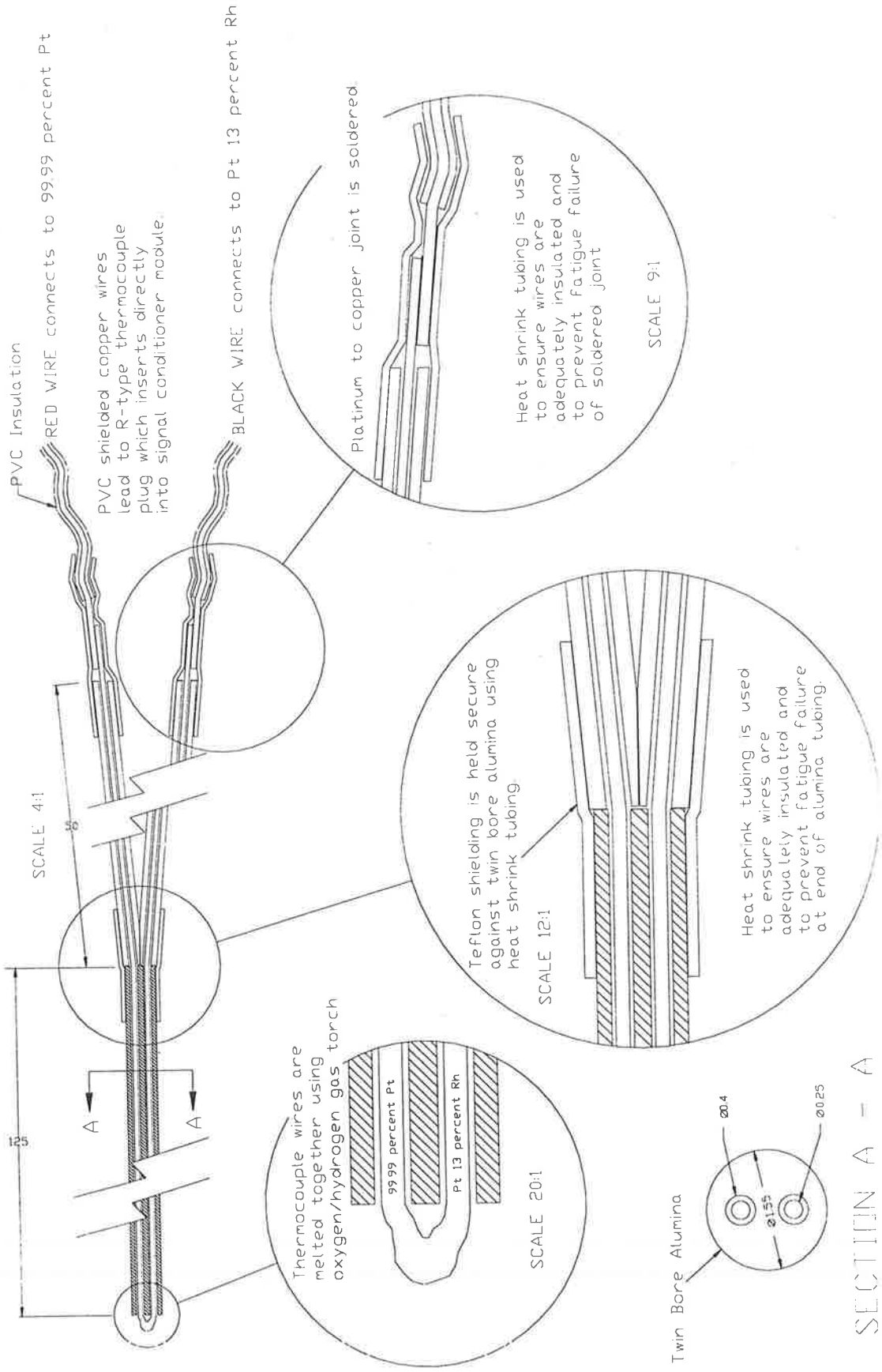

Figure 4-6 Thermocouple Probe Assembly

4.5.3. Thermal Data Collection

When an R-type thermocouple is heated to temperatures found in the weld pool, only a few mV of output is produced (typically 10 to 20 mV). As the thermocouple is also in the vicinity of an arc with peak currents in the order of 400 to 500 amps and voltages of up to 35 volts, some sort of signal conditioning is necessary to obtain a relatively noise-free output. The system available was an Analogue Devices 3B-01 signal conditioner. Unfortunately this system consistently proved cantankerous and much time was spent attempting to find the cause of faults. This system continued to behave unreliably until an intermittent power supply fault was discovered. Regrettably this fault was discovered at a critical point in experimentation resulting in the loss of valuable data.

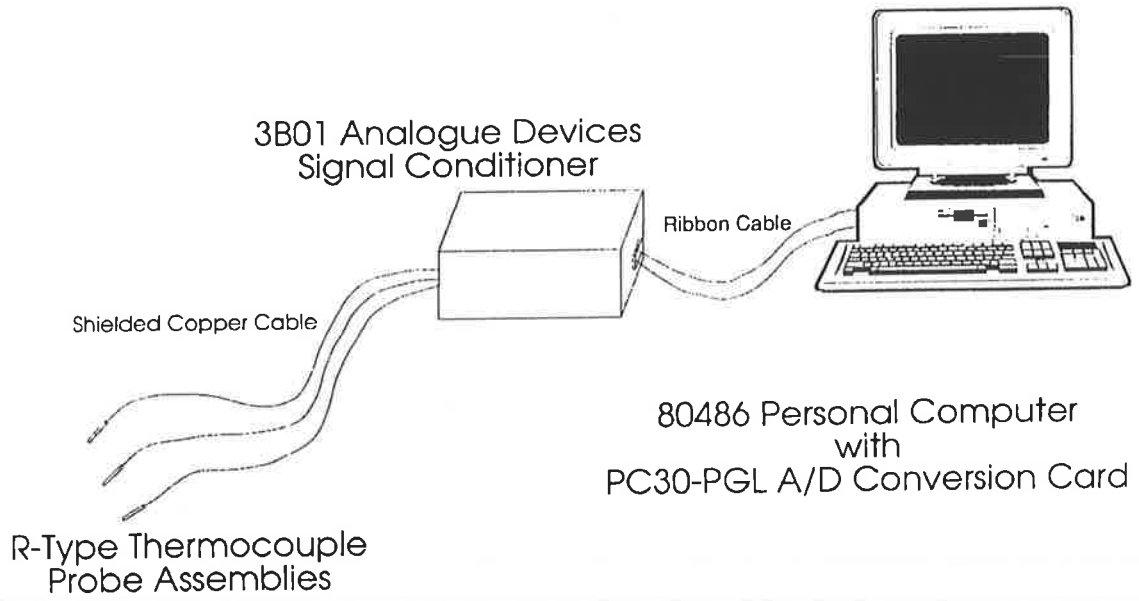

Figure 4-7 Thermal Data Collection System

When the reading of data is complete, software checks to see if the PC-30 has set the data read flag in one of its registers. If this flag is set then the data is read into the program in high byte/low byte form before being converted to an integer value. The data read flag is then reset to data not ready. As the PC-30 has 12 bit resolution the 4 highest bits of the high byte register are discarded. This leaves a binary number which is converted into an integer value between 0 and 4095. This value is then directly mapped to a temperature value using the look-up table previously generated. The screen is then updated and if the record option is set the data is recorded to file.

Software operation is described best in flow chart form in figure 4-8 while a listing of the code can be found in appendix A.

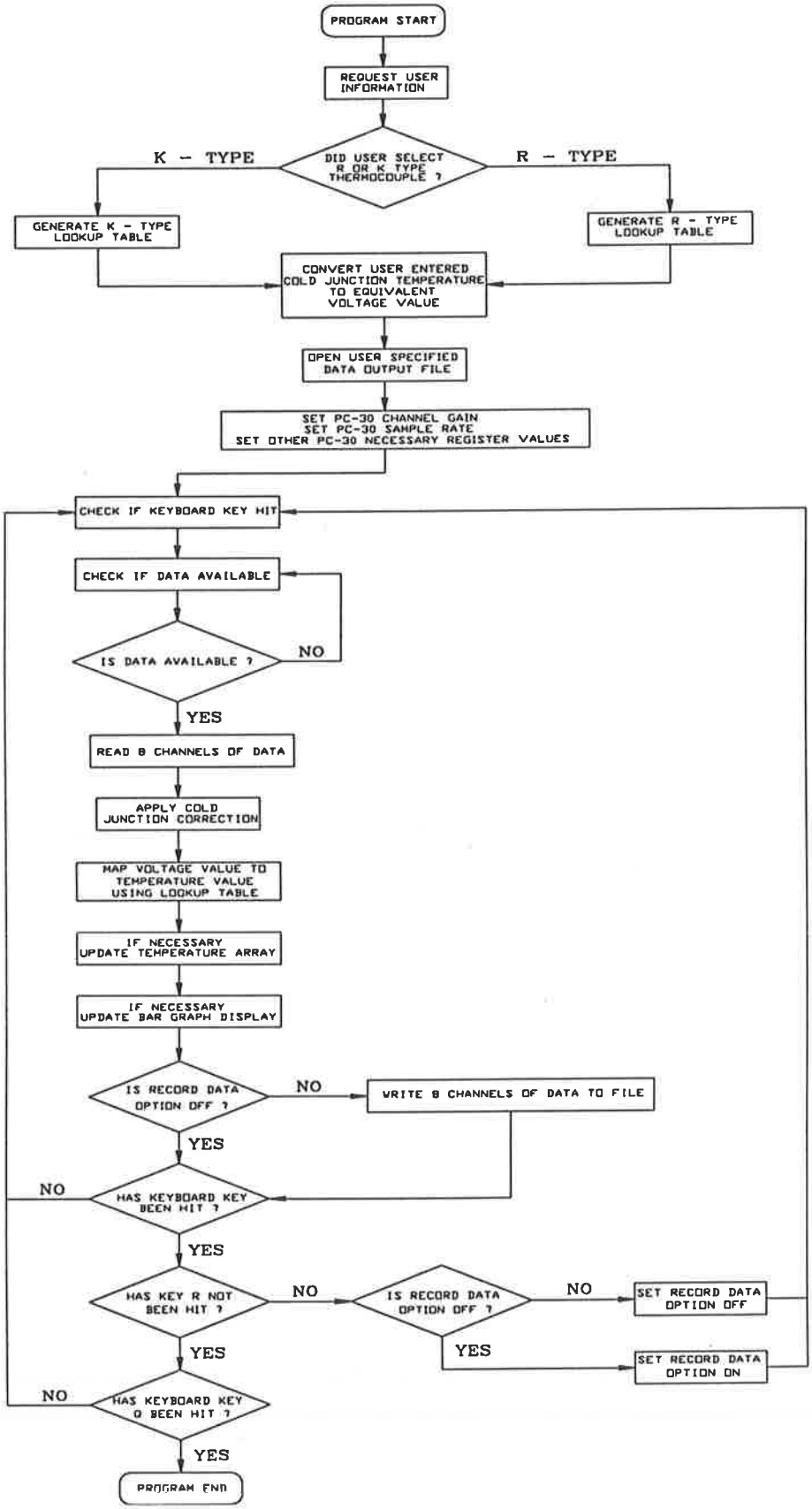

Figure 4-8 Software Function Flow Chart

4.5.5. Thermal Data Analysis and Results

An example of the header of a data file and the first few lines of data from the thermocouple collection software can be found in appendix B. A sample rate of 50 Hz was used which allowed relatively detailed thermal profiles while not generating excessively large data files.

Relevant cooling rates and peak temperatures were obtained using graphs of this data processed with Microsoft Excel. Graphs were then generated using Gnuplot. Simple software programs were also written to manipulate the data files to simplify data processing due to the large data files obtained.

HEAT INPUT (kJ/mm)	*THEORETICAL COOLING RATE (°C per second at 700°C)*	*EXPERIMENTAL COOLING RATE (°C per second at 700°C)*
1.12	89.0	117
1.19	83.5	113
1.21	80.8	nd
1.66	58.5	81
1.74	55.1	nd
1.94	49.4	nd
1.97	48.4	nd

Table 4-2 Weld Deposit Cooling Rates

As can be seen in table 4-2, the results obtained from the thermocouples were far from satisfying due to the effects of power supply faults, unexpected software crashes and thermocouples failing in the hostile environment of the arc. This is unfortunate considering the time invested in developing the instrumentation. Results shown in table 4-2 are the mean averages of data recorded (ie if three thermocouples recorded valid data then the value shown is the average value of these three).

The statistical variation of the results (not shown here) prevents their use for anything other than confirming that the theoretically calculated results are of the correct order of magnitude. It should be noted that the theoretical estimates, are for bead on plate welds with the assumption of a 70% arc efficiency. This arc efficiency was taken from French [139]. The V-groove welds here will have a greater cooling rate than the theoretical estimates made in table 4-2. Theoretical bead on plate weld welds will cool slightly slower than a V-preparation. In practice this has proven to be the case as can be clearly seen in figure 4-9. It was hoped that information such as a thermal arrest of the molten steel solidifying might be recorded verifying thermocouple accuracy, however, no thermal arrest could be identified.

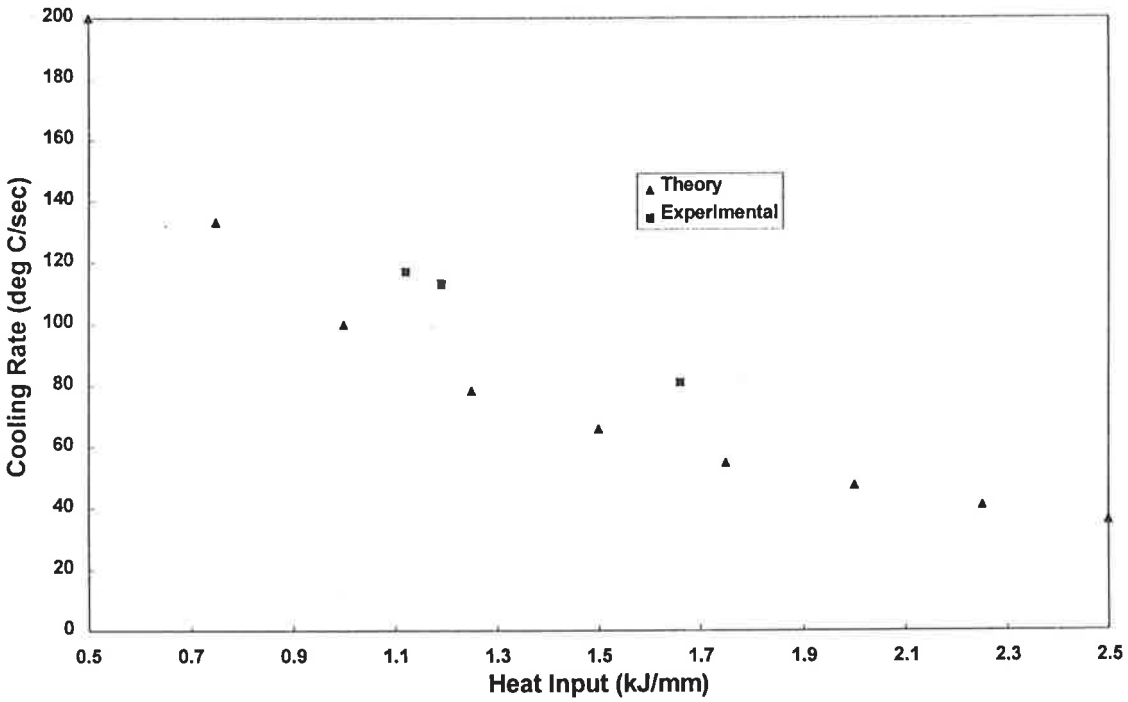

Figure 4-9 Cooling Rate Comparisons at 700 °C

4.6. WELDING PROCEDURE AND RESULTS

4.6.1. Test Welds

Before the final welds to be used for metallurgical examination and mechanical testing could be made, a number of test welds were prepared. As the welding process was inconsistent and buttered test plates, which take considerable resources to prepare could not be wasted, these trials were essential. In addition to this, the thermocouples to be implanted were of significant value and these could not be needlessly wasted either. Finally, much of the equipment required was in use by other research projects and was only available for limited periods of time. During testing there were numerous problems encountered and in all over 60 welds were made, many of which were sectioned and examined as macro's before satisfactory welds could be assured.

4.6.2. Welding and Monitoring Procedure

The procedure for making the final welds was:

1. Set welding speed on BUG-9600 (based on equation 4-2).
2. Adjust weld parameters of voltage and current once the weld had started.
3. Insert a thermocouple.
4. Record a sample of the voltage and current waveforms on the NICOLET.
5. Insert a second thermocouple.
6. Insert the last thermocouple.
7. Wait for temperature to decrease to 200°C then stop recording.

The above procedure required two people. A welder adjusted the alignment of the torch and maintained the correct arc length while another person (the author) inserted thermocouples and operated the instrumentation. The welding equipment and inserted thermocouples can be seen in figures 4-10 and 4-11.

After use, the thermocouple assemblies were cut off close to the weld and the end 5mm of twin bore alumina broken off to expose clean thermocouple wires. These wires were then melted together to form a new hot junction. The thermocouple probe was then ready for re-use.

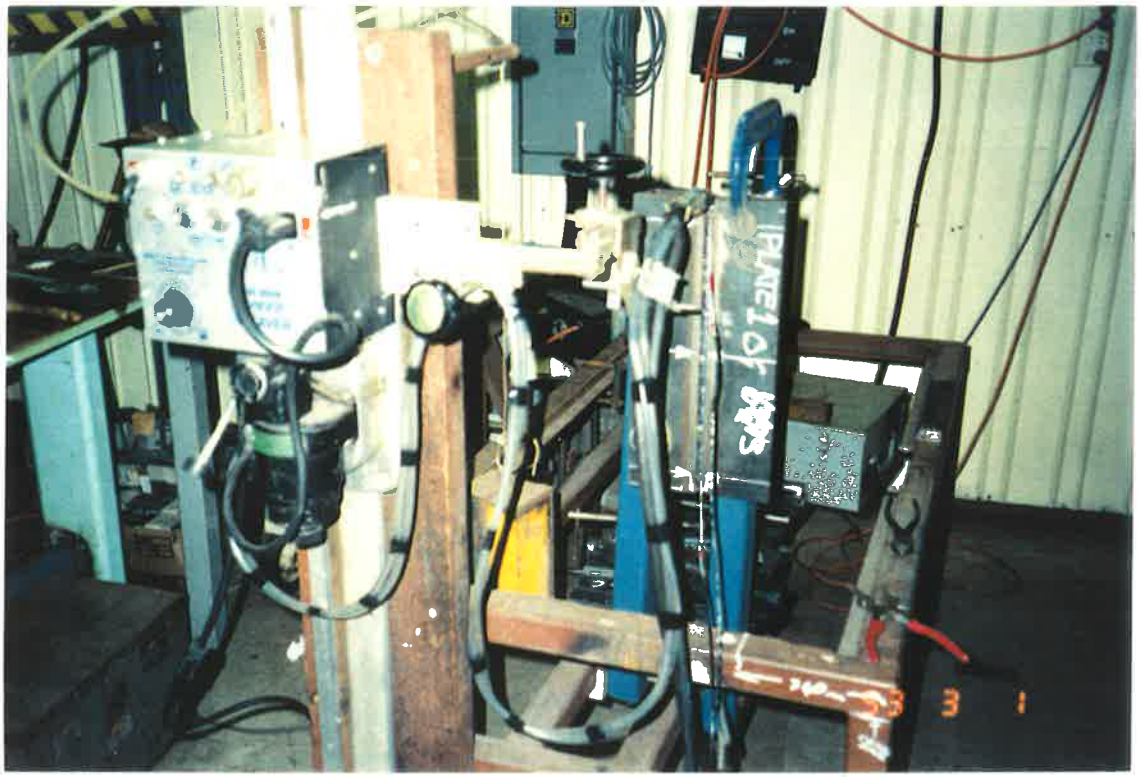

Figure 4-10 Photograph of Welding Equipment

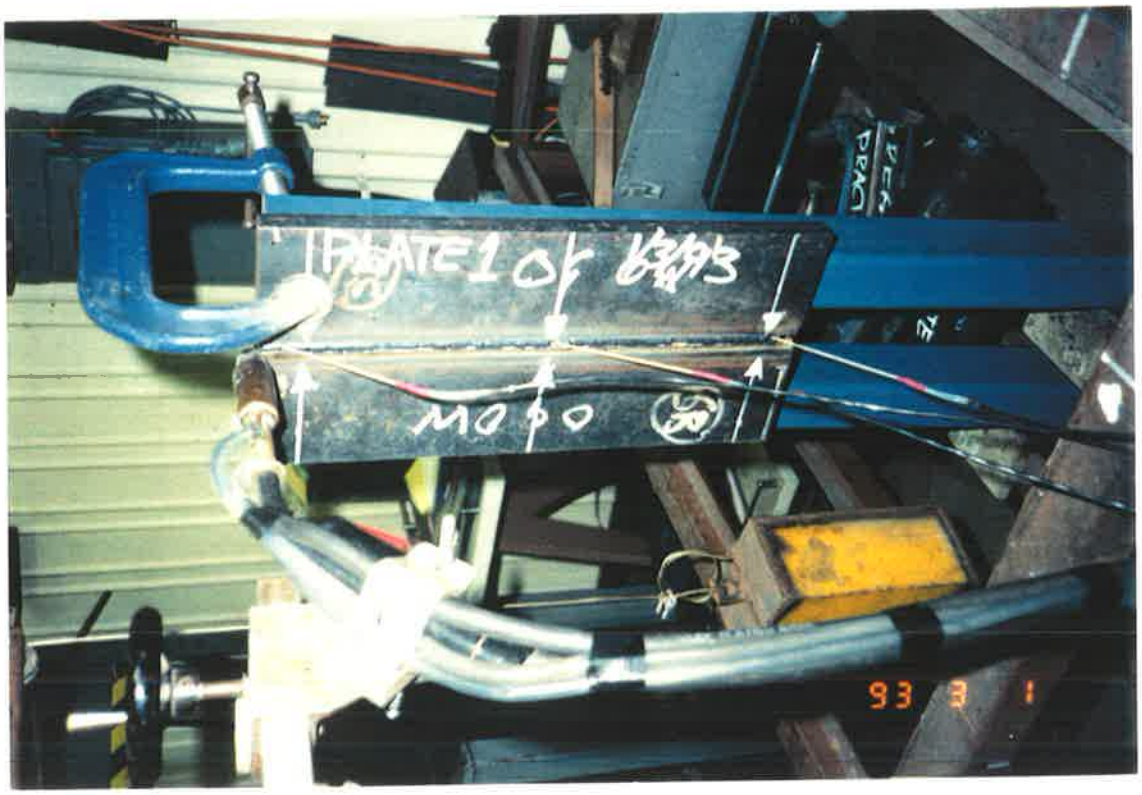

Figure 4-11 Photograph of Inserted Thermocouples

4.6.3. Welding Results

In all, six of the seven heat inputs were successfully welded but, as was seen in table 4-1, the target values were difficult to achieve. The weld deposit which was unsuccessful was the heat input target of 1.25 kJ/mm. In addition to the failure to obtain a satisfactory weld with a heat input of 1.25 kJ/mm the other welds which formed satisfactory deposits had minor root defects.

4.6.4. Effect of Heat Input on Chemical Composition

Heat Input (kJ/mm)	Fe	C	Ni	Mo	Si	Mn
1.12	Bal	0.059	3.52	0.30	0.51	1.18
1.21	Bal	0.061	3.36	0.30	0.54	1.22
1.66	Bal	0.059	3.76	0.30	0.55	1.25
1.74	Bal	0.064	3.50	0.29	0.52	1.21
1.94	Bal	0.061	3.38	0.30	0.55	1.16
1.97	Bal	0.056	3.06	0.29	0.53	1.20
In all welds S < 0.02, P < 0.015, O < 0.04, N < 0.005						

Table 4-3 Weld Chemical Compositions (% weight)

It was not possible to analyse chemistries using an optical emission spectrometer as the area of available weld metal was not large enough to allow sparking exclusively on the as-deposited weld metal. Chemical analysis of C, O, S and N were determined using Leco induction furnace equipment and the remaining elemental compositions were subsequently determined by ICP analysis. Analysis results can be seen in table 4-3. Comparison of table 4-3 and table 3-1 shows that a slightly lower nickel content and a slightly higher carbon content was encountered than expected while all other elements were of the expected concentration levels.

CHAPTER 5. MECHANICAL PROPERTIES

5.1. INTRODUCTION

There are many mechanical tests for welds and metals commonly accepted by organisations such as Australian Standards, British Standards, Lloyd's and the American Society for Testing of Materials. Selection of which test (or tests) to employ is based upon a number of factors such as the welding application, availability of test material, allowable time and expense, required test accuracy and most importantly the properties of interest.

In this study the mechanical properties of strength, hardness and toughness of the weld deposit were considered to be the most important engineering properties. These properties were tested and the results are shown in the following sections.

Due to the difficulty of measuring the mechanical properties for such a small weld deposit, modifications of standard tests were necessary.

5.2. HARDNESS

Hardness data is particularly useful to complement trends in other data. The relative ease in which hardness data can be obtained also makes it an attractive mechanical property to measure. Vickers hardness with a 5 kg load was measured by taking a hardness traverse across the centre of the weld deposit as shown in figure 5-1.

The tests were conducted to AS~~1203~~ 2205 5.1 "Non-Destructive Testing of Weld Metal" [96] using the following procedure:

1. Specimens were prepared for metallographic examination by polishing with 1μm diamond then etching with 2% Nital solution.
2. The hardness testers calibration was checked using a 295 HV5 Vickers calibration block by making two measurements before and after each session of hardness testing and then comparing these to the expected value.
3. Tests were then done to "AS2205.6.1 Weld Joint Hardness Tests" [97] with the following exceptions:
    - Due to the small size of the welds, one hardness traverse only was made of each specimen through its approximate centre line as shown in figure 5-1. Additional hardness traverses were made on the 1.74 and 1.94 kJ/mm weld specimens to confirm that no significant differences occurred between hardness values obtained from different parts of the weld deposit. The 1.74 and 1.94 kJ/mm

weld deposits were chosen for the additional testing as they had deposits of sufficient size to allow the additional traverses.

- Due to sample size, and the buttering layer thickness, parent metal which was not heat-affected was not always available for testing in each hardness traverse. It was therefore not possible, in all cases, to extend the hardness traverses outwards from the weld to the point where at least two hardness indentations gave hardness values to within 5 HV5 of the unaffected parent metal.

Hardness data was entered into Microsoft Excel. From this data the averages of the most representative hardness values from the weld deposit region were selected. This was done with the assistance of the graphical results shown in appendix D.

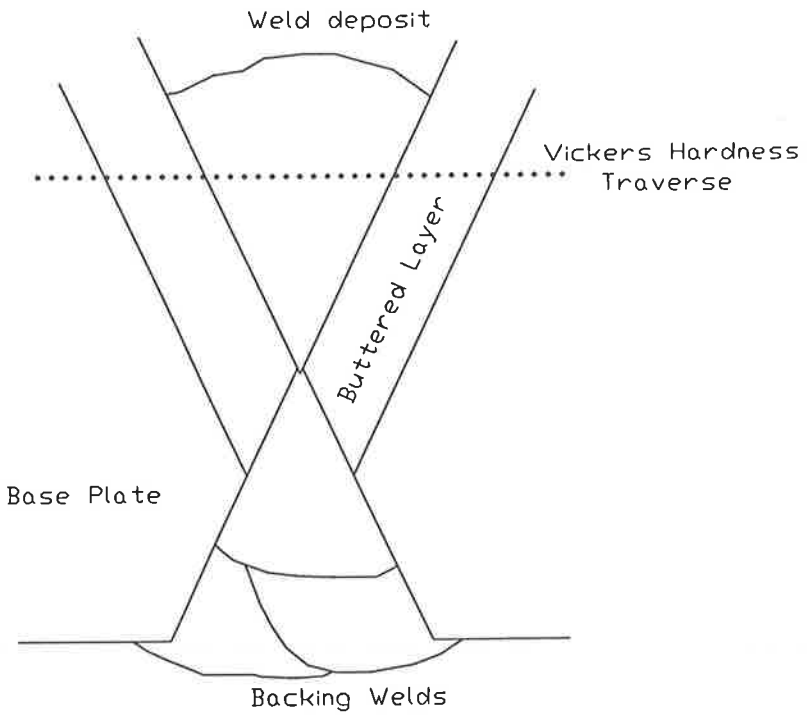

Figure 5-1 Hardness Traverse Location

As is apparent from figure 5-2, the use of the Vickers hardness test ensures the hardness of the bulk material is measured and not individual phases, particles or specific crystal orientations. In figure 5-2 a Vickers hardness indent is shown which has been heavily etched with a 2% Nital solution after indentation. This shows the sampled weld microstructure.

As previously mentioned, in addition to the hardness traverse shown in figure 5-1, hardness traverses were also taken just below the weld surface and near the weld root to determine if differences existed. No significant differences in hardness were found. This suggests the weld deposit has uniform hardness properties throughout.

Figure 5-3 is of interest as it clearly shows differences in hardness between as deposited and the re-heated buttering layer deposits. It is reasonable to conclude the lower value of hardness is not primarily due to the weld metal in the buttered layer being diluted by the base plate, as different hardness values would have been encountered as the layers of buttered weld metal were traversed. Figure 5-3 also makes a direct comparison of the weld metal hardness to that of the mild steel base plate material.

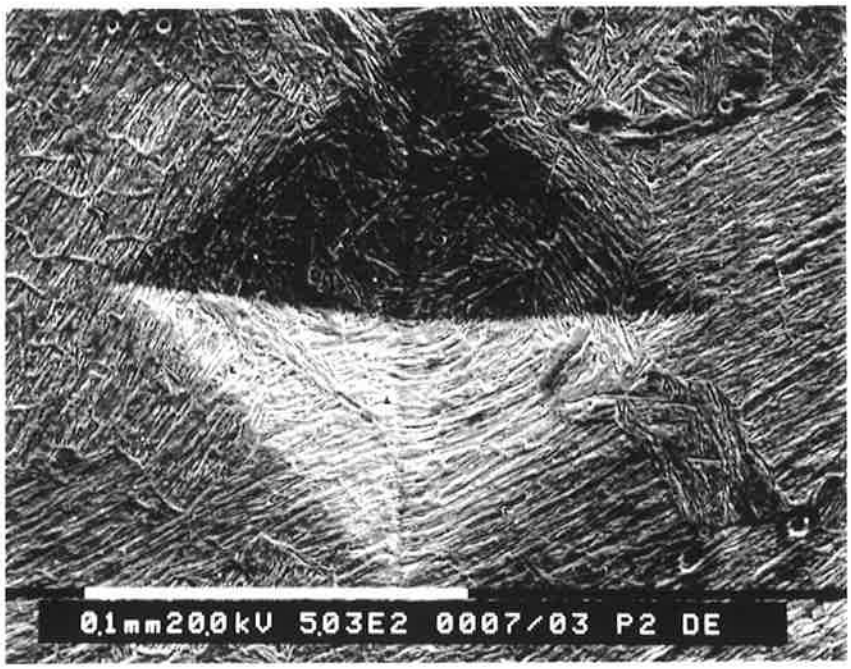

Figure 5-2 SEM Micrograph of Hardness Indent

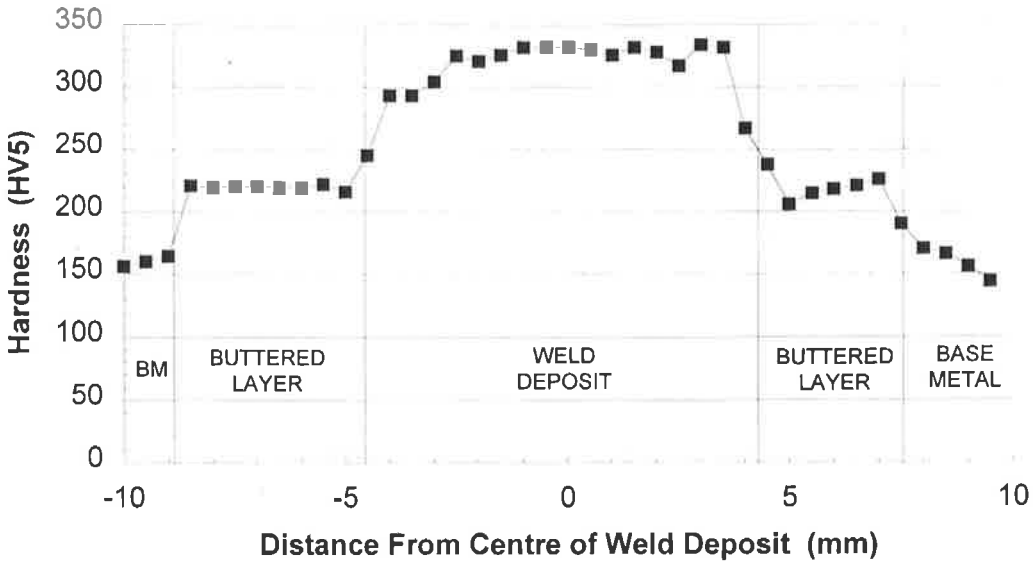

Figure 5-3 Hardness Values Across 1.21 kJ/mm Weld Deposit

The results of hardness tests are graphically illustrated in figure 5-4 and are also tabulated with statistical information in table 5-1. A general trend of decreasing hardness as the heat input is increased is apparent. The reason there are different numbers of indents recorded for different welds is based upon the size of the weld deposit and uncertainties in the accurate location of the fusion line.

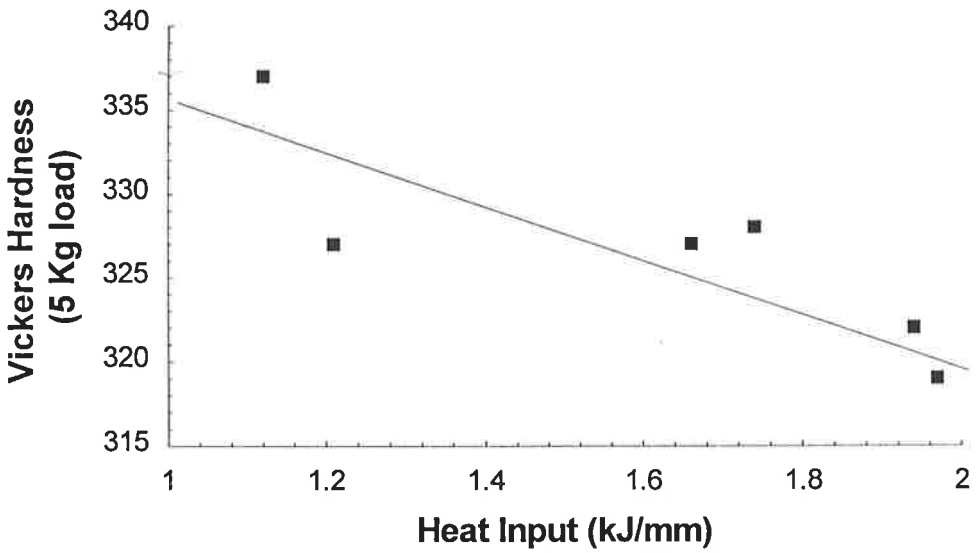

Figure 5-4 Variation of Vickers Hardness as a Function of Heat Input

Heat Input	1.12	1.21	1.66	1.74	1.94	1.97
Indents in Weld	13	11	12	10	10	9
Standard Deviation	12	5	8	7	3	5
Hardness (HV5)	337	327	327	328	322	319

Table 5-1 Variation of Vickers Hardness

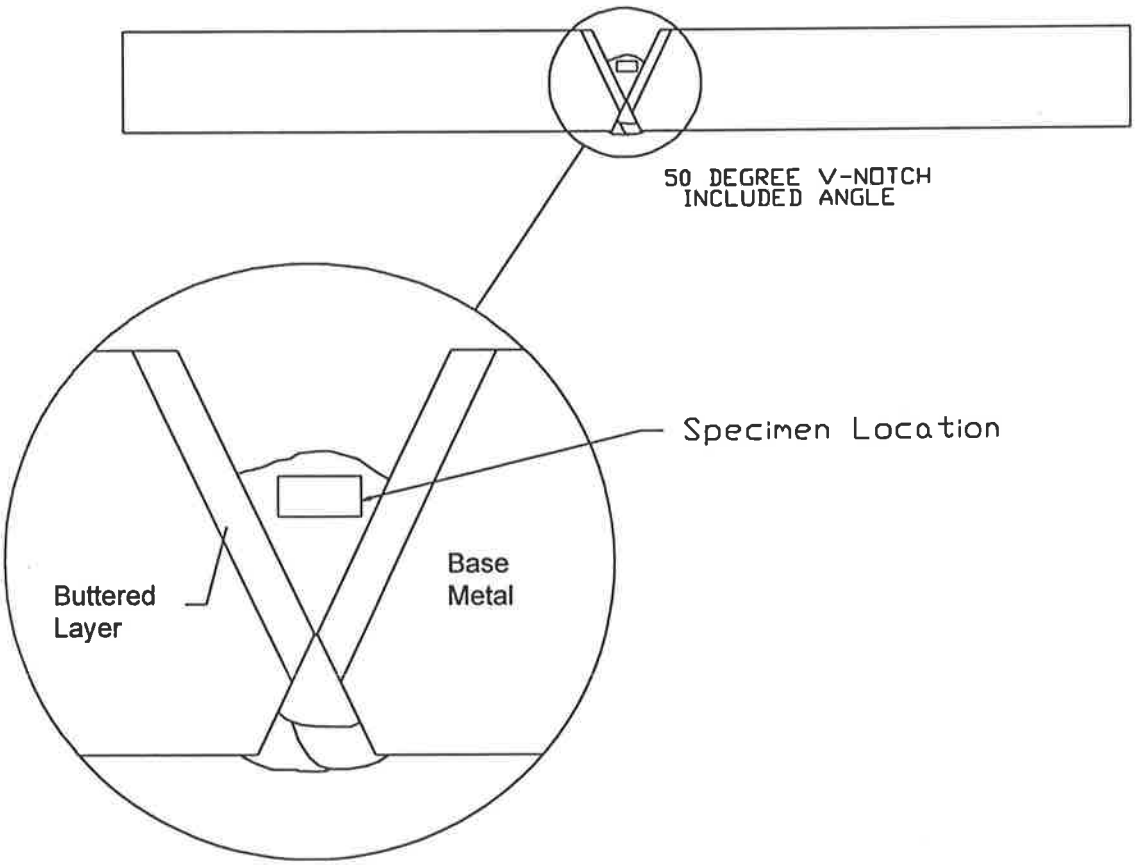

Figure 5-5 Origin of Tensile Specimens

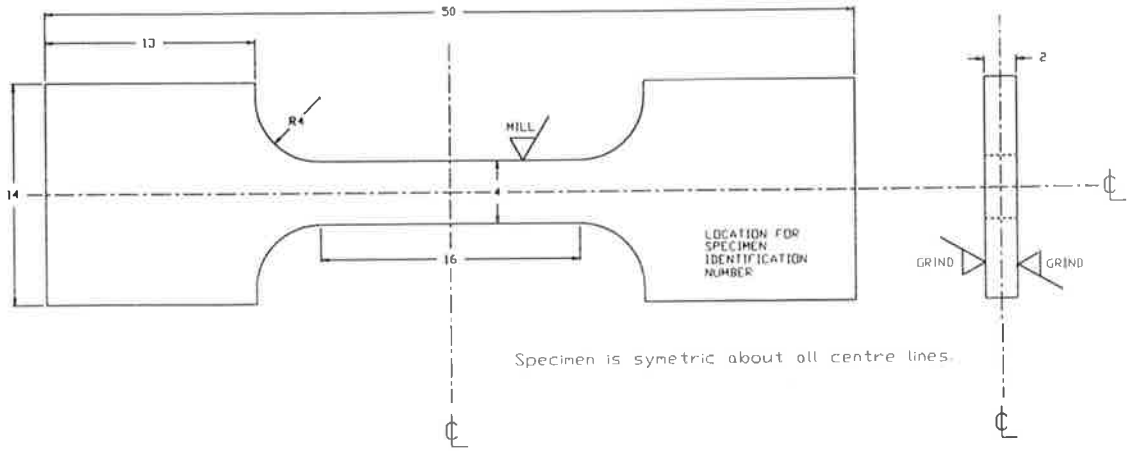

Figure 5-6 Dimensions of Tensile Specimen

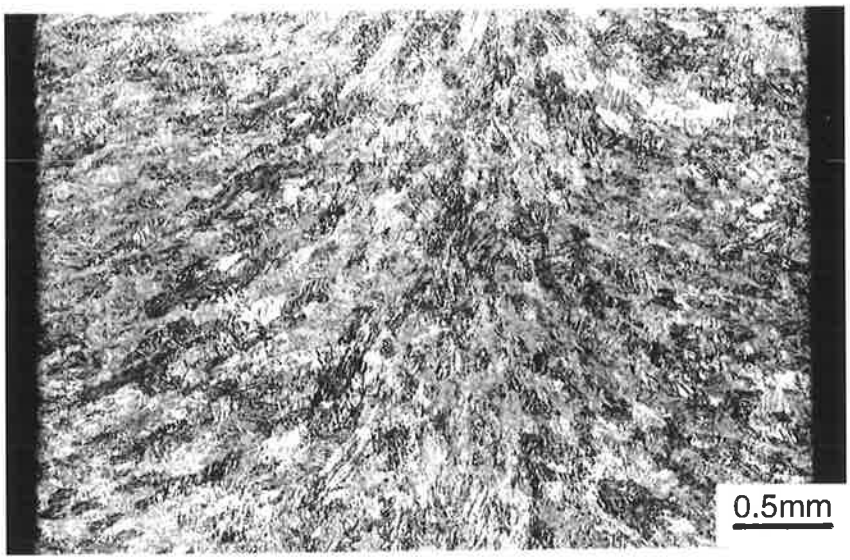

Figure 5-7 Micrograph of Tensile Specimen Cross Section

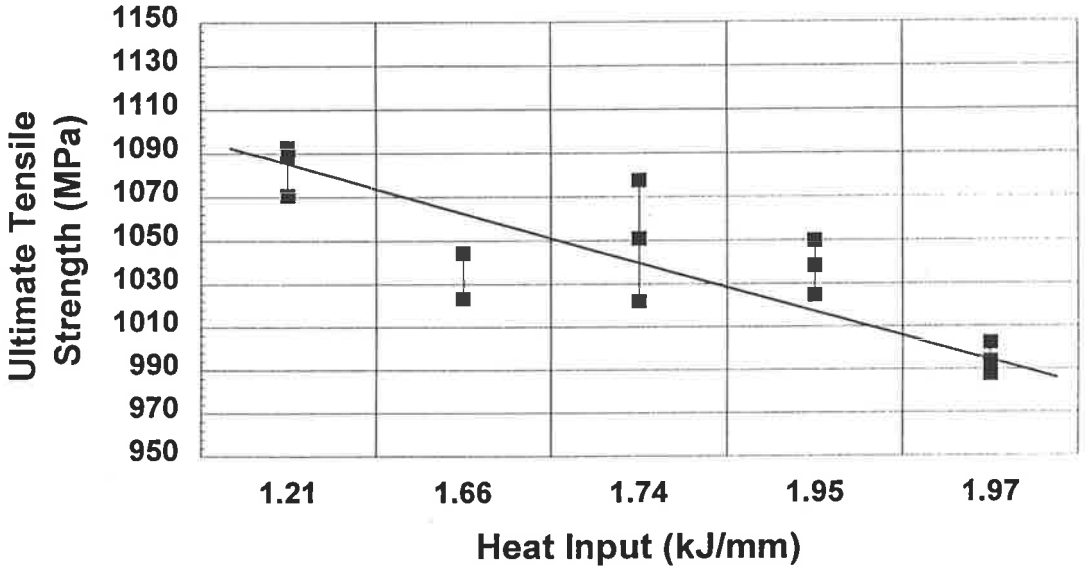

Figure 5-8 Weld Tensile Properties as a Function of Heat Input

Heat Input(kJ/mm)	1.12	1.21	1.66	1.74	1.95	1.97
UTS (MPa)	N/A	1084	1034	1050	1038	995

Table 5-2 Weld Tensile Data

As can be seen from the above results, as the heat input increased a general trend of decreasing tensile strength was observed. It was unfortunate that results could not be obtained for the lowest heat input of 1.12 kJ/mm. This was due to the presence of cracks along prior austenite grain boundaries as shown in figures 5-9 and 5-10.

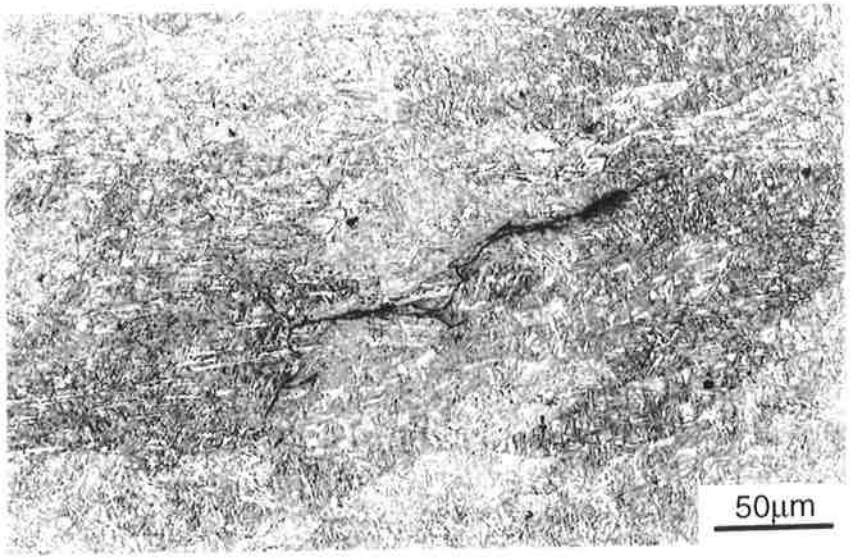

Figure 5-9 Grain Boundary Crack Transverse to Direction of Strain

(Etchant in figure 5-9 was 2% Nital)

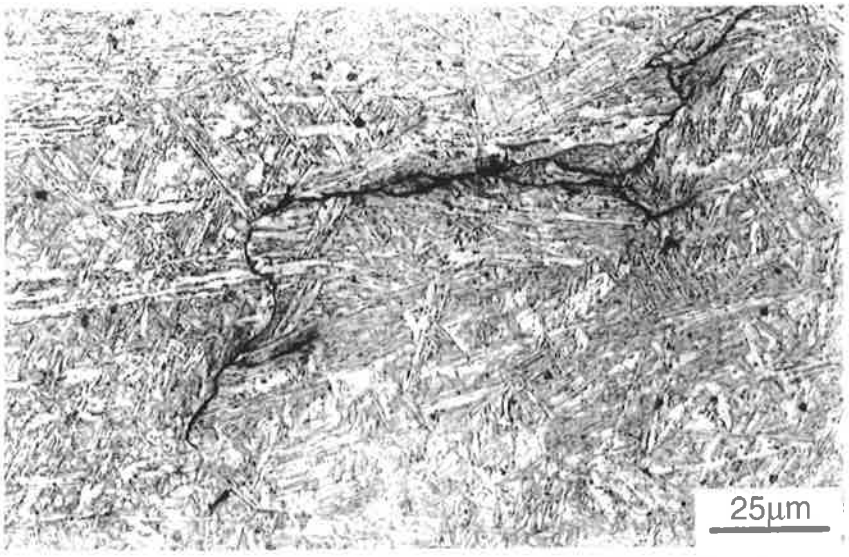

Figure 5-10 End of Crack Shown in Figure 5-9

(Etchant in figure 5-10 was 2% Nital)

5.4. FRACTURE TOUGHNESS

5.4.1. Introduction

CTOD tests were chosen due to the small amount of weld metal available for testing. Sub-size 5mm x 5mm Charpy specimens would have been an alternative, however it was felt that a unique sub-sized CTOD test would provide results with far less scatter. It was not possible to obtain standard K_{IC} values with samples of this size as the testing would have been in a plain strain condition rather than in a plain stress condition. A plain stress condition is required to obtain valid K_{IC} values.

5.4.2. Test Rig Construction

No mechanical testing rigs were available for testing of sub-size CTOD specimens of this size. A custom-made apparatus was subsequently designed which was then manufactured by the University of Adelaide engineering workshop. Detailed analysis was performed on the apparatus geometry to ensure maximum stresses and deflections would be within allowable limits. So as to ensure the CTOD test deviated as little as possible from recognised standards, the apparatus was also made to conform to ASTM E1290 and BS 5762 standards for CTOD testing. This also had the added advantage of increasing the range of equipment in the laboratory which could later be used for other projects. A schematic of the apparatus is shown in figure 5-11 and engineering drawings of individual components can be found in appendix D.

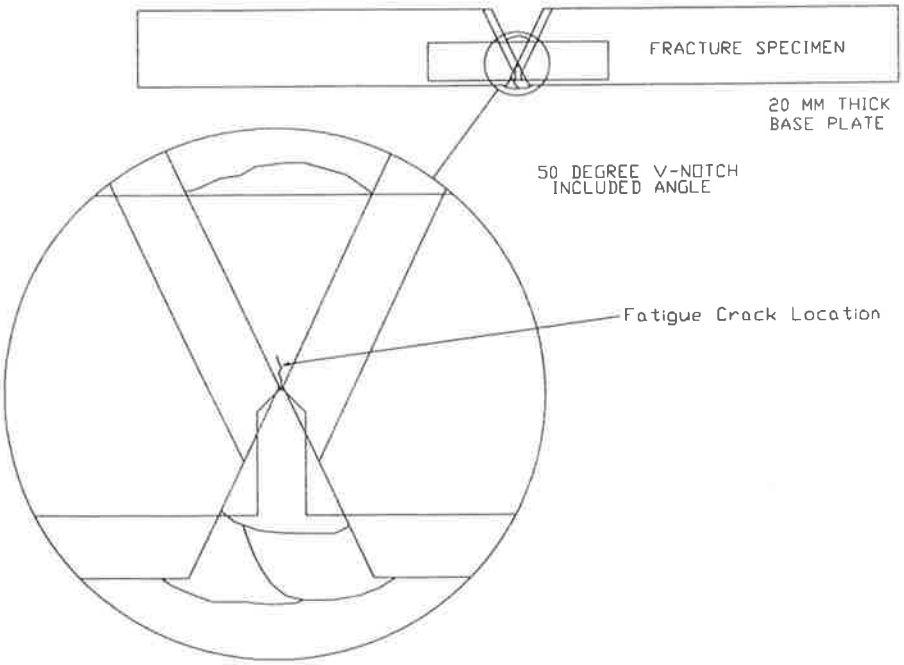

Figure 5-13 Location of Fracture Specimen In Weld Deposit

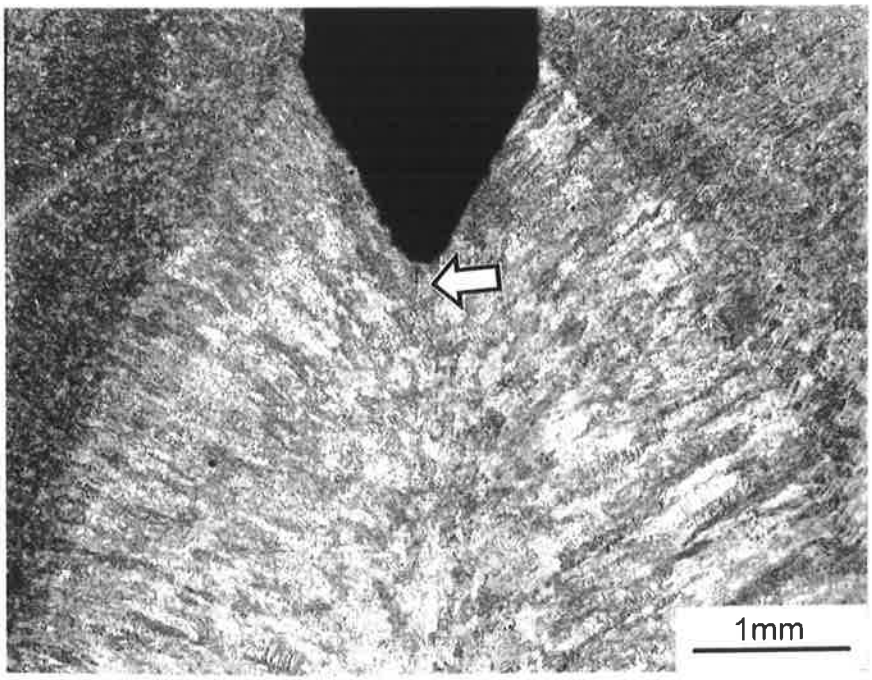

Figure 5-14 Location of Notch and Fatigue Crack (arrowed)

5.4.4. Testing, Analysis and Results

As previously stated in chapter 3, two test temperatures were used. For testing of cryogenic specimens a small insulated tank was constructed around the specimen in the MTS machine. This was filled with alcohol to which liquid nitrogen was added. Mixing was done by a small stirrer motor while the temperature was monitored with a NATA certified digital thermometer. This arrangement can be seen in figure 5-15. The ambient temperature tests were relatively easy to perform, although great care was still necessary to ensure the specimens were correctly aligned. The cryogenic specimens were much more difficult to test due to the time required for the specimen temperature to reach equilibrium and the difficulty of maintaining the correct temperature in the alcohol bath. All specimens were loaded at 90N per second.

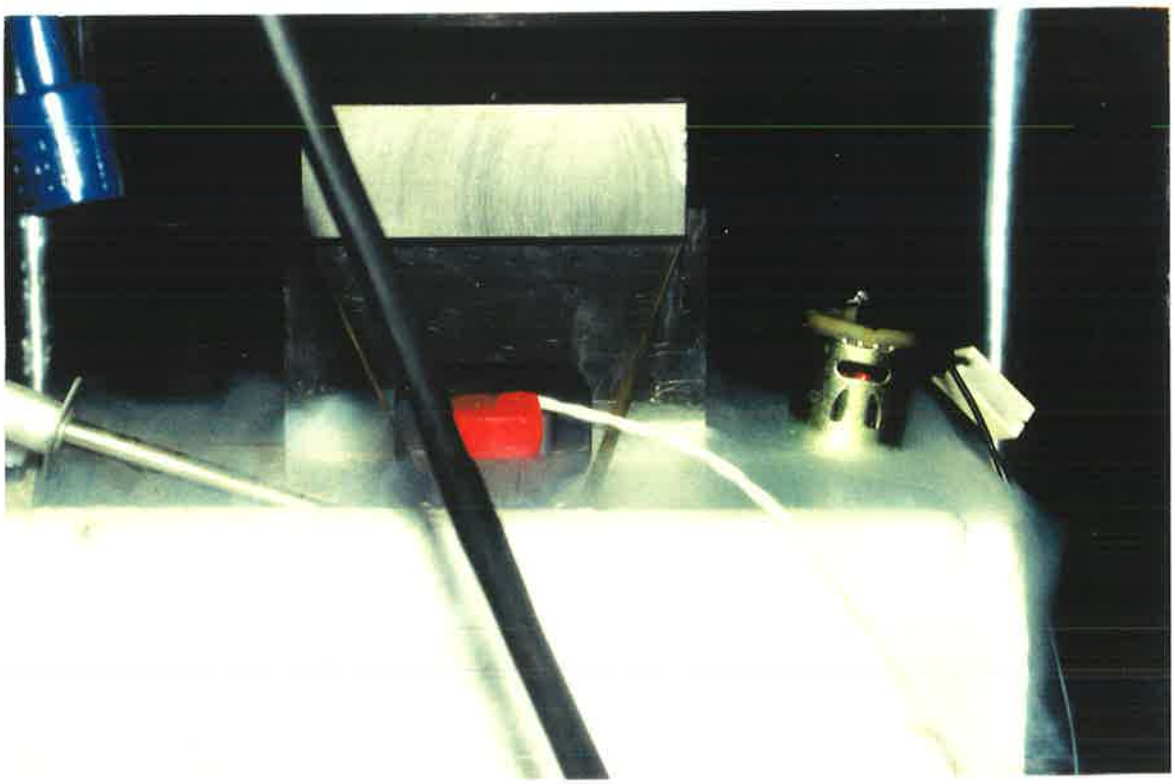

Figure 5-15 MTS Apparatus

Once the specimens had been tested the load versus displacement records were examined to determine the failure mode, the load corresponding to the failure or pop in and the clip gauge displacement. These values were then used with measurements of the fatigue notch length to determine the CTOD using equations 5-2, 5-3 and 5-4 in Microsoft Excel. The fatigue notch length was determined in accordance with BS 5762 and ASTM E1290 using a stereo light microscope with calibrated graticules and a Vernier stage.

$$\delta = \frac{K^2\left(1-\nu^2\right)}{2\sigma_y E} + \frac{0.4(W-a)V_p}{0.4W+0.6a+z}$$

Equation 5-2 Crack Tip Opening Displacement

$$K = \frac{YP}{BW^{1/2}}$$

Equation 5-3 Stress Intensity Factor

$$Y = \frac{6\left(\frac{a_0}{W}\right)^{1/2}\left(1.99 - \frac{a_0}{W\left(1-\frac{a_0}{W}\right)\left(2.15 - \frac{3.93a_0}{W} + 2.7\left(\frac{a_0}{W}\right)^2\right)}\right)}{\left(1+\frac{2a_0}{W}\right)\left(1-\frac{a0}{W}\right)^{3/2}}$$

Equation 5-4 Stress Intensity Coefficient

5.5. DISCUSSION

The mechanical tests done have obtained a measure of the basic mechanical properties of the weld metal. In the case of the tensile specimens, and especially the CTOD tests, the small number of samples has resulted in a large amount of statistical uncertainty in the results. Despite this uncertainty a number of trends were apparent.

Trends observed were a decrease in the hardness, and a corresponding decrease in tensile strength as the heat input increased. The welds also appeared to have higher resistance to fracture at the high heat inputs. These trends correlated well with each other and literature shows these trends are generally accepted as being the normal situation.

The small heat input range over which these trends occur is of interest. This combined with the fact that no other researchers have conducted mechanical tests of this nature on single pass welds of this type makes this approach unique. For this reason further work is required to verify the results. This is especially the case for the CTOD tests where the statistical uncertainty is large.

It should also be noted that the CTOD tests predominantly tested the toughness of the equiaxed grains in the centre of the weld deposit. Further mechanical tests should also be conducted in other areas of the weld deposit.

Work on larger mechanical test specimens prepared using a weld thermal simulator would also be of benefit in determining the validity of the sub size tests conducted in this study. This would provide data for comparison of these tests and tests done using specimens of normal size.

CHAPTER 6. MICROSTRUCTURE

6.1. INTRODUCTION

The microstructure of a weld has great influence on the mechanical properties. This is especially the case for fracture toughness. Examination of microstructural features such as lath sizes and orientations, grain boundaries and precipitates provide a wealth of information to help explain and predict mechanical properties. They also indicate how the microstructure developed and what roles features such as prior austenite grain boundaries and non-metallic particles played in the development of the final microstructure.

High strength ferrous weld microstructures commonly contain large amounts of martensite and bainite. Microstructures containing phases such as bainite and martensite are, however, difficult to identify using light microscopy. Positive identification of such phases requires the use of electron microscopy. This is especially the case for low carbon weld metals. This is because low levels of carbon result in the absence of carbide precipitates thus making the differentiation of acicular ferrite, bainite and martensite difficult.

The weld metal examined in this study was low in carbon, however, a number of phases were positively identified. Microstructural features were also found that may explain the variations in mechanical properties. The use of electron microscopy allowed the examination of the fracture surfaces of the tensile

absence of particle nucleation, this is despite the apparent abundance of available nucleation sites. This absence of nucleation on non-metallic particles does not however prove that the microstructure is martensitic. One possibility is that the microstructure could be mostly bainite and due to the attributes of the particles seen in this micrograph they were not conducive to nucleation of ferrite.

A further limitation of light microscopy is that it did not have the resolution to examine the laths in the microstructure to determine what would likely occur if a crack were to propagate through the weld. For this reason SEM was then used.

Figure 6-1 1.12 kJ/mm Representative Microstructure

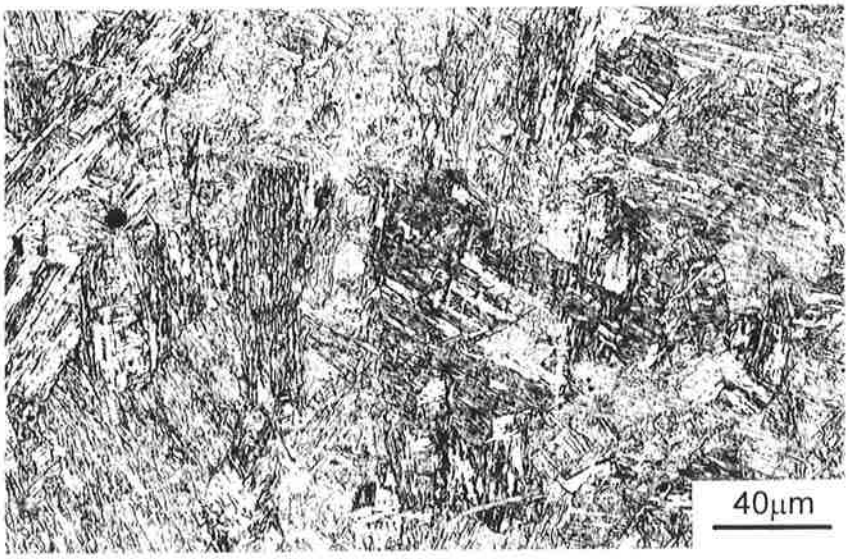

Figure 6-2 1.21 kJ/mm Representative Microstructure

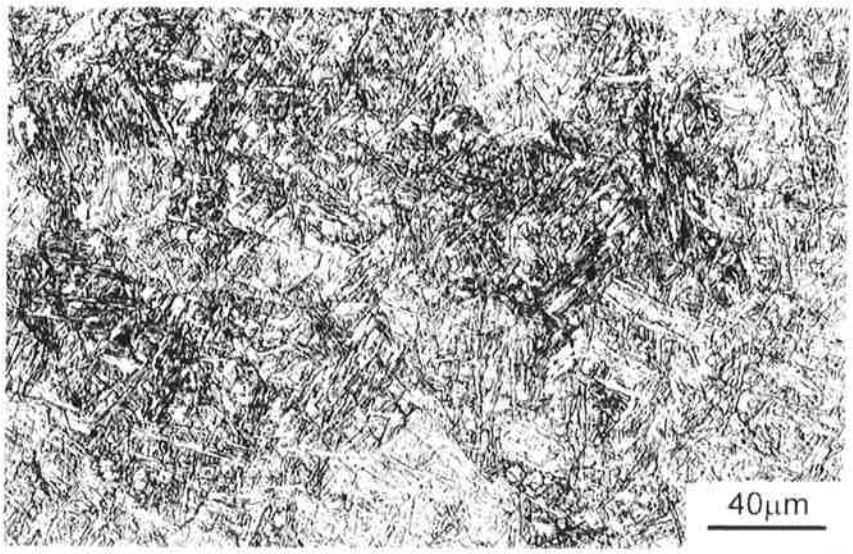

Figure 6-3 1.66 kJ/mm Representative Microstructure

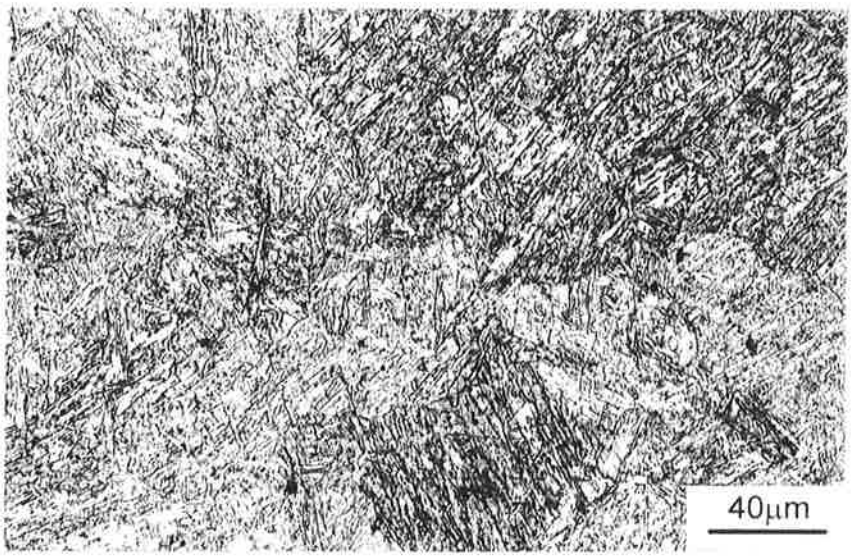

Figure 6-4 1.74 kJ/mm Representative Microstructure

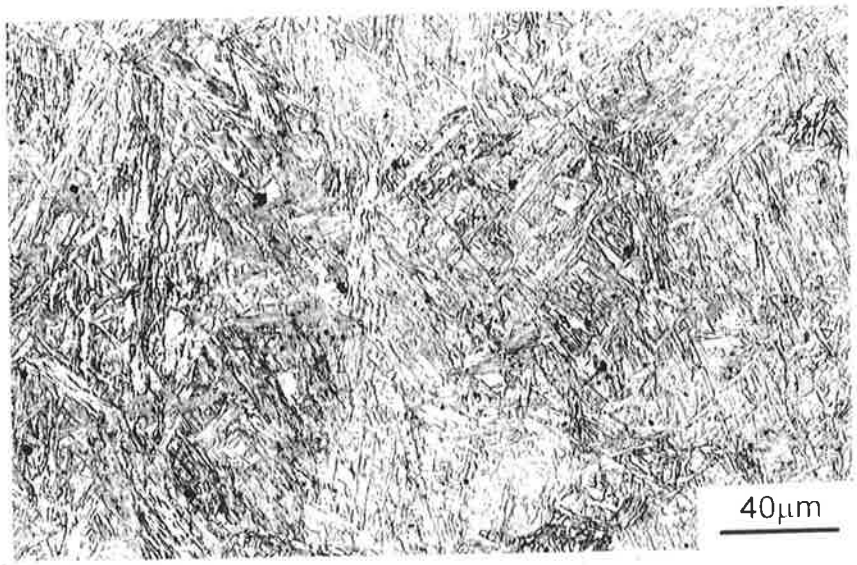

Figure 6-5 1.94 kJ/mm Representative Microstructure

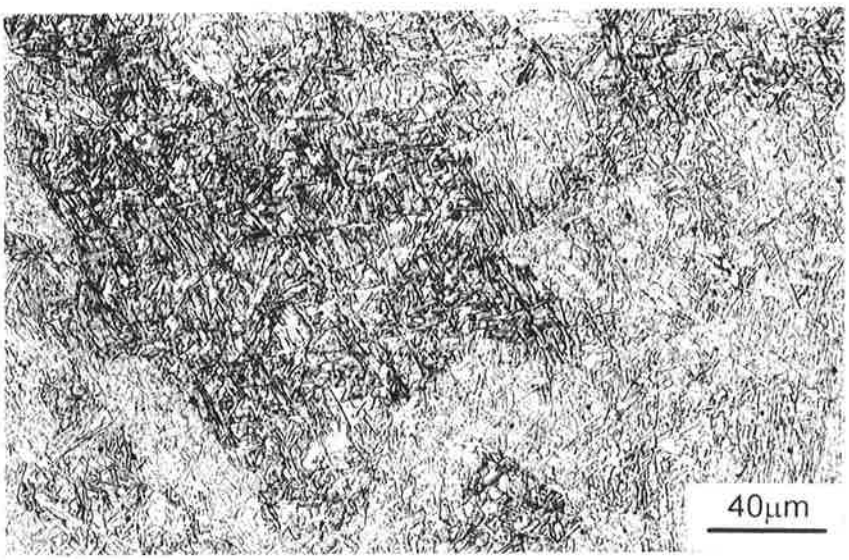

Figure 6-6 1.97 kJ/mm Representative Microstructure

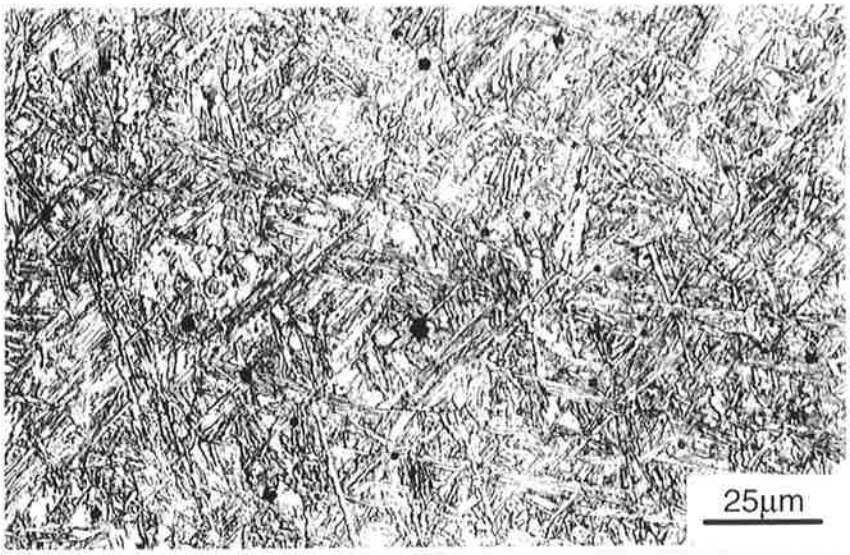

Figure 6-7 Representative High Heat Input Microstructure

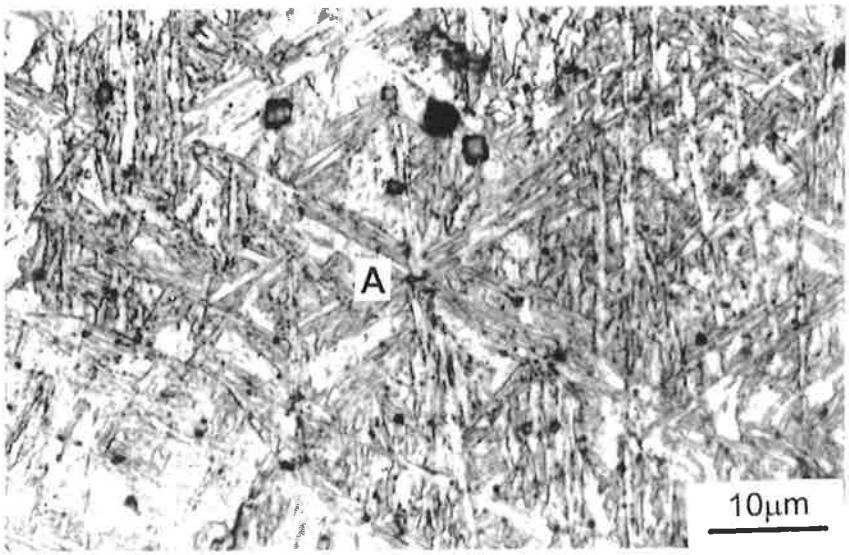

Figure 6-8 Nucleation of Ferrite on Particles at High Heat Input

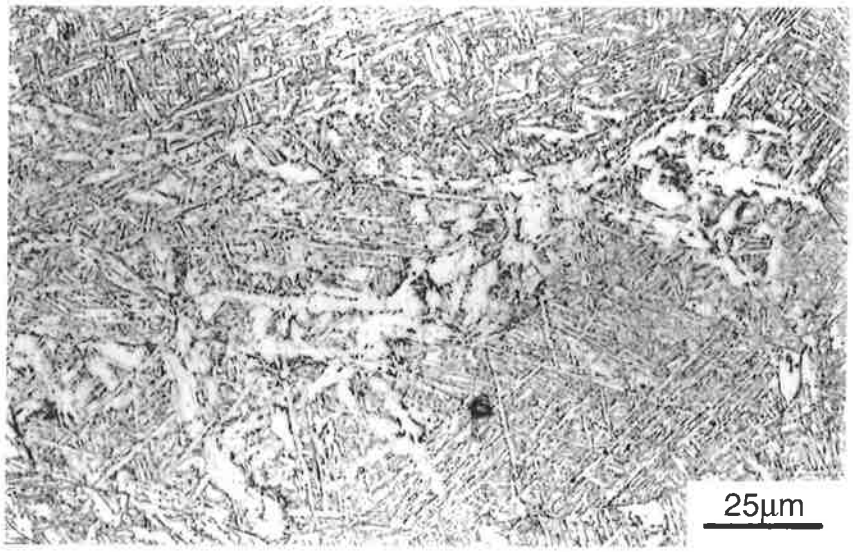

Figure 6-9 Grain Boundary Ferrite at High Heat Input

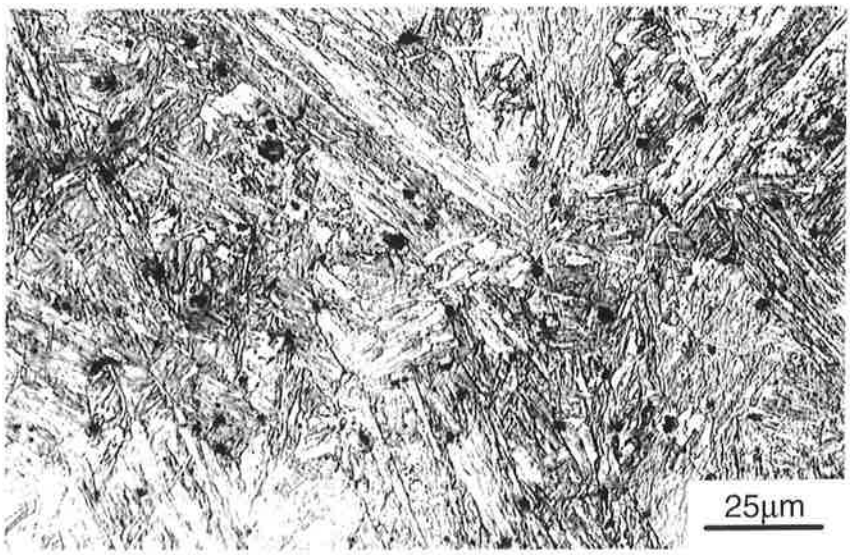

Figure 6-10 Particles Without Ferrite Nucleation

As light microscopy techniques were unable to positively identify the microstructure and could not fully explain the mechanical properties observed on a micro scale, SEM was used to provide better resolution at high magnification. Initial work was done on a Phillip's 505 SEM with a Tracor Northern EDS analysis unit. Later work was done on a Phillips XL20 with an EDAX EDS analysis unit.

Like figure 6-8, figure 6-11(a) shows ferrite nucleation on an intra-granular non-metallic particle (labelled B). Further examples of ferrite nucleation on non-metallic particles can be seen in figure 6-11(b) (labelled C). There also appear to be large areas of broad (1μm) plates rather than packets of fine lath martensite in this micrograph. This can be more clearly seen in figure 6-12(a) which shows prior austenite grain boundaries which have either nucleated ferrite or have acted as barriers to laths of martensite. Figure 6-12(b) shows a selected area of figure 6-12 (a) at higher magnification where this may be occurring.

Another mechanism which may be occurring is the refinement of the martensite packet size within the boundaries of the prior austenite grains. An area where this could be occurring is shown in figure 6-12(a) (vicinity of label D). The sequence of microstructure development would be that prior austenite grain boundary nucleated ferrite laths first grow into the austenite grains so that when the martensite forms the volume of available austenite is segmented resulting in smaller packets of martensite laths.

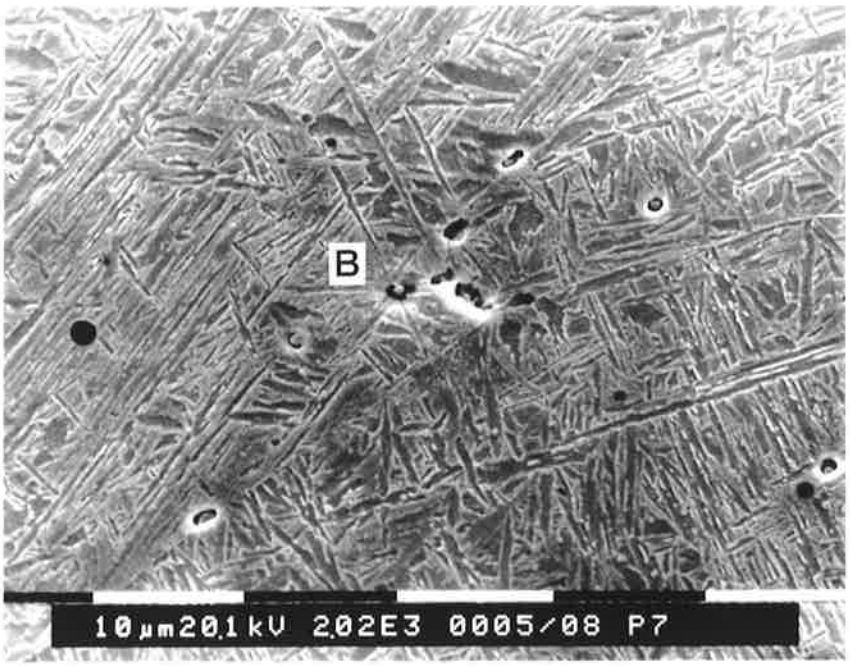

(a)

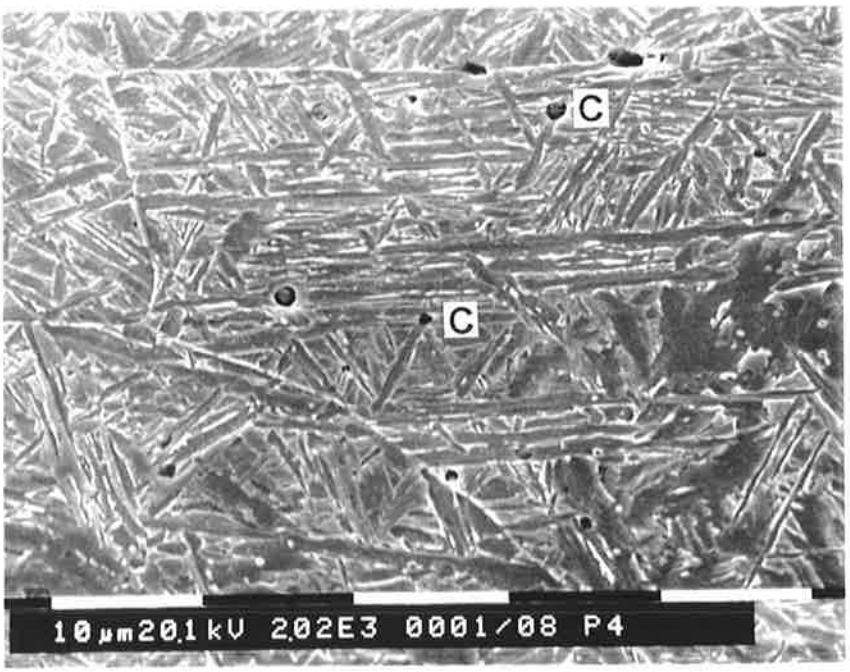

(b)

Figure 6-11 SEM Micrographs of Ferrite Nucleation

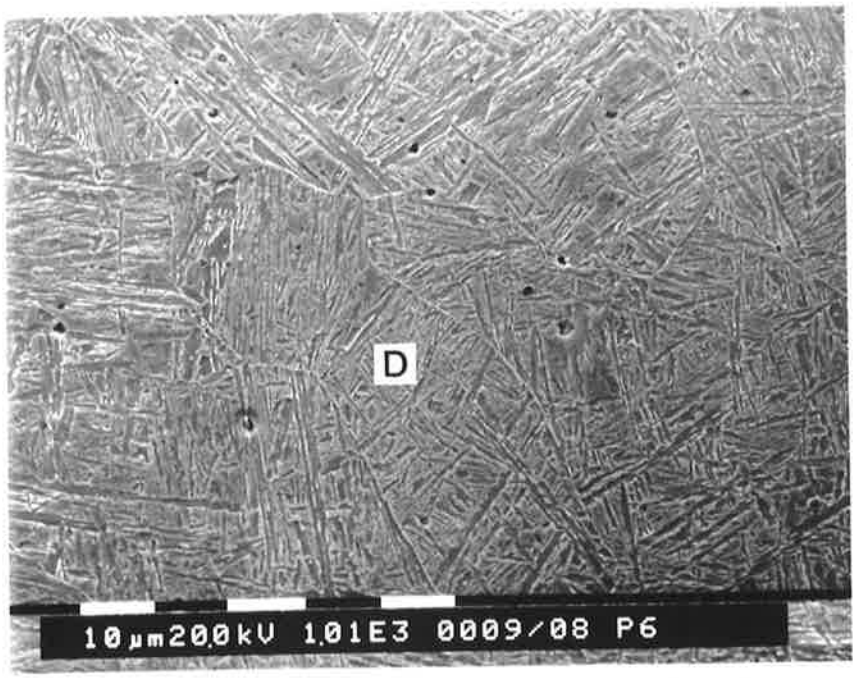

(a)

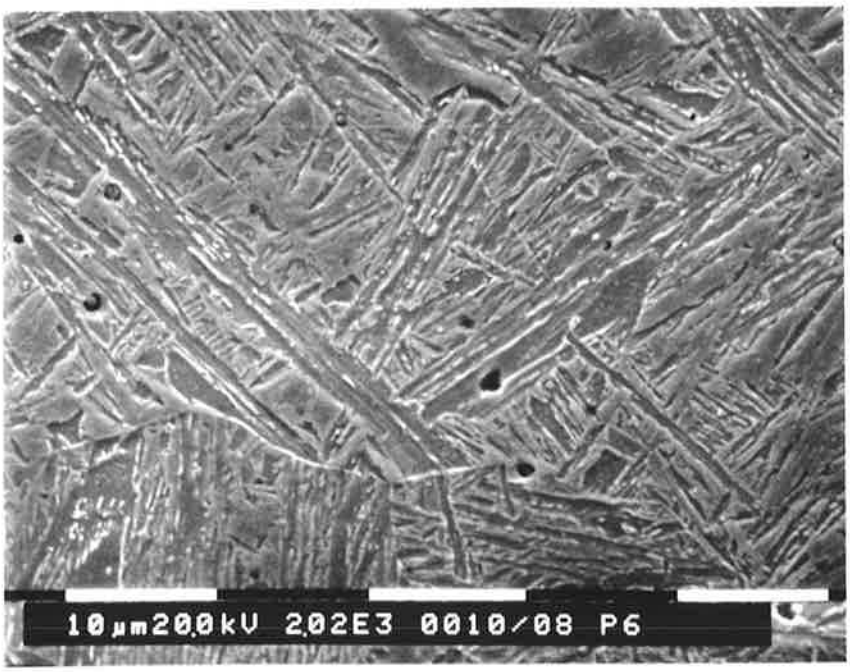

(b)

Figure 6-12 Prior Austenite Grain Boundaries

Apart from the presumption, based upon figures 6-1 to 6-6, that martensite is present in the lower heat input welds (and they therefore have a lower toughness) there is no evidence to prove that martensite is present, or for that matter, any other evidence to suggest why a lower fracture toughness would be expected.

However, the reduction in toughness may be explained by the micrographs in figures 6-13 and 6-14. This explanation is independent of whether the phase present is martensitic or ferritic but instead relies on the geometry and orientations of the laths. These SEM micrographs show that there are differences between the path which a crack would need to propagate along in the cases of both low and high heat input. In the microstructure of the high heat input case shown in the micrographs of figure 6-13 the microstructure consists of laths with a large included angle between them through which a crack would need to change its direction of propagation frequently on its path through the weld deposit. The micrographs in figure 6-14 however, show a microstructure consisting of mostly aligned laths through which a crack can propagate without frequently changing direction.

Unfortunately these micrographs do not positively identify the microstructure as containing martensite, even though the mechanical properties of hardness and tensile strength depend upon the presence of martensite to explain the higher values associated with the lower heat input welds. To identify martensite and other microconstituents present TEM was used.

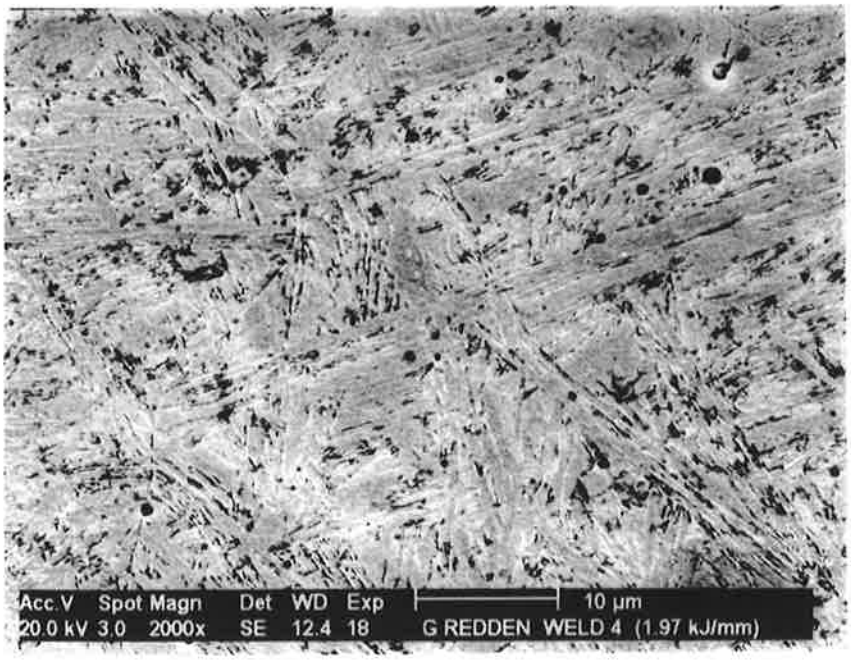

(a)

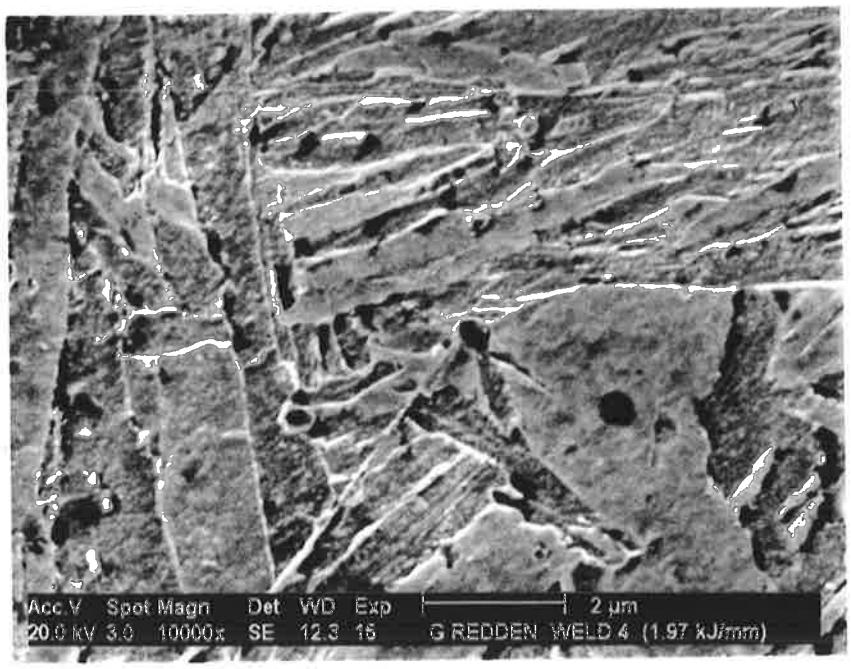

(b)

Figure 6-13 SEM Micrographs of Unaligned Microstructure (1.97 kJ/mm)

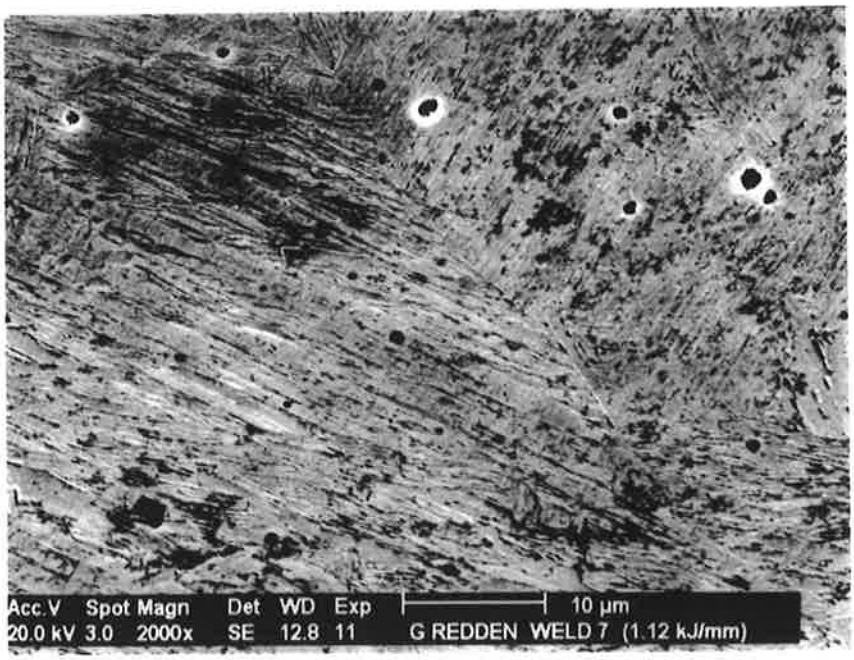

(a)

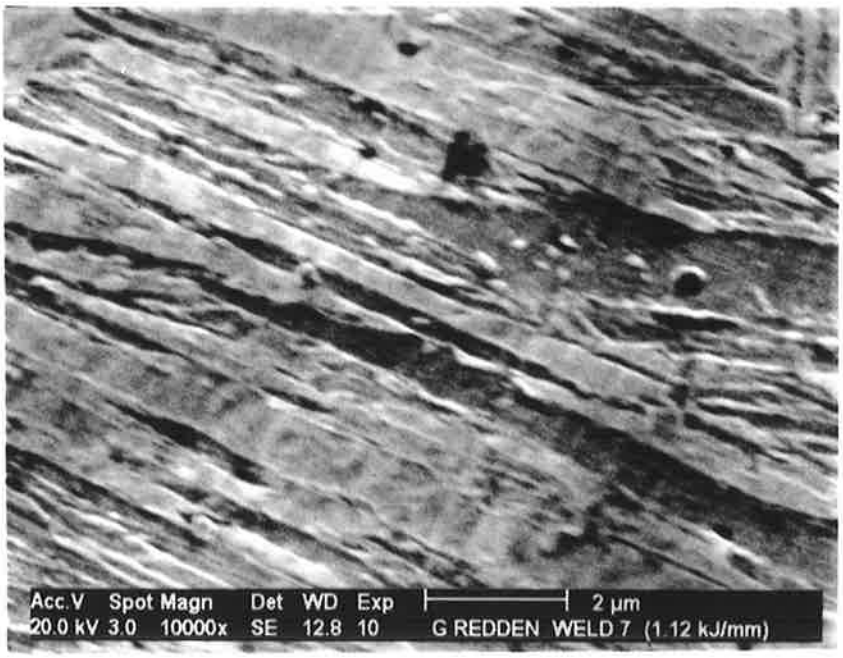

(b)

Figure 6-14 SEM Micrographs of Aligned Microstructure (1.12 kJ/mm)

Transmission electron microscopy provides a wealth of information about the microstructure. In general it was determined that the microstructure consists of a mix of martensite, carbide free bainite and retained austenite. TEM was able to identify these phases due to its ability to detect features characteristic of martensite and the ability to obtain selected area electron diffraction patterns.

In figure 6-15(a), a prior austenite grain boundary is arrowed and there is a broad martensite lath (labelled E) which can be identified due to the high dislocation density and evidence of fine twinning (labelled F). A lath martensite structure is clearly visible (labelled G) and there is no evidence of ferrite nucleation on non-metallic inclusions (eg. at H). The martensite twinning can be more clearly seen in figure 6-15(b) (arrowed).

Figure 6-16 is a selected area diffraction pattern from the lath martensite (labelled G) in figure 6-15. There is some spread in the spot positions which indicates that the martensite laths are separated by low angle boundaries.

Figure 6-17 shows a TEM image of a non-metallic inclusion which appears to have acted as a nucleus for ferrite lath growth as seen in previous light microscopy and SEM images.

Figure 6-18(a), shows ferrite or martensite laths with dark contrast features in the lath boundaries (eg at J). Figure 6-18(b) shows a selected area diffraction

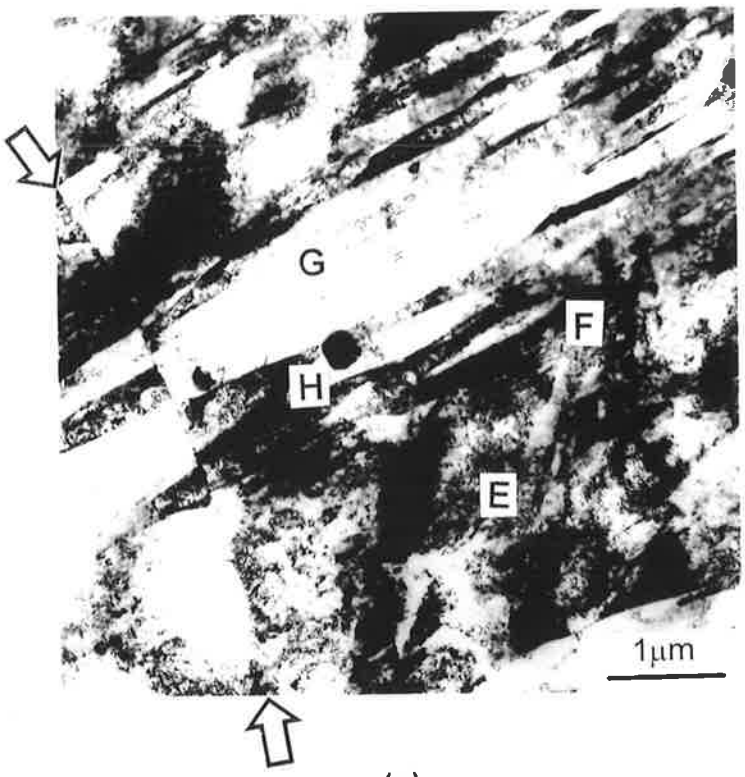

(a)

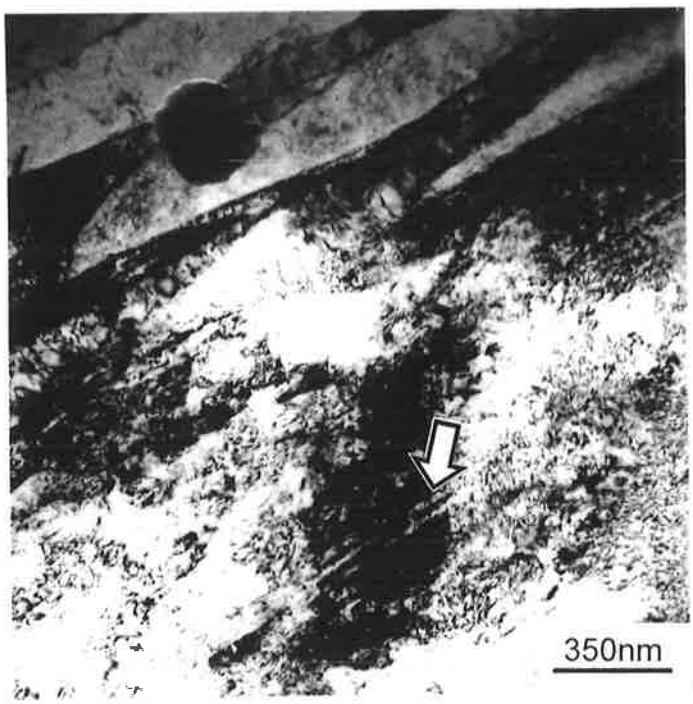

(b)

Figure 6-15 TEM Micrographs of Martensite Laths and Twinning

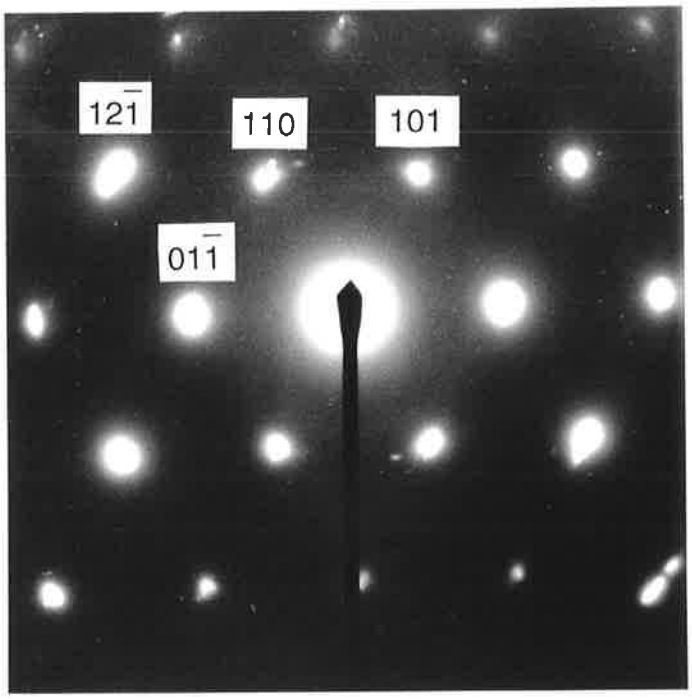

Figure 6-16 Electron Diffraction Pattern of Martensite

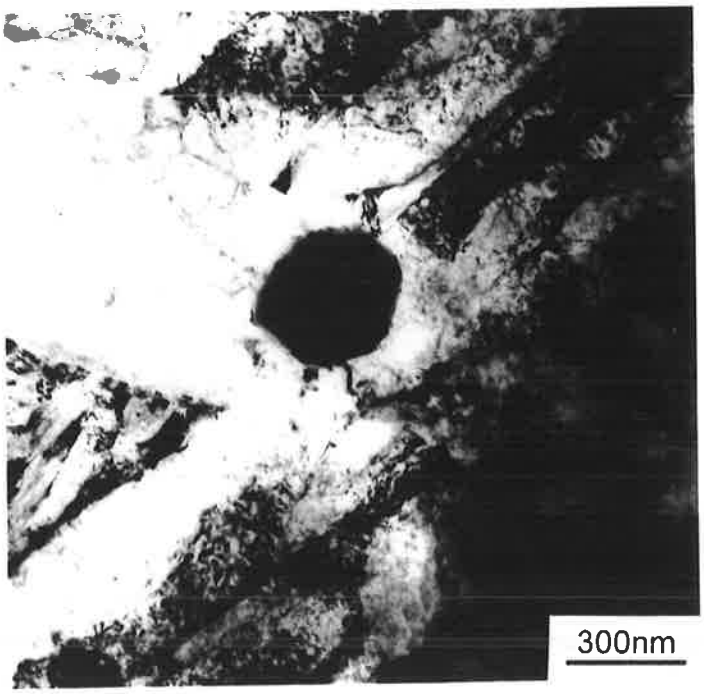

Figure 6-17 TEM Micrograph Showing Ferrite Nucleation

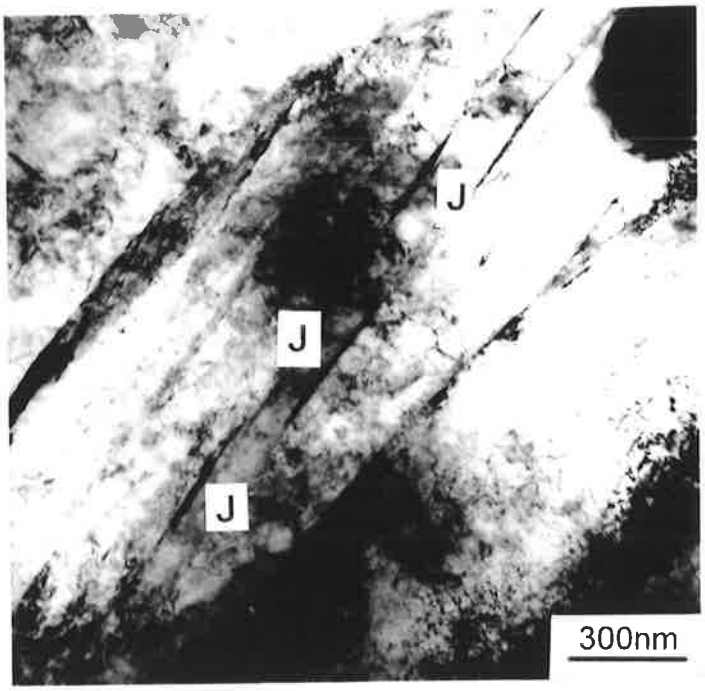

Figure 6-18 (a) TEM Bright Field of Laths

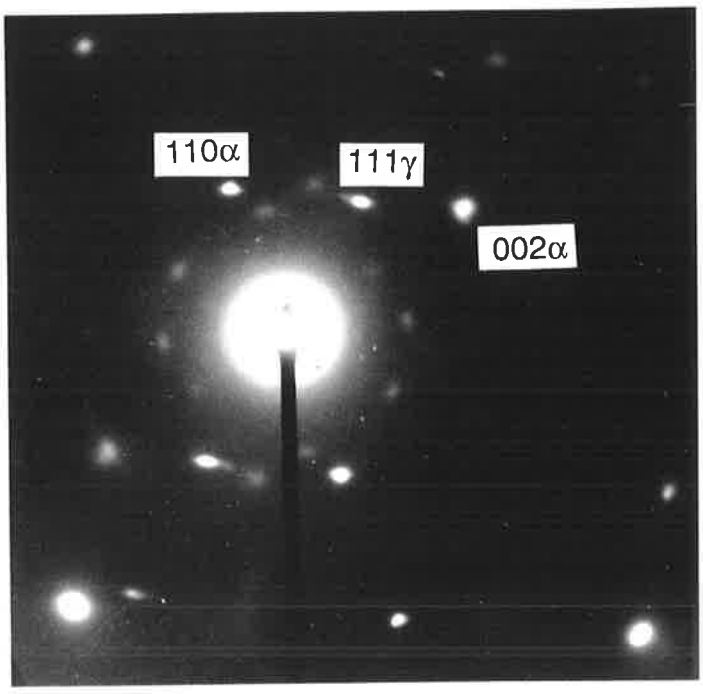

Figure 6-18 (b) Selected Area Diffraction Pattern

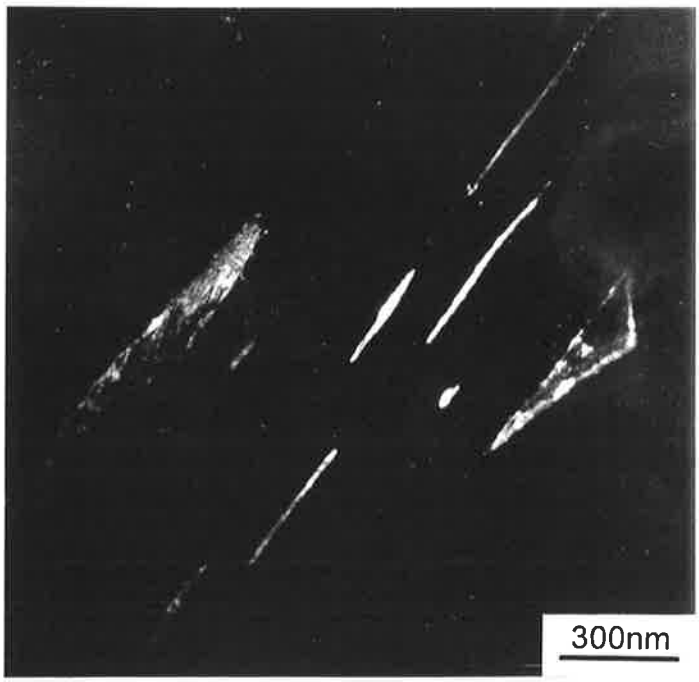

Figure 6-18 (c) Retained Austenite

6.3. NON-METALLIC PARTICLE ANALYSIS

6.3.1. Particle Analysis Techniques

Due to the importance of inclusions, discussed in chapter 2, they were closely examined using electron microscopy techniques. Figure 6-19 shows inclusions of interest in a mechanically polished specimen. The scratches on the surface are artefacts from polishing with 1 micron diamond.

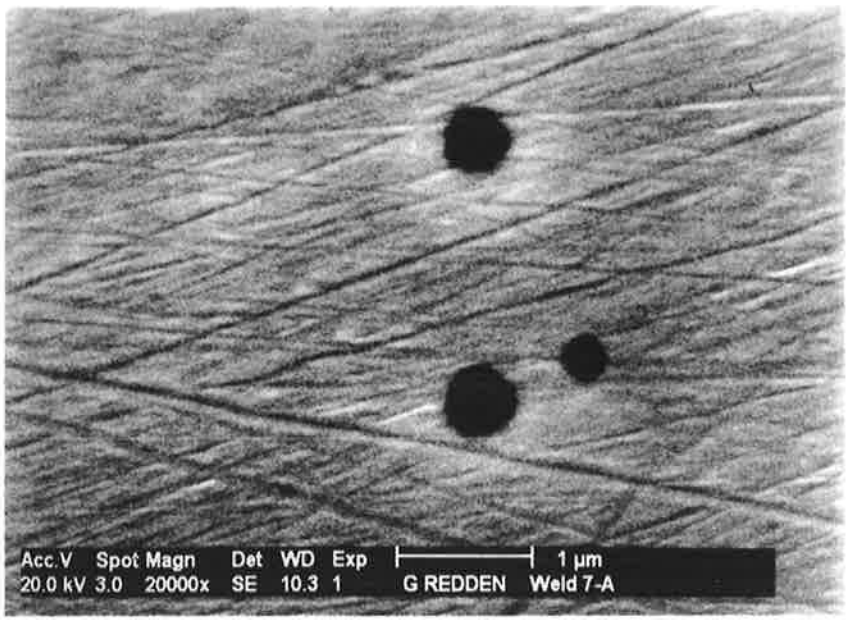

Figure 6-19 Weld Inclusions in 1µm Diamond Polished Surface

To avoid interference from the matrix either the use of carbon extraction replicas or the electrolytic dissolution of the surrounding iron matrix is generally used. Examples of carbon extraction micrographs can be seen in the work of Court [80]. The analysis of particle volume fraction of the weld is the only measurement where a planer polished specimen is necessary.

In the present study no time or resources were available for preparation of specimens to use with these techniques. Subsequently, all analysis was done using mechanically polished specimens.

Early particle analysis work used a Phillips 505 SEM with Tracor Northern particle recognition and EDS analysis software. Only low heat input welds were examined with this system. To eliminate any uncertainties in the spatial comparison data, this data was not used. All spatial comparisons were made from data collected with the newer XL20 SEM.

6.3.2. Size Distributions and Volume Fractions

Images for determining inclusion spatial data were collected using the Phillips XL20 SEM. These images were then processed using the software package AnalySIS 2.0. To obtain images suitable for analysis the SEM was operated with a spot size of 3.0, accelerating voltage of 10 kV and a backscattered detector at a working distance of 10.3 mm. A greater working distanced would have been preferred to allow the use of larger samples thus minimising sample preparation, however, larger working distances could not provide suitable particle definition. At large working distances (eg 30 mm) the particles had poor contrast with the matrix thus resulting in inaccurate measurements.

An image with high contrast was required as the AnalySIS software, like most image analysis software packages, uses a thresholding technique to

corresponds to a backscatter emission depth of about 0.035 microns which results in negligible errors.

A further, but unavoidable error, is because a plane cut through a three dimensional system of polydispersed spheres, will indicate a larger number of small inclusions and less large inclusions than reality. The distribution in figure 6-20 is therefore biased. For purposes of comparison this is not important as this bias is applied to all particles from both high and low heat input welds. No corrections have been made for this reason. If these results must be adjusted to remove the bias then methods such as those detailed in Underwood [141] must be applied.

The results of particle size distribution analysis, shown in figure 6-20, indicate little difference between the high and low heat input welds but compare well to distributions found in other studies [80,142-144]. What differences do exist show that inclusions in high heat input welds may be slightly larger. This would be expected as the high heat input welds remain molten for longer allowing a greater time for inclusion growth as discussed by Kluken et al [143]. Like the inclusion size distributions there was also little difference in the volume fractions of inclusions in the welds produced with different heat inputs. Volume fraction statistics can be found in table 6-1 with a number of other spatial statistics.

Spatial Statistic	1.12 kJ/mm	1.97kJ/mm
Frames of area 1720 μm^2 analysed	32	37
Total area analysed	55066 μm^2	63671 μm^2
No. of inclusions in analysis area	511	522
Volume fraction	0.19 %	0.24%
Inclusion density	$2.02x10^7$ per mm^3	$1.70x10^7$ per mm^3
Mean inclusion diameter	0.49 μm	0.54 μm
Inclusion diameter std deviation	0.33 μm^2	0.37 μm^2

Table 6-1 Inclusion Spatial Analysis Statistics

6.3.3. Elemental Compositions

In addition to determining size distributions of weld inclusions typical inclusion elemental compositions were also characterised. This characterisation was done using X-ray Analysis in the SEM. A typical X-ray spectrum from an inclusion is shown in figure 6-21. Note the high iron peaks in this spectrum emanating from the iron matrix.

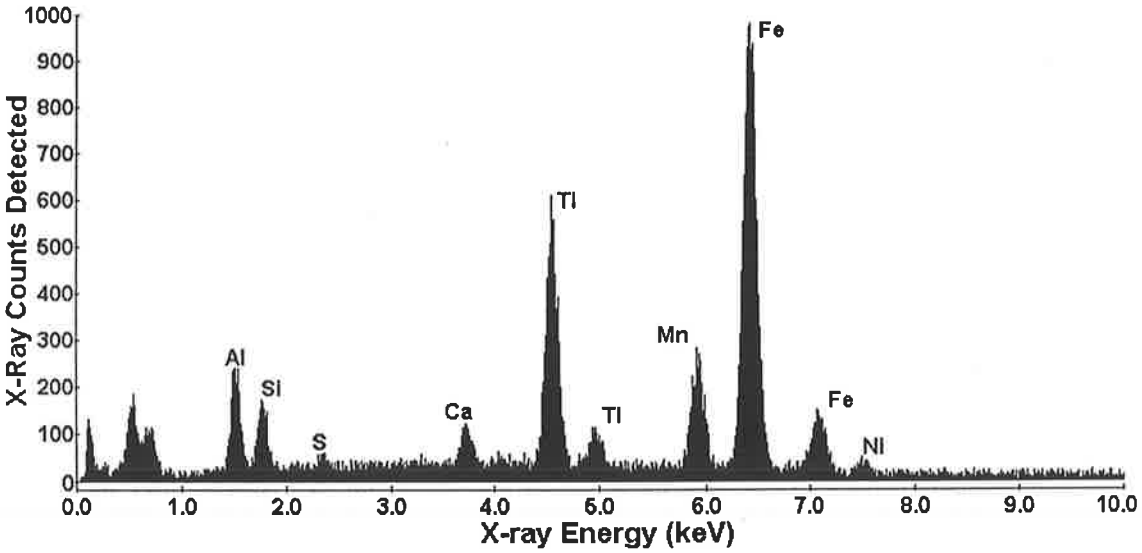

Figure 6-21 EDS X-Ray Spectrum of Selected Weld Inclusion

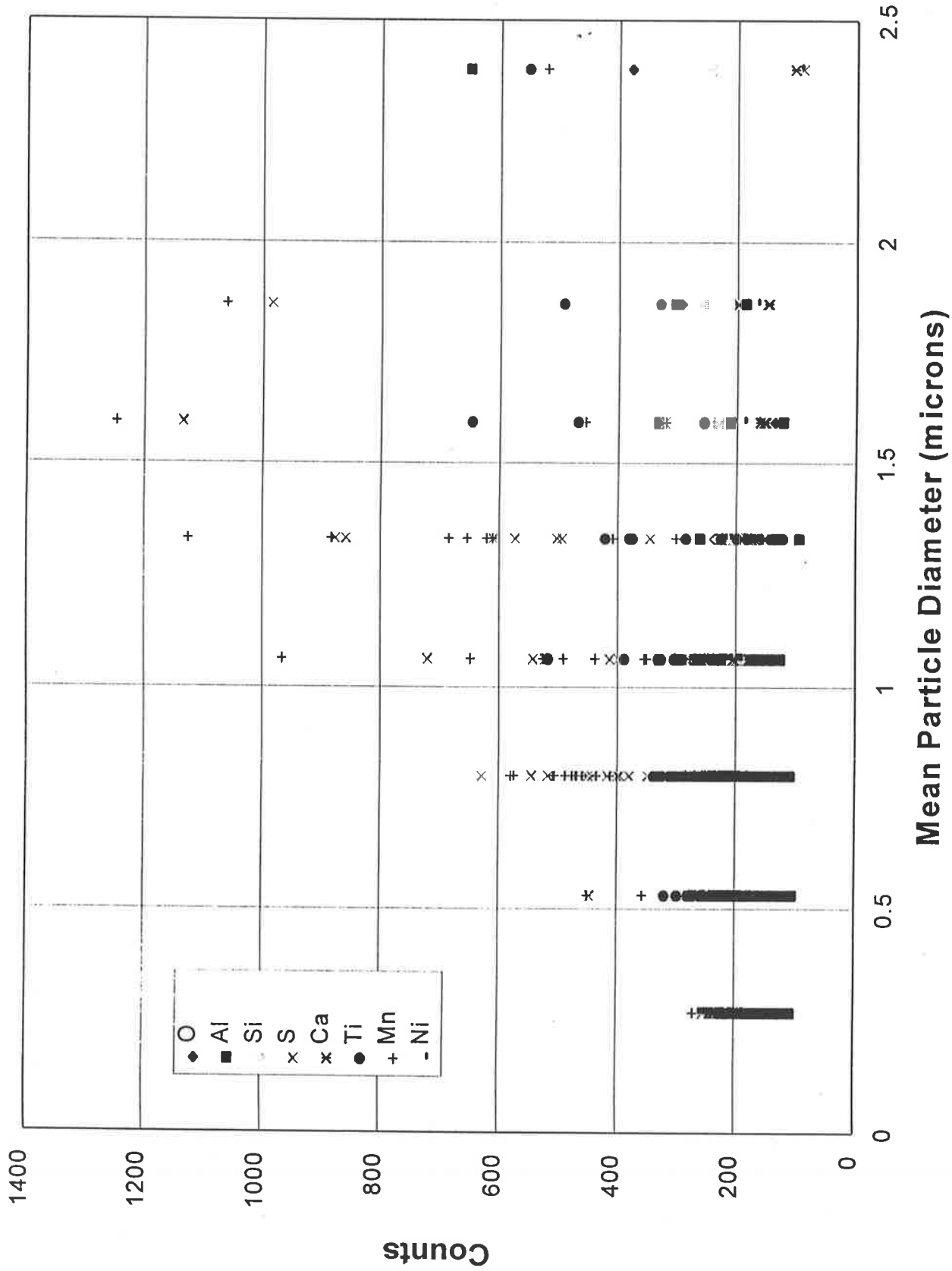

Figure 6-22 X-Ray Counts Collected from Weld Particles

6.4. FRACTURE SURFACES

All tensile specimens had a ductile mode of failure initiated by microvoid coalescence on the weld inclusions. There was some evidence of quasi-cleavage on the low heat input specimens but this played a minor role in the failure. Similar results on fracture test specimens for C-Mn-Ni welds have also been reported by Abson [35]. Figures 6-23 (a) and (b) show a micrograph of this microvoid coalescence with the characteristic inclusion based at the bottom of the equiaxed dimples.

Of interest was that there were minimal differences in dimple size between the weld deposits of different heat inputs. This would suggest the nucleation sites for microvoid coalescence are uniform and indicates a similar spatial distribution of nucleating particles in the weld deposits of different heat inputs.

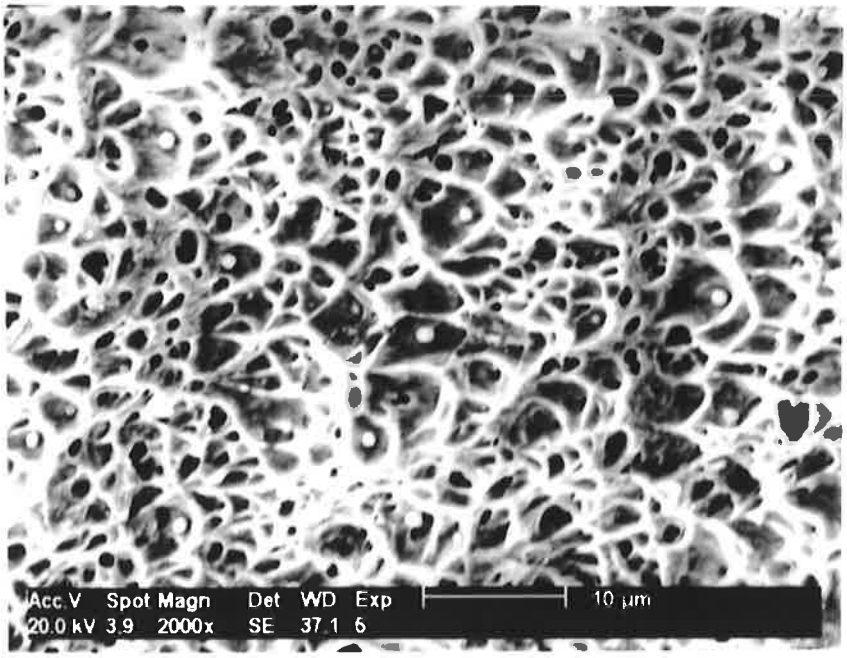

(a)

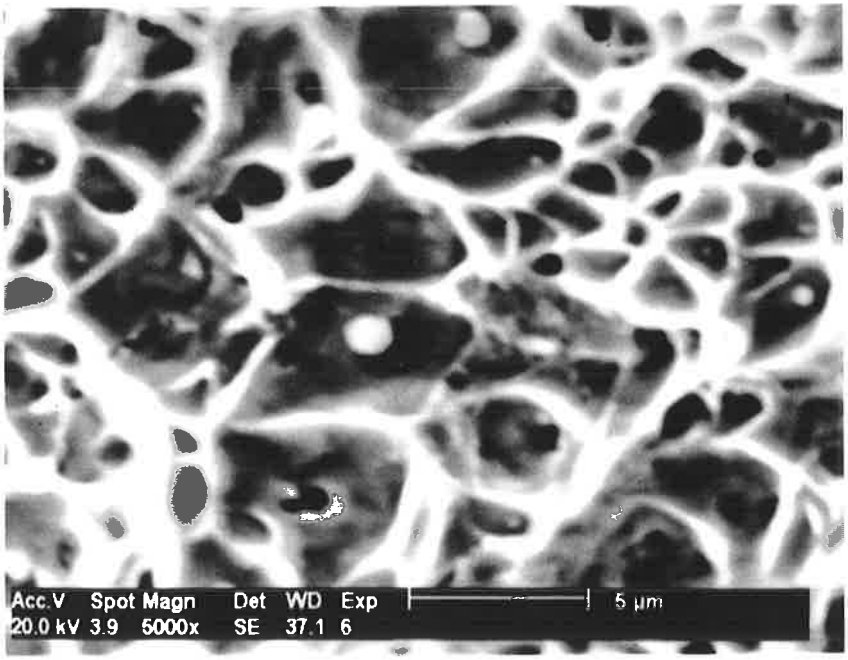

(b)

Figure 6-23 Microvoid Coalescence on Tensile Specimens

6.5. DISCUSSION

Examination of the welds produced in this study has revealed a highly complex microstructure which ranged from mostly martensitic at low heat inputs to mostly bainitic at high heat inputs.

The identification of this microstructure was not straightforward. Transmission electron microscopy was required to positively identify microconstituents present. Light microscopy was capable of identifying ferrite nucleation but was unable to identify the characteristics of martensite. For positive identification of martensite TEM was required. TEM revealed very high dislocation densities and evidence of martensite twinning. Features unique to martensite. In addition to this, the use of TEM revealed the presence of retained austenite as thin films between martensite laths.

SEM was also used to highlight microstructural features of interest and to explain why the fracture resistance of the low heat input welds appeared to be reduced. This was explained as being due to the aligned laths in the microstructure of the low heat input welds and the randomly oriented laths occurring in the high heat input welds. Aligned laths allow crack propagation to occur relatively easily whereas a propagating crack would need to frequently change direction in a microstructure of unaligned laths.

In many cases the microstructure was influenced by the presence of non-metallic particles while at other times they appeared to have little effect. Size

distributions were examined as were the elemental compositions of the particles. Distributions correlated well with those of other studies. Of interest was the presence of a number of large particles of above 1μm in diameter. These were mostly rich in manganese and sulphur.

Fracture surfaces of the tensile specimens were examined revealing a surface characteristic of microvoid coalescence on particles in the weld deposit. The examination of large particles in the weld deposit and their effects on ductile fracture initiation is an area requiring further study.

CHAPTER 7. CONCLUSIONS AND FUTURE WORK

7.1. CONCLUSIONS

This study has examined microstructural development as a function of heat input for a high strength weld metal produced using flux cored consumables. It has also made correlations between the microstructure and mechanical properties.

Techniques used to characterise the microstructure were light microscopy, SEM and TEM. Standard sample preparation techniques were used for microstructural examination but, to determine the mechanical properties, non-standard tests were required due to the unusually small amount of weld metal available for testing. The use of such tests has provided results not previously seen which has allowed a number of conclusions to be made relating to the influence of heat input on the microstructure and mechanical properties of this high strength weld metal in the as deposited state.

The conclusions of this study are:

1. This high strength weld metal is sensitive to heat input with microstructures ranging from mostly martensitic, at low heat inputs of less than 1.5 kJ/mm, to mostly bainitic at over 1.5kJ/mm. Near the upper heat input examined (approx 2 kJ/mm) grain boundary ferrite was observed in small quantities. This could possibly lead to a reduction in fracture properties at even higher heat inputs where greater amounts of grain boundary ferrite would be expected.

2. An increase in heat input resulted in a decrease in the tensile strength, hardness and resistance to fracture. This conforms with the observed change in microstructure.
3. The decreased resistance of the weld to fracture at low heat inputs may be due to the microstructure of aligned laths (of either martensite or bainite) at low heat inputs. At high heat inputs the improved fracture toughness was possibly due to the random orientation of the ferrite laths. The transition from aligned laths in the microstructure to randomly oriented laths appears to occur at about 1.5 kJ/mm which correlated with the observed change from a mostly martensitic to a mostly bainitic microstructure.
4. Heat input was shown to have an insignificant effect on the elemental composition of the weld deposit over the range of heat inputs studied. This would suggest that the variations in microstructure and mechanical properties was due to either cooling rate differences or differences in the non-metallic particles and their propensity to nucleate ferrite.
5. Variations in the size distributions of non-metallic particles (as a function of heat input) was small. This would suggest that differences observed in the microstructure and mechanical properties are not attributable to variations in the sizes of particles in this heat input range.
6. Mechanical testing of as deposited weld metal at low heat inputs is possible but only with the use of non-standard specimens. The results obtained can only be used for comparison to other results obtained using the same specimen type.

7.2. FUTURE WORK

The results of this study, as well as many of the studies examined in the literature review, leave many questions unanswered. Explanations to these questions will only come from further studies focussed on individual aspects of high strength welding metallurgy. General studies (such as this one) will continue to be of value to examine the many effects of altering process parameters, but concentrated efforts on individual aspects are required to further the understanding of microstructural development and its relationship with mechanical properties.

The results of this study suggest a number of areas in which further work can be done. These areas are discussed below:

- ***Quantitative Microstructure Examination***

  Further progress into the effects of welding parameters on mechanical properties will require quantitative examination of the microstructure. High strength weld microstructures are currently difficult to identify using techniques which can observe areas of the microstructure large enough to be considered representative, thus allowing quantitative examination. Techniques to allow positive identification of different phases using light microscopy must therefore be investigated.

  The ability to identify phases using light microscopy would allow techniques such as point counting to be used to determine the percentage

fractions of different microconstituents thus allowing direct correlations to mechanical properties. Advanced image analysis techniques could also be developed to be used in conjunction with either light microscopy or SEM images.

There are also other microstructural features which this study has not been able to examine. For example, the use of etchants such as LePera's to reveal the solidification structure may provide valuable information.

- ***Mechanical Test Development***

  Any study of mechanical properties for as deposited weld metals using low heat inputs will be confronted with a limited amount of material from which to obtain samples to perform mechanical testing. For this reason, non-standard tests are often required, however, such tests being modifications of proven test methods, require verification if the results are to be compared to those obtained in other studies. This is especially the case for the sub-size CTOD specimens used in this study.

  The verification of such tests could involve the testing of materials with known properties using the subsize specimens. The results obtained would then be compared to results obtained using standard test methods.

- ***Multi-Pass Welds***

  The present study focussed on the as deposited weld metal. In a real situation, multi-pass welds are often used. In such welds the as deposited pass only constitutes the last welds made which are not reheated by subsequent passes. For this reason a study should be made of the effects of reheating high strength weld microstructures. The use of weld thermal simulation may be of benefit in such a study.

  To perform such a study would require considerable resources as full Charpy or CTOD transition curves should be obtained, as should be tensile strength data, hardness and microstructural characterisation.

- ***Non-Metallic Particle Characterisation***

  This would be especially relevant as, as discussed in chapter 2 and clearly seen in chapter 6, it is these particles which are responsible for much of the development of microstructure.

  It is envisaged that a study focussed on this would require a number of welds to be made under identical welding parameters but with consumable fluxes specifically designed to vary the inclusion properties. Subsequent weld analysis would be highly dependent upon electron microscopy techniques to determine microstructures and inclusion composition and structure.

It would have been valuable if, in the present study, the size distributions of inclusions containing different elements could have been determined. To make an assessment such as this the inclusions would need to be removed from the weld using dissolution techniques and then many hours of electron microscopy done to build a database of statistical significance.

The information obtained could then be correlated with differences in the microstructure to make an assessment of what elements in particles are important and what sizes of particles containing elements of importance influence the microstructure. In addition to this, inclusion inhomogeneities could also be examined.

REFERENCES

[1] Vines M.J., "Effects of Shielding Gas Composition on Operating Characteristics and Weld Metal Properties of Flux-Cored Wires", AWRA Document P2-46-85, December 1985, pp 21-40

[2] Vaidya V.V., "Flux Cored Arc Welding Wires - Factors Affecting Selection", Canadian Welder and Fabricator, November, 1989, pp 33-38

[3] Ahlblom B., "Oxygen and its Role in Determining Weld Metal Microstructure and Toughness: A state of the Art Review", Doc. IX-J-81-84 of the IIW, 1984

[4] Chai C.S. and Eagar T.W., "Slag-Metal Equilibrium During Submerged Arc Welding", Metallurgical Transactions, Vol 12B, September, 1981, pp 539-547

[5] Francis R.E., Jones J.E and Olson D.L., "Effect of Shielding Gas Oxygen Activity on Weld Metal Microstructure of GMA Welded Microalloyed HSLA Steel", Welding Journal Research Supplement, Vol. 69, November, 1990, pp 408-414

[6] Vines M.J. and Bailey N., "Manual Metal Arc Welding - Effects of Core Wire Deoxidisation Practice", Welding Institute Research Report 197, November, 1982

[7] Den Ouden G., "The Role of Nitrogen in Electric Arc Welding", Phillips Welding Reporter, Vol. 13, No.1, January, 1977, pp 45-51

[8] Lathabai S. and Stout R.D., "Shielding Gas and Heat Input Effects on Flux Cored Weld Metal Properties", Welding Journal Research Supplement, Vol. 64, November, 1985, pp 303-313

[9] David S.A. and Vitek J.M., "Correlation Between Solidification Parameters and Weld Microstructures", International Materials Reviews, Vol. 34, No. 5, May, 1989, pp 213-245

[10] Bramfit B.L., "Solidification Structures of Steel", Metals Handbook 9th Ed., Vol. 9, 1985, pp 623-628

[11] Kluken A., Grong Ø. and Hjelen J., "The Origin of Transformation Textures in Steel Weld Metals Containing Acicular Ferrite", Metallurgical Transactions A, Vol. 22A, March, 1991, pp 657-663

[12] Lancaster J.F., "Metallurgy of Welding 3rd Ed.", George Allen & Unwin Ltd, 1980

[13] Easterling K., "Introduction to the Physical Metallurgy of Welding 2nd Ed.", Butterworth-Heinemann, 1992

[14] Rosenthal D., "Mathematical Theory of Heat Distribution During Welding and Cutting", Welding Journal Research Supplement, Vol. 20, May, 1941, pp 220-234

[15] Adams C.M. Jr., "Cooling Rates and Peak Temperatures in Fusion Welding", Welding Journal Research Supplement, Vol. 37, May, 1958, pp 210-215

[16] Blodgett O.W., "Calculating Cooling Rates by Computer Programming", Welding Journal, March, 1984, pp 19-34

[17] David S.A. and Liu C.T., "High Power Laser and Arc Welding of Thorium Doped Iridium Alloys", Welding Journal Research Supplement, Vol. 61, May, 1982, pp 157-163

[18] Oldland P.T., Ramsay C.W., Matlock D.K. and Olson D.L., "Significant Features of High-Strength Steel Weld Metal Microstructures", Welding Journal Research Supplement, Vol. 68, April, 1989, pp 158-168

[19] Bhadeshia H., "Control of Weld Metal Microstructure and Properties", Proceedings of International Conference on the Metallurgy, Welding and Qualification of Micro-Alloyed (HSLA) Steel Weldments, November, 1990, pp 34-69

[20] Bhadeshia H., "Modelling of Steel Welds", Materials Science and Technology, Vol 8, February, 1992, pp 123-133

[21] Sudgen A. and Bhadeshia H., "The Non-Uniform Distribution of Inclusions in Low Alloy Steel Weld Deposits", Metallurgical Transactions A, Vol 19A, March, 1988, pp 669-764

[22] IIW Doc No. IX-1533-88, "Guide to the Light Microscope Examination of Ferritic Steel Weld Metals", June, 1988

[23] Ali A. and Bhadeshia H., "Nucleation of Widmanstätten Ferrite", Materials Science and Technology, Vol. 6, August, 1990, pp 781-784

[24] Garland J. and Kirkwood P., "Towards Improved Submerged Arc Weld Metal", Metal Construction, Vol 7, No. 7, June, 1975, pp 320-330

[25] Billy J., Johansson T., Loberg B. and Easterling K., "Stress Relief Heat Treatment of Submerged Arc Microalloyed Steels", Metals Technology, Vol. 7, February, 1980, pp 67-78

[26] Munning Schnidt-Van Der Burg M., Hoekstra S. and Den Ouden G., "Influence of Microstructure on Mechanical Properties of Two Single-Bead Ferritic Weld Metals", Welding Journal Research Supplement, Vol. 64, March, 1985, pp 63-70

[27] Svensson L. and Gretoft B., "Microstructure and Impact Toughness of C-Mn Weld Metals", Welding Journal Research Supplement, Vol. 69, December, 1990, pp 454-461

[28] Yang J.R. and Bhadeshia H., "Orientation Relationships Between Adjacent Plates of Acicular Ferrite in Steel Weld Deposits", Materials Science and Technology, Vol. 5, January, 1989, pp 93-97

[29] Ali A. and Bhadeshia H., "Microstructure of High Strength Steel Refined with Intragranularly Nucleated Widmanstätten Ferrite", Materials Science and Technology, Vol. 7, October, 1991, pp 895-903

[30] Yang J., Yang C. and Huang C., "The co-existence of acicular ferrite and bainite in an alloy steel weld metal", Journal of Materials Science Letters, November, 1992, pp 1145-1146

[31] Bhadeshia H., "Models for Acicular Ferrite", Proceedings of 3rd International Conference on Trends in Welding Research, Gatlinburg, Tennessee USA, June, 1992, pp 213-222

[32] Sudgen A. and Bhadeshia H., "Lower Acicular Ferrite", Metallurgical Transactions A, Vol 20A, September, 1989, pp 1811-1818

[33] Ito Y., Nakanishi M. and Komizo Y., "Effect of Oxygen Transformation of Low Carbon Weld Metal", IIW Document IX-1194-81, International Institute of Welding, 1981

[34] Evans G.M., "The Effect of Heat Input on the Microstructure and Properties of C-Mn All-Weld-Metal Deposits", Welding Journal Research Supplement, Vol. 61, April, 1982, pp 125-132

[35] Abson D.J., "Microstructure and Mechanical Properties of Gas Shielded Welding of C-Mn-Ni Steel", Welding Journal Research Supplement, Vol. 72, May, 1993, pp 173-187

[36] Edmonds D.V., "Bainitic Structures", Metals Handbook 9th ed., Vol. 9, 1985, pp 662-667

[37] Honeycombe R., "Steels - Microstructure and Properties", Edward Arnold Publishers Ltd, 1981

[38] Yang J.R., Huang C.Y., Huang C.F. and Aoh J.N., "Influence of Acicular Ferrite and Bainite Microstructures on Toughness for an Ultra-Low-Carbon Steel Weld Metal", Journal of Materials Science Letters, December, 1993, pp 1290-1293

[39] Speich G.R., "Ferrous Martensitic Structures", Metals Handbook 9th ed., Vol. 9, 1985, pp 668-674

[40] Bilby B.A. and Christian J.W., "The Crystallography of Martensite Transformations", Journal of Iron and Steel Institute, April, 1961, pp 187-195

[41] Chandrasekharaiah M., Dubben G. and Kolster B., "An atom probe study of retained austenite in ferritic weld metal", Welding Journal Research Supplement, Vol. 71, July, 1992, pp 247-251

[42] Biss V. and Cryderman R., "Martensite and Retained Austenite in Hot Rolled, Low Carbon Bainitic Steels", Metallurgical Transactions, Vol 2, August, 1971, pp 2267-2276

[43] Narasimha-rao V., Bangaru and Sachdev A., "Influence of Cooling Rate on the Microstructure and Retained Austenite in an Intercritically Annealed Vanadium Containing HSLA Steel", Metallurgical Transactions A, Vol 13A, November, 1982, pp 1899-1906

[44] Harrison P., "Microstructural Development and Toughness of C-Mn and C-Mn-Ni Weld Metals - Part 1: Microstructural Development", Metal Construction, July, 1987, pp 392-399

[45] Harrison P.L., "Microstructural Development and Toughness of C-Mn and C-Mn-Ni Weld Metals - Part 2: Toughness", Metal Construction, August, 1987, pp 447-450

[46] Harrison P.L. and Farrar R.A., "Application of Continuous Cooling Transformation Diagrams for Welding of Steels", International Materials Reviews, Vol. 34, No. 1, January, 1989, pp 35-51

[47] Horii Y. and Ohkita S., "Prediction of weld metal microstructure: Part 1 Low-alloy steels", Welding International, Vol. 10, June, 1992, pp 761-765

[48] Kenny B., Kerr H., Lazor R. and Graville B., "Ferrite transformation characteristics and CCT diagrams in weld metals", Metal Construction, Vol. 17, June, 1985, pp 374-381

[49] Surian E., "Influence of Carbon on Mechanical Properties and Microstructure of Weld Metal From a High Strength SMA Electrode", Welding Journal Research Supplement, Vol. 70, June, 1991, pp 133-140

[50] Evans G.M., "The Effect of Carbon on the Microstructure and Properties of C-Mn All-Weld-Metal Deposits", Welding Research Abroad WRC, Vol. 28, No. 1, January, 1983, pp 1-69

[51] Den Ouden G., "The Influence of Chemical Composition on Mild Steel Weld Metal Notch Toughness", Welding Journal Research Supplement, Vol. 54, September, 1975, pp 311-319

[52] Paxton H.W., in "Alloys for the Eighties", Greenwich, Conn., Climax Molybdenum Company, 1981, pp 185-211

[53] Evans G.M., "The Effect of Manganese on the Microstructure and Properties of C-Mn All-Weld-Metal Deposits", Welding Research Abroad WRC, Vol. 28, No. 1, January, 1983, pp 1-69

[54] Evans G.M., "Effect of Electrode Diameter on the Microstructure and Properties of C-Mn All-Weld Metal Deposits", IIW Document, II-A-469-79, 1979

[55] Grong O. and Matlock D., "Microstructural Development in Mild and Low-Alloy Steel Weld Metals", International Metals Reviews, Vol. 31, No. 1, January, 1986, pp 27-48

[56] Evans G.M., "The Effect of Chromium on the Microstructure and Properties of C-Mn All-Weld-Metal Deposits", Welding and Metal Fabrication, August/September, 1989, pp 346-358

[57] Evans G.M., "The Effect of Nickel on the Microstructure and Properties of C-Mn All-Weld-Metal Deposits", Joining Sciences, Vol. 1, No. 1, January, 1991, pp 2-13

[58] Dolby R.L., in "Steels for Linepipe and Pipeline Fittings", London, The Metals Society, 1983, pp 302-312

[59] Levine E. and Hill D., "Toughness in HSLA steel weldments", Metal Construction, August,1977, pp 346-353

[60] Evans G.M., "Effects of niobium in manganese containing MMA weld deposits", Welding International, July,1993, pp 518-528

[61 Evans G.M., "The Effect of Vanadium in Manganese Containing MMA Weld Deposits", Welding International, July,1993, pp 438-448

[62 Abson D.J., "The Influence of Aluminium Additions to Tubular Cored Welding Electrodes on the Microstructure and Toughness of As-deposited C-Mn-Ni Weld Metal", TWI, July, 1992, pp 100-127

[63] Oh D.W., Olson D.L. and Frost R.H., "The Influence of Boron and Titanium on Low-Carbon Steel Weld Metal", Welding Journal Research Supplement, Vol. 69, April,1990, pp 151-158

[64] Mori N., Homma H., Ohkita S. and Wakabayashi M., "Mechanisms on Notch Toughness Improvement in Ti-B Bearing Weld Metals", IIW Doc IX-1196-81, 1981

[65] Ohkita S., Homma H., Tsushima S. and Mori N., "The Effect of Oxide Inclusions on the Microstructure of Ti-B Containing Weld Metal", IIW Doc II-1070-86, 1986

[66] Snyder J.P. and Pense A.W., "Effect of Ti on Submerged Arc Weld Metal" Welding Journal Research Supplement, Vol. 61, July, 1982, pp 201-211

[67] Evans G.M., "The Effect of Titanium in Manganese Containing SMA Weld Deposits", Welding Journal Research Supplement, Vol. 72, March, 1993, pp 123-133

[68] Evans G.M., "The Effect of Titanium in SMA C-Mn Steel Multi-Pass Deposits", Welding Journal Research Supplement, Vol. 71, December, 1992, pp 447-454

[69] Yang J.R. and Bhadeshia H., "Acicular Ferrite Transformation in Alloy-Steel Weld Metals", Journal of Materials Science, Vol. 26, 1991, pp 839-845

[70] Bhadeshia H. and Svensson L., "The Austenite Grain Structure of Low Alloy Steel Weld Deposits", Journal of Materials Science, Vol. 21, No. 11, November, 1986, pp 3947-3951

[71] Dallam C.B. and Olson D.L., "Stress and Grain Size Effects on Weld Metal Ferrite Formation", Welding Journal Research Supplement, Vol. 68, May, 1989, pp 198-205

[72] Barritte G.S., Ricks R.A. and Howell P.R., "Application of STEM/EDS to Study of Microstructural Development in HSLA Steel Weld Metals", Proceedings of the Conference on Qualitative Microanalysis with High Spatial Resolution, The Metals Soc., 1981, pp 112-118,

[73] Babu S. and Bhadeshia H., "Mechanism of the Transformation from Bainite to Acicular Ferrite", Materials Transactions, Vol. 32, No. 8, August, 1991, pp 679-688

[74] Farrar R.A., Zang Z., Bannister S. and Barritte G., "The Effect of Prior Austenite Grain Size on the Transformation Behaviour of C-Mn-Ni Weld Metal", Journal of Materials Science, Vol. 28, 1993, pp 1385-1390

[75] Handeland T., Erkkila E. and Gjonnes J., "A Combined Electron Microscope and Optical Metallographic Study of Microstructures in High Strength Low Alloy (HSLA) Steels After Welding", Journal of Microscopy, Vol. 144, December, 1986, pp 251-259

[76] Kokak M., Es-Souni M. and Schwalbe K., "Effect of Microstructure on Weld Metal Toughness", Proceedings of the 2nd International Conference on Trends in Welding Research, Gatlinburg, Tennessee, USA, 14-18 May, 1989, pp 727-731

[77] Tweed J.H. and Knott J.F., "The Effect of Preheat Temperature on the Microstructure and Toughness of a C-Mn Weld Metal", Metal Construction, March, 1987, pp 153-158

[78] Abson D.J., "Non-Metallic Inclusions in Ferritic Steel Weld Metals - A Review", Welding in the World, Vol. 27, No. 3/4, 1989, pp 76-101

[79] Barbaro F.J., "Intragranular Ferrite Formation on Second Phase Particles in C-Mn Steels", Materials Processing and Performance - Extended Abstracts, September, 1991, pp 235-240

[80] Court S.A. and Pollard G., "Inclusion Chemistry and Morphology in Shielded Metal Arc (SMA) Steel Weld Deposits", Metallography Vol. 22, 1989, pp 219-243

[81] Liao F. and Liu S., "Effect of Deoxidisation Sequence on Carbon Manganese Steel Weld Metal Microstructures", Welding Journal Research Supplement, Vol. 71, March, 1992, pp 94-103

[82] Homma H., Ohkita S. and Matsuda Y., "Improvement of HAZ Toughness in HSLA Steel by Introducing Finely Dispersed Titanium Oxide", Welding International, Vol. 7, March, 1989, pp 567-671

[83] Es-Souni M. and Beaven P.A., "Micro-Analysis of Inclusion/Matrix Interfaces in Weld Metals", Surface and Interface Analysis, Vol. 16, July, 1990, pp 504-509

[84] Es-Souni M., Beaven P.A. and Evans G.M., "Microstructure and AEM Studies of Self Shielded Flux Cored Arc Weldments", Welding Journal Research Supplement, Vol. 71, February, 1992, pp 35-45

[85] Thewlis G., Amin R.K., Cochrane R.C. and Reasbeck L., "The Effect of Calcium Treatment of Steels on Weld Metal Microstructure and Toughness", Proceedings of the 2nd International Conference on Trends in Welding Science and Technology, Gatlinburg, Tennessee, USA, May, 1989, pp 879-887

[86] Ramsay C.W., Matlock D.K. and Olson D.L., "Microstructures and Properties of a High Strength Weld Metal", Proceedings of The 2nd International Conference on Trends in Welding Research, Gatlinburg, Tennessee, USA, 1989, pp 763-767

[87] Fleck N., Masters Thesis, Colorado School of Mines, 1984

[88] Gonzalez J.C., Llorente C.L. and Biloni H., "Correlation Between Microstructure and Mechanical Properties for Two Self-Shielded Flux Cored Wires", Canadian Metallurgical Quarterly, Vol. 25, No. 4, April, 1986, pp 319-326

[89] Gianetto J.A., Smith N.J., McGrath J.T. and Bowker J.T., "Effect of Composition and Energy Input on Structure and Properties of High-Strength Weld Metals", Welding Journal Research Supplement, Vol. 71, November, 1992, pp 407-419

[90] Rørvik G., Onsøien M.I., Kluken A.O. and Akselsen O.M., "High Heat Input Welding of Offshore Structures - Procedures and Weld Properties", Welding Journal Research Supplement, Vol. 71, September, 1992, pp 331-339

[91] Bhadeshia H. and Svensson L., "The Microstructure and Properties of Submerged Arc-Weld Deposits for High Strength Welds", Journal of Materials Science, Vol. 24, 1989, pp 3180-3188

[92] Hasson D.F., Zanis C.A. and Anderson D.R., "Fracture Toughness of HY-130 Steel Weld Metals", Welding Journal Research Supplement, Vol. 63, June, 1984, pp 197-202

[93] Kluken A.O., Onsøien M.I., Akselsen O.M. and Rørvik G., "Mechanical Properties of High Heat Input Deposited Weld Metals", Joining Sciences, Vol. 1, No. 1, January, 1991, pp 14-22

[94] Smith N.J., "Microstructure/Mechanical Property Relationships of Submerged Arc Welds in HSLA 80 Steel", Welding Journal Research Supplement, Vol. 68, March, 1989, pp 112-120

[95] Dixon B. and Håkansson K., "Effects of Welding Parameters on Weld-Zone Toughness and Hardness in 690 MPa Steel", Proceedings of 41st Annual Welding Conference, FABCON/FABFAIR '93 - Towards a Compeditive Edge, 1993, pp 197-203

[96] Standards Association of Australia, "AS1203 5.1, Non-Destructive Testing of Weld Metal", August, 1988

[97] Standards Association of Australia, "AS 2205, Methods of Destructive Testing of Welds in Metal", August, 1988

[98] B4 Committee on Mechanical Testing of Welds, "Mechanical Testing of Welds Part 1 - Tension Testing of Welds", Welding Journal, Vol. 60, January, 1981, pp 33-37

[99] B4 Committee on Mechanical Testing of Welds, "Mechanical Testing of Welds Part 2 - Bend Testing of Welds", Welding Journal, Vol. 60, February, 1981, pp 34-37

[100] B4 Committee on Mechanical Testing of Welds, "Mechanical Testing of Welds Part 3 - Fracture Toughness Testing of Welds", Welding Journal, Vol. 60, March, 1981, pp 37-40

[101] Barclay J., "Fracture Toughness Properties of Some Australian Electroslag Welds - AWRA Contract 91", Australian Welding Research, December, 1982, pp 63-68

[102] American Society for Testing and Materials, "ASTM E92-82 Standard Test Method for Vickers Hardness of Metallic Materials", 1982

[103] American Society for Testing and Materials, "ASTM E1290 - Standard Test Method for Crack Tip Opening Displacement (CTOD) Fracture Toughness Measurement", November, 1989

[104] Askerland D., "The Science and Engineering of Materials SI ed.", Van Nostrand Reinhold, 1988

[105] Chen J.H., Ma H. and Wang G.Z., "Fracture Behaviour of C-Mn Steel and Weld Metal in Notched and Pre-Cracked Specimens: Part 2 Micromechanism of Fracture", Metallurgical Transactions A, Vol 21A, February, 1990, pp 321-330

[106] Chen J., Xia T. and Yan C., "Study on Impact Toughness of C-Mn Multi-layer Weld Metal at -60°C", Welding Journal Research Supplement, January, 1993, pp 19-27

[107] Choi C.L. and Hill D.C., "A Study of Microstructural Progression in As-Deposited Metal", Welding Journal Research Supplement, Vol. 57, August, 1978, pp 232-236

[108] Cox E., "A Methodology for Characterising Weldment Fracture Behaviour", Welding Journal Research Supplement, Vol. 66, February, 1987, pp 39-49

[109] Crawford D.G. and Baker T., "Microstructure and Toughness of Low Carbon Steel Weld Metal", Materials Science and Engineering, A131, 1991, pp 255-263

[110] Deb P., Challenger K.D. and Burna R.F., "Microstructural Characterisation of Shielded Metal Arc Weldments of a Copper Bearing HSLA Steel", Materials Science and Technology, Vol. 1, November, 1985, pp 1000-1006

[111] Deb P., Challenger K. and Therrien A., "Structure-Property Correlation of Submerged Arc and Gas Metal Arc Weldments in HY-100 Steel", Metallurgical Transactions A, Vol 18A, June, 1987, pp 987-999

[112] Denys R.M., "Difference Between Small and Large Scale Testing of Weldments", Welding Journal Research Supplement, Vol. 68, February, 1989, pp 33-43

[113] Henderson I. and Steffens H., "Fracture Toughness of Narrow Gap Welded Joints in the Nuclear Pressure Vessel Steel 22 NiMoCr 37", Nuclear Engineering and Design, Vol. 36, No. 2, February, 1976, pp 273-285

[114] Matsoukas G., Cotterell B. and Mai Y., "On the plastic rotation constant used in standard COD tests", Australian Welding Research, December, 1984, pp 50-51

[115] Matsoukas G., Cotterell B. and Mai Y., "Fracture Toughness of Pressure Vessel Steels", Australian Welding Research, December, 1985, pp 1-7

[116] Morgenstern V., Herrera R., Mejías H. and Patchett B., "Inexpensive Computer Controlled Fracture Toughness Testing", Welding Journal Research Supplement, Vol.68, June, 1989, pp 223-229

[117] Williams J.F., Jones R. and Goldsmith N., "An Introduction to Fracture Mechanics - Theory and Case Studies", Mechanical Engineering Transactions, The Institution of Engineers Australia, Vol. ME 14, No. 4, 1989

[118] Signes E.G., "A Simplified Method for Calculating Cooling Rates in Mild and Low Alloy Steel Weld Metals", Welding Journal Research Supplement, Vol. 51, October, 1972, pp 273-284

[119] Kim Y. and Eagar T., "Metal Transfer in Pulsed Current Gas Metal Arc Welding", Welding Journal Research Supplement, Vol. 72, July, 1993, 279-287

[120] Bosworth M., "Effective Heat Input in Pulsed Current Gas Metal Arc Welding with Solid Wire Electrodes", Welding Journal Research Supplement, Vol. 70, May, 1991, pp 111-117

[121] Bosworth M., Unpublished, 1993

[122] Jhaveri P., Moffatt W.G. and Adams C.M. Jr., "The Effect of Plate Thickness and Radiation on Heat Flow in Welding and Cutting", Welding Journal Research Supplement, Vol. 41, January, 1962, pp 12-16

[123] Barry J.M., Paley Z. and Adams C.M. Jr., "Heat Conduction from Moving Arcs During Welding", Welding Journal Research Supplement, Vol. 42, March, 1963, pp 97-104

[124] Christensen N., Davies V. and Gjermundsen K., "Distribution of Temperatures in Arc Welding", British Welding Journal, February, 1965, pp 54-75

[125] Clyde M. and Adams Jr., "Cooling Rates and Peak Temperatures in Fusion Welding", Welding Journal Research Supplement, Vol. 47, May, 1958, pp 210-215

[126] Eagar T.W. and Tsai N.S., "Temperature Fields Produced by Travelling Distributed Heat Sources", Welding Journal Research Supplement, Vol. 62, December, 1983, pp 346-355

[127] Myhr O.R. and Grong Ø., "Dimensionless Maps for Heat Flow Analysis in Fusion Welding", Acta. metall. mater., Vol. 38, No. 3, 1990, pp 449-460

[128] Paley Z., Lynch J.N. and Adams C.M., "Heat Flow In Welding Heavy Steel Plate", Welding Journal Research Supplement, Vol. 53, February, 1964, pp 71-79

[129] Kannatey-Asibu E. Jr., Kikuchi N. and Jallad A.R., "Experimental Finite Element Analysis of Temperature Distribution During Arc Welding", Sensors and Controls for Manufacturing, 1988, pp 1-14

[130] Bradstreet B.J., "Effect of Welding Conditions on Cooling Rate and Hardness in the Heat Affected Zone", Welding Journal Research Supplement, Vol. 58, November, 1969, pp 499-504

[131] Chakravarti A., Thibau R. and Bala S., "Cooling characteristics of bead-on-plate welds", Metal Construction, March, 1985, pp 178-183

[132] Dorschu K.E., "Control of Cooling Rates in Steel Weld Metal", Welding Journal Research Supplement, Vol. 57, February, 1968, pp 49-62

[133] Krantz B. and Coppolecchia V., "The Effects of Pulsed Gas Metal-Arc Welding Parameters on Weld Cooling Rates", Welding Journal Research Supplement, Vol. 60, November, 1971, pp 474-479

[134] Lukens W.E., "Infrared Temperature Sensing of Cooling Rates for Arc Welding Control", Welding Journal, Vol. 71, January, 1982, pp 27-33

[135] Eller F.C. Jr., "Thermocouples - Essential Devices for Proper Control of Local Weld Heat Treatment", Welding Journal, Vol. 72, December, 1983, pp 38-40

[136] Kinzie P.A., "Thermocouple Temperature Measurement", Wiley Interscience, 1973

[137] Lenk J.D., "ABC's of Thermocouples", Foulsam-Sams, 1968

[138] Bentley R., "Theory and Practice of Thermoelectric Thermometry", CSIRO Division of Applied Physics, 1990

[139] French I., "Influence of Shielding Gas Composition on Heat Transfer in Flux Cored Arc Welding", Australian Welding Journal, Spring, 1984, pp 25-28

[140] Kluken A., Grong Ø. and Hjelen J., "SEM based automatic image analysis of non-metallic inclusions in steel weld metals", Materials Science and Technology, Vol. 4, July, 1988, pp 649-654

[141] Underwood E., "Quantatative Stereology", London, Addison-Wesely, 1970

[142] Grong Ø., Siewart T.A., Martins G.P. and Olson D.L., "A Model for the Silicon-Manganese Deoxidation of Steel Weldments", Metallurgical Transactions, 17A, 1986, pp 1797-1807

[143] Kluken A. and Grong Ø., "Mechanisms of Inclusion Formation in Al-Ti-Si-Mn Deoxidised Steel Weld Metals", Metallurgical Transactions A, Vol 20A, August, 1989, pp 1335-1349

[144] St-Laurent S. and L'Espérance G., "Effects of chemistry, density and size distribution of inclusions on the nucleation of acicular ferrite in C-Mn steel shielded-metal-arc-welding weldments", Materials Science and Engineering, A149, 1992, pp 203-216

Appendix A TMS Software Listing

```
/*****************************************************************************
THERMOCOUPLE MEASUREMENT SYSTEM 1.3

This program is for use in aquiring data from a PC-30PGL D/A board.

Written By GREG REDDEN
University of Adelaide, South Australia
CRC for Welding and Joining Technology

Language TURBO C++ version 3.0

This software may be freely modified under the provision that all
modifications are documented in the space below.

This software may be used for any purpose the user wishes with the provision
that it may not be sold or leased for gain or profit in any form.

NOTE: Requires library containing the diagnostic routines.
NOTE: THE ABOVE MENTIONED LIBRARY IS NOT REQUIRED AS THE DIAGNOSTIC ROUTINES
      ARE NOT CURRENTLY USED.

*****************************************************************************/


// #define tcc
// The above compiler directive is required so that BORLAND TURBO products
// can use the predefined libraries and headers correctly.

#include <conio.h>
#include <ctype.h>
#include <dos.h>
#include <math.h>
#include <stdio.h>
#include <io.h>

//#include "pc30.h"
//#include "reg_30.h"
// The only function requiring the use of these headrers is the
// diagnostic routine.

//*******************
// At present the diagnostic routines are not used. Ideally they should be
// however due to time restraints and difficulties encountered in utilising
// them they have not yet been used.
//*******************


// Definitions to describe where registers are located relative to base.


#define BADD 0x700  /* Base address setting of board (Jumper setting) */

#define BLKCNT    (BADD  + 0)  /* Block counter reg. W.     */
#define ADDATL     (BADD + 0)  /* A/D low byte. R.          */
#define ADDATH     (BADD + 1)  /* A/D high byte. R.         */
#define ADDSR      (BADD + 1)  /* Data/status register      */
#define ADCCR      (BADD + 2)  /* Control/Channel register  */
#define ADMDE      (BADD + 3)  /* Mode register             */
#define PRESCALER (BADD + 4)  /* Clock prescaler. R/W.     */
#define DIVIDER   (BADD + 5)  /* Clock divider. R/W.       */
#define TMRCTR     (BADD + 7)  /* Clock control byte. R/W.  */
#define DIOCNTRL  (BADD  + 11) /* Digital I/O control. R/W. */
#define GAIN_REG  (BADD  + 24) /* Gain memory address R/W.  */


// Send video writes direct to video ram
// Be careful that video card is 100 % IBM compatible

int directvideo = 1;

// global constant declarations

const int max_thermocouples = 8 ;
const int channels          = 8 ;
const int maxbarheight      = 40;
```

```
// NOTE: Changing the value of channels is not all that is required to
// change the number of channels which are sampled.

// global variable declarations
char  filename[80],t_type;
float maxtemp,cjtemp,fsamplerate,samplerate;
int gain,ingain,sig_gain,cjmodify,temp[8];
int oldbarheight[9],a_d[8],lut[4097],peaktemp[8];

// file handle declarations

FILE *fh;

// function declarations

void   screen_draw(void);
void   gen_lut(void);
double r_volt2temp(double);
double k_volt2temp(double);
void   displaybar(float);
void   get_user_info(void);
void   bars(int);
void   write_file_header(void);
void   draw_border(int);
void   draw_vertline(int,int,int,int,int);
void   draw_horline(int,int,int,int);
void   beep(int, int);
void   set_sample_rate(void);
int    cjtempconv(void);
void   initialise(void);
void   set_channel_gain(void);
static b_test(int, int, int, int);


// function definitions

void get_user_info(void)

// This function gets values for some global variables
// it is not in function main() in order to keep main() simpler.

{
 char reply,answer, buffer[3];
 int file_stat;

 textcolor(WHITE);

 gotoxy(5,21);
 cputs("Cold Junction Temperature    :");
 gotoxy(5,22);
 cputs("Maximum expected temperature :");
 gotoxy(5,23);
 cputs("Name of output file          :");
 gotoxy(5,26);
 textcolor(RED);
 cputs("WARNING: Setting high gain may overload PC-30 causing damage");
 textcolor(WHITE);
 gotoxy(5,27);
 cputs("PC-30 input gain (1,10,100,1000):");
 gotoxy(5,28);
 cputs("Signal conditioner input gain   :");
 gotoxy(5,30);
 cputs("Thermocouple type (R,K):");
```

```
label2:; // For the goto statement a few lines below.

// Lines below ensure the previous values which are not default values
// are not displayed.
gotoxy(36,21);
puts("                          ");
gotoxy(36,22);
puts("                          ");
gotoxy(36,23);
puts("                          ");
gotoxy(5,24);
puts("                                                          ");
gotoxy(39,27);
puts("                          ");
gotoxy(39,28);
puts("                           ");
gotoxy(30,30);
puts("                          ");
gotoxy(5,35);
puts("                                                            ");

do
{
 gotoxy(5,20);
 cputs("Required samplerate (Hz)     :");
 gotoxy(35,20);
 puts("                       ");
 gotoxy(36,20);
 scanf("%f",&fsamplerate);
 // fsamplerate is only used to keep value that user entered.
 samplerate = fsamplerate;
 if (fsamplerate < 1)
 {
  beep(700,200);
  gotoxy(5,20);
  cputs("A samplerate of less than 1Hz is not supported.              ");
  delay(2000);
 }
} while (fsamplerate < 1);


// Gets cold junction temperature from user.
gotoxy(36,21);
scanf("%f",&cjtemp);

// Gets maximum expected temperature from user.
gotoxy(36,22);
scanf("%f",&maxtemp);


// Gets filename to output data to from user and checks to see if file
// already exists. If it does user gets prompted to decide to overwrite
// or to give a different file name.

do
{
 gotoxy(36,23);
 puts("                          ");
 gotoxy(5,24);
 puts("                                                          ");
 gotoxy(36,23);
 scanf("%s",filename);

 file_stat = access(filename,0);
 if (file_stat == 0)
  do
   {
    beep(700,200);
    textcolor(YELLOW);
    gotoxy(5,24);
    cprintf("File '%s' already exists, overwrite (Y/N) : ",filename);
    textcolor(LIGHTGRAY);
    scanf("%c",&answer);
    answer = toupper(answer);
    textcolor(WHITE);
   } while ((answer != 'Y') && (answer != 'N'));
} while ((answer != 'Y') && (file_stat == 0));
```

```
 draw_border(LIGHTBLUE);
 draw_horline(1,80,15,LIGHTBLUE);
 draw_horline(1,80,17,LIGHTBLUE);
}

void draw_border(int color)
{
 int i;

 textcolor(color);

 for (i=2;i<80;i++)
 {
  gotoxy(i,1);
  cprintf("%c",char(196));
  gotoxy(i,49);
  cprintf("%c",char(196));
 }

 for (i=2;i<49;i++)
 {
  gotoxy(1,i);
  cprintf("%c",char(179));
  gotoxy(80,i);
  cprintf("%c",char(179));
 }

 gotoxy(1,1);
 cprintf("%c",char(218));
 gotoxy(80,1);
 cprintf("%c",char(191));
 gotoxy(1,49);
 cprintf("%c",char(192));
 gotoxy(80,49);
 cprintf("%c",char(217));

}

void draw_vertline(int startx,int starty, int finishx,int finishy,int color)
{
 int i,j;
 int a,b,c,d;

 if (startx > finishx) {b = startx; a = finishx;}
  else {a = startx; b = finishx;}

 if (starty > finishy) {d = starty;c = finishy;}
  else {c = starty; d = finishy;}

 textcolor(color);

 for (i=a;i<(b+1);i++)
  for (j=c;j<(d+1);j++)
  {
   gotoxy(i,j);
   cprintf("%c",char(179));
  }
}

void draw_horline(int startx, int finishx,int yloc,int color)
{
 int i;
 int a,b;

 if (startx > finishx) {b = startx; a = finishx;}
  else {a = startx; b = finishx;}

 textcolor(color);

 for (i=(a+1);i<b;i++)
  {
   gotoxy(i,yloc);
   cprintf("%c",char(196));
  }
```

```
  // Put ends on the line
  gotoxy(a,yloc);
  cprintf("%c",char(195));
  gotoxy(b,yloc);
  cprintf("%c",char(180));
}

void paint_data_screen()
{
 int i,j,value;
 const int tick_number = 8; // number of ticks on bar y-axis

 clrscr();

 draw_border(LIGHTBLUE);
 draw_vertline(31,48,31,2,LIGHTBLUE);
 gotoxy(31,1);
 cprintf("%c",char(194));
 gotoxy(31,49);
 cprintf("%c",char(193));

 draw_horline(31,80,45,LIGHTBLUE);
 draw_horline(31,80, 4,LIGHTBLUE);

 gotoxy(35,2);
 textcolor(YELLOW);
 cputs("THERMOCOUPLE MEASUREMENT SYSTEM version 1.3");
 textcolor(CYAN);
 gotoxy(34,3);
 cputs("Written by Greg Redden Adelaide Uni Feb 1993");

 textcolor(LIGHTRED);
 gotoxy(43,6);
 cputs("PEAK TEMPERATURE VALUES");


 textcolor(WHITE);
 for (i=0;i < max_thermocouples/2;i++)
 {
  gotoxy(34,7+i);
  cprintf("\nT%i",i);
 }

 j = 0;
 for (i=max_thermocouples/2;i < max_thermocouples;i++)
 {
  gotoxy(57,7+j);
  cprintf("\nT%i",i);
  j++;
 }

 draw_horline(31,80,13,LIGHTBLUE);

 textcolor(LIGHTRED);
 gotoxy(51,15);
 cputs("MESSAGES");
 gotoxy(33,17);
 textcolor(WHITE);
// puts("Data collection operating correctly");
 draw_horline(31,80,19,LIGHTBLUE);

 textcolor(LIGHTRED);
 gotoxy(47,21);
 cputs("CURRENT SETTINGS");
 textcolor(WHITE);
 gotoxy(33,23);
 cputs("User entered Cold Junction Temp :       deg. C");
 gotoxy(33,24);
 cputs("User entered sample rate        :       Hz");
 gotoxy(33,25);
 cputs("Actual sample rate              :       Hz");
 gotoxy(33,27);
 cputs("Gain setting on PC-30PGL           :");
 gotoxy(33,28);
 cputs("Gain setting on signal conditioner :");
 gotoxy(33,29);
 cputs("Total gain on all channels         :");
```

```
   if (oldbarheight[l] <= maxbarheight)
   {
    if (newbarheight[l] < oldbarheight[l]) /* erase a bit of bar */
    {
     textcolor(BLACK);
     height = newbarheight[l];
     for (k=1;k < (1+oldbarheight[l]-height);k++)
     {
      newbarheight[l] = oldbarheight[l] - k;
      gotoxy((7+3*l),(43-newbarheight[l]));
      cprintf("%c%c",char(219),char(219));
     }
    }
   }
    /* if (newbarheight = oldbarheightheight) do nothing */

    oldbarheight[l] = newbarheight[l];

 }
}

void write_file_header()
{
 int j;

 struct date d;
 struct  time t;
 getdate(&d);
 gettime(&t);


 fprintf(fh,"THERMOCOUPLE MEASUREMENT SYSTEM version 1.3");


 fprintf(fh,"\nDATE: %d/%d/%d",d.da_day,d.da_mon,d.da_year);
 fprintf(fh,"\nTIME: %2d:%02d:%02d",t.ti_hour, t.ti_min, t.ti_sec);

 fprintf(fh,"\nUser entered Cold Junction Temp    : %4.1f deg. C",cjtemp);
 fprintf(fh,"\nUser entered sample rate           : %f Hz",fsamplerate);
 fprintf(fh,"\nActual sample rate                 : %f Hz",samplerate);
 fprintf(fh,"\nGain setting on PC-30PGL           : %i",ingain);
 fprintf(fh,"\nGain setting on signal conditioner : %i",sig_gain);
 fprintf(fh,"\nTotal gain on all channels         : %i",(ingain*sig_gain));
 fprintf(fh,"\nThermocouple type used             : %c",t_type);

 fprintf(fh,"\n\n");
 for (j=0;j<channels;j++)
 {
  fprintf(fh,"   T%i  ",j);
 }
} // end of function write_file_header

void set_sample_rate()
{
 unsigned long int pre_div,clock_div,clock_div2;

  // samplerate is a global variable

  // The PC-30PGL board has an internal clock frequency of 2 MHz
  // The maximum value for either the clock or prescaler is 65536 (base 10)

  // When the user enters sample rate a value less than 1 Hz is disallowed.
 gotoxy(1,1);

 clock_div = (2e6 / samplerate);
 clock_div2 = clock_div/2;
 pre_div = 1;

 if (clock_div > 65530)
 {
  pre_div = 31;
  clock_div = clock_div/(pre_div);

  outp(DIVIDER, (clock_div));
  outp(DIVIDER, (clock_div >> 8));
 }
```

```
 if (clock_div <= 65530)
 {
  outp(DIVIDER, (clock_div2));
  outp(DIVIDER, (clock_div2 >> 8));
 }

 outp(PRESCALER, (pre_div));
 outp(PRESCALER, ((pre_div) >> 8));

 samplerate  = 2e6 / (pre_div*clock_div);

}

int cjtempconv()
// lookup table must be initialised before this function is used.
{
 int cjeqval;
 cjeqval = -1;
 do
 {
  cjeqval++;
 } while (cjtemp > (float(lut[cjeqval])));
 return(cjeqval);
}

void initialise()
// This function performs the operations specified on page 79 of the
// user manual.
{
 // Write 92(hex) to the A/D mode register (ADMDE).
 outp(ADMDE, 0x92);

 // Write 34(hex) to the counter control register (TMRCTR). This sets the
 // mode of the A/D clock prescaler to 2.
 outp(TMRCTR, 0x34);

 // Write 74(hex) to the counter control register (TMRCTR). This sets the
 // mode of the A/D clock divider to 2.
 outp(TMRCTR, 0x74);

 // Write B6(hex) to the counter control register (TMRCTR). This sets the
 // mode of the uncommitted counter/timer to 3.
 outp(TMRCTR, 0xb6);

 // Write 02(hex) to the A/D control/channel register (ADCCR). This disables
 // DMA and interrupts, and sets the A/D for software strobes.
 outp(ADCCR, 0x02);

 // Write 0 to the digital I/O control register (DIOCNTRL). This configures
 // all digital input lines as inputs.
 outp(DIOCNTRL, 0);

 // Write 0 to the GMEM0, GMEM1, GMEM2 and GMEM3 registers. This selects a
 // channel gain of 1 for all channels.
 outp(GAIN_REG+0, 0);
 outp(GAIN_REG+1, 0);
 outp(GAIN_REG+2, 0);
 outp(GAIN_REG+3, 0);

 // Wait at least 100 microseconds.
 delay(10); // 10 milliseconds delay.
}

void set_channel_gain()
// This function sets the gain of all channels to that specified by the user.
{
 int i;

 if (gain == 0) for (i=0;i<4;i++) outp(GAIN_REG+i, 0x00);
 if (gain == 1) for (i=0;i<4;i++) outp(GAIN_REG+i, 0x55);
 if (gain == 2) for (i=0;i<4;i++) outp(GAIN_REG+i, 0xaa);
 if (gain == 3) for (i=0;i<4;i++) outp(GAIN_REG+i, 0xff);

} // end function set_channel_gain()
```

```
void clear()
// Clears the A/D subsystem as decribed on page 76 of manual.
{
 unsigned i;

 // Write 92(hex) to the A/D mode register (ADMDE).
 outp(ADMDE, 0x92);

 // Write 02(hex) to the A/D control/channel register (ADCCR). This disables
 // DMA and interrupts, and sets the A/D for software strobes.
 outp(ADCCR, 0x02);

 // Read the high and low byte of the A/D data register.
 inp(ADDATL);
 inp(ADDATH);

 // Wait at least 100 microseconds or at least until the done bit is set.
 for (i = 0; ((i < 20) && (!(inp(ADDSR) & 0x70))); i++);

 // Read the high and low byte of the A/D data register.
 inp(ADDATL);
 inp(ADDATH);
}


void load_chan_list()
{
 // Using block mode so write (257-N) to the BLKCNT register, where N is
 // the number of samples per block.
 outp(BLKCNT, 0xf9);

 // Clear the A/D subsystem.
 clear();

 // Write the first channel address to the ADCCR. All other bits except the
 // STBC should be cleared. The channel list now contains only the first
 // channel.
 outp(ADCCR, 0x1);

 // Set A/D mode register to (ADMDE) to 9f(hex).
 // This sets the channel list mode to add.
 outp(ADMDE, 0x9f);

 // Write in sequence the rest of the channels to be converted to the ADCCR
 // as above. On read the the ADCCR will reflect the first channel
 // address written.

 outp(ADCCR, 0x00);
 outp(ADCCR, 0x10);
 outp(ADCCR, 0x20);
 outp(ADCCR, 0x30);
 outp(ADCCR, 0x40); // loads the channel list with
 outp(ADCCR, 0x50); // the 8 channels to be sampled
 outp(ADCCR, 0x60);
 outp(ADCCR, 0x70);

 // Set the A/D mode register (ADMDE) to 91(hex) for block trigger mode.
 // To set A/D mode to normal trigger mode write 90(hex) to register.
 // This sets the channel list mode to ignore. You can now write control
 // bits to the ADDCR without disturbing the channel list.
 outp(ADMDE, 0x91);

 // Channel list is now ready for operation.
}

main()
{
 // int diag_result;  // Diag result is not currently in use.
 int i,t,chan_list[8],index,rec_disp_test;
 char looptest;

 textmode(C4350);

 paint_title_screen();
```

```
// NOTE: THE DIAGNOSTIC ROUTINE LOCATED IN THE LIBRARY FILE IS NOT
//       CURRENTLY IN USE.

// Call the diagnostic routine located in the library file.
// diag_result = diag();

 textcolor(GREEN);
 gotoxy(5,16);
 cprintf("PC-30 diagnostics not performed.");
//cprintf("PC-30 diagnostics report:");

// if (diag_result != 0)
// {
//  textcolor(LIGHTRED + BLINK);
//  gotoxy(36,16);
//  cputs("PC-30 not found, or failed.");
//  delay(5000);
//  textmode(C80); // set textmode to normal
//  puts("\nPC-30 not found, of failed.");
//  puts("\nCheck to make sure card is properly inserted into computer.");
//  puts("\nIf card is secure try rebooting.");
// puts("\If neither of the above have worked - TRY TO HAVE A NICE DAY");
//  return 0;      // exit the program
// }
// else
// {
//  textcolor(LIGHTGREEN + BLINK);
//  gotoxy(36,16);
//  cputs("PC-30 found and operating.");
// }

 get_user_info();

 // Set initial barheight.
 for (i=0;i<8;i++) oldbarheight[i] = 0;

 // Initialise values of array to store peak temperatures
 for (i=0;i<8;i++) peaktemp[i] = 0;

 // GENERATE THE LOOKUP TABLE
 // There are 4096 possible values the PC-30PG may give as an A/D conversion.
 // This assumes the PC-30PG is configured in 0 -> +10V input range.
 // Conversion is made on microvolts as  r_volt2temp and k_volt2temp
 // is set up to take microvolts not volts.

 if (t_type == 'R')
 {
  for (i=0;i<4096;i++)
  {
   lut[i] = int(r_volt2temp((1e7*i)/(4095.0*ingain*sig_gain)));
  }
 }

 if (t_type == 'K')
 {
  for (i=0;i<4096;i++)
  {
   lut[i] = int(k_volt2temp((1e7*i)/(4095.0*ingain*sig_gain)));
  }
 }

// Convert user entered cold junction temperature to an equivalent
// number between 0 and 4095 to change value of data from PC-30PGL
// before conversion to temperature using the lookup table.

 cjmodify = cjtempconv();

 // turn off the cursor to get a cleaner more "graphics like" display
 _setcursortype(_NOCURSOR);

 paint_data_screen();

 fh = fopen(filename,"w"); // Open file for writing of data.
 write_file_header();      // writes a header on the output file

 rec_disp_test = 0;
 looptest = 'R';
```

```
    if ((rec_disp_test == 1) && (looptest == 'R'))
    {
     gotoxy(63,47);
     textcolor(LIGHTRED + BLINK);
     cputs("RECORDING    ");
     rec_disp_test = 3;
    }

    if ((rec_disp_test == 0) && (looptest == 'R'))
     {
      textcolor(LIGHTBLUE + BLINK);
      gotoxy(63,47);
      cputs("NOT RECORDING");
      rec_disp_test = 2;
     }


  } while (looptest != 'Q'); // end of the data read loop


  // clean up before exit
  fclose(fh);
  textmode(C80);
  return 0;
} // end  of function main
```

Appendix B TMS Data File Example

THERMOCOUPLE MEASUREMENT SYSTEM version 1.3
DATE: 24/3/1993
TIME: 17:26:59
User entered Cold Junction Temp : 24.0 deg. C

User entered sample rate : 50.000000 Hz

Actual sample rate : 50.000000 Hz

Gain setting on PC-30PGL : 1
Gain setting on signal conditioner : 200
Total gain on all channels : 200
Thermocouple type used : R

Time	T0	T1	T2
0	28	25	25
0.02	28	25	25
0.04	25	25	25
0.06	25	25	25
0.08	25	25	25
0.1	25	25	25
<Data removed>			
2.3	25	25	112
2.32	25	25	142
2.34	25	25	167
2.36	25	25	192
2.38	25	25	206
2.4	25	25	217
2.42	25	25	228
2.44	25	25	230
2.46	25	25	229
2.48	25	25	228
2.5	25	25	222
<Data removed>			
3.16	25	25	445
3.18	25	25	524
3.2	25	25	621
3.22	25	25	727
3.24	25	25	840
3.26	25	25	951
3.28	25	25	1054
3.3	25	25	1147
3.32	25	25	1228
3.34	25	25	1292
3.36	25	25	1341
3.38	25	25	1377
3.4	25	25	1401
3.42	25	25	1417

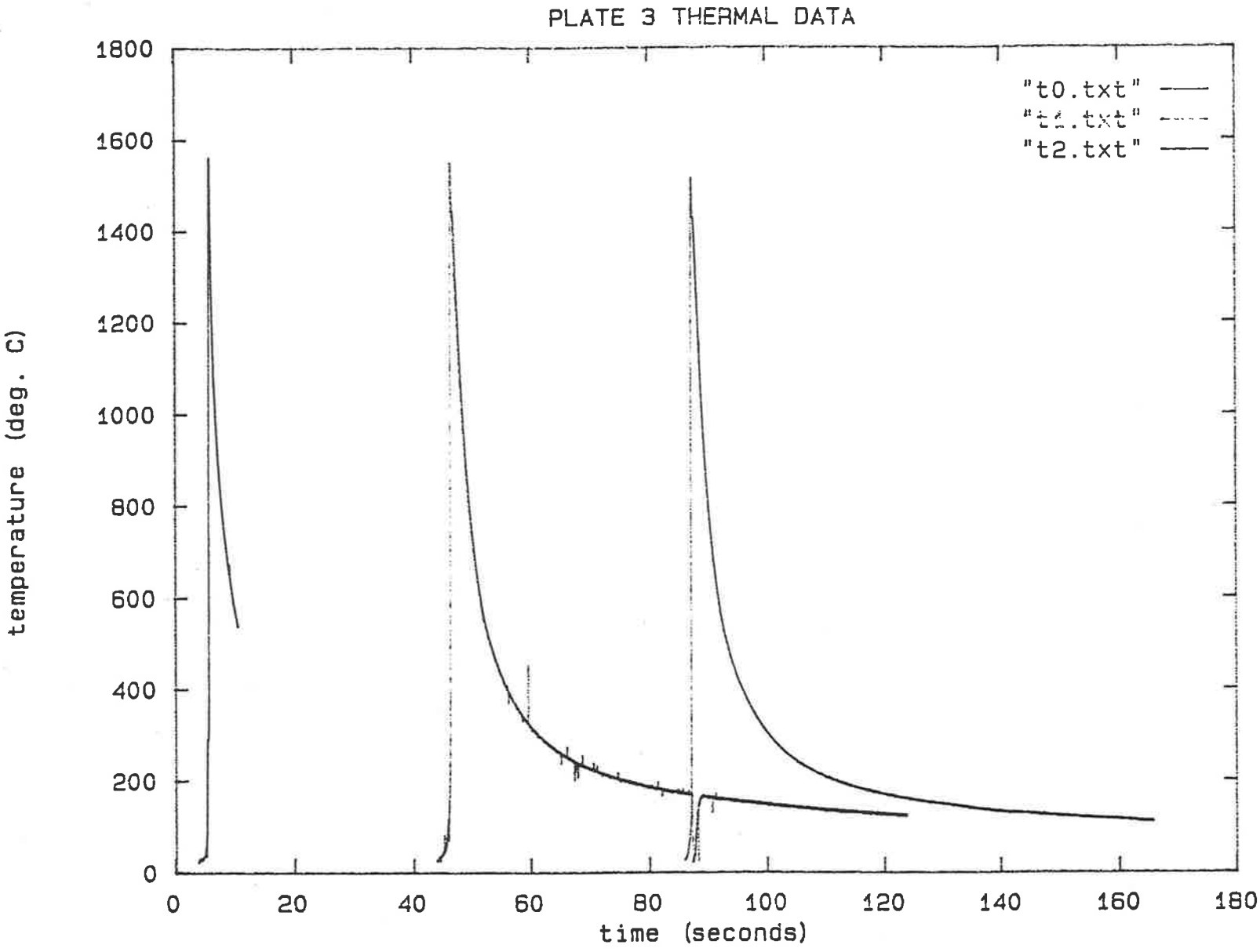
PLATE 3 THERMAL DATA
"t0.txt"
"t1.txt"
"t2.txt"
temperature (deg. C)
time (seconds)
0
200
400
600
800
1000
1200
1400
1600
1800
0
20
40
60
80
100
120
140
160
180

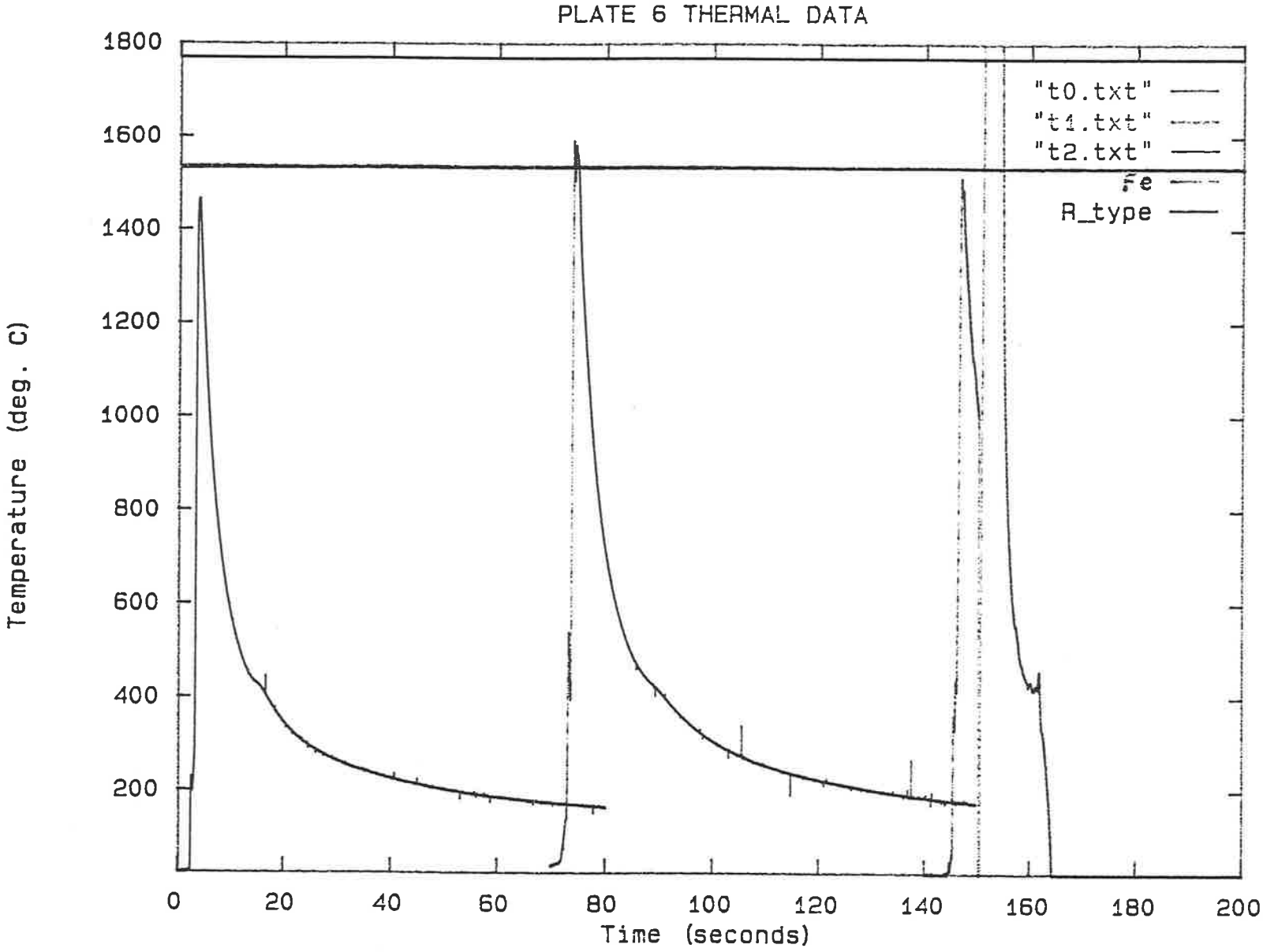
PLATE 6 THERMAL DATA
"t0.txt"
"t1.txt"
"t2.txt"
Fe
R_type
Temperature (deg. C)
1800
1600
1400
1200
1000
800
600
400
200
0
20
40
60
80
100
120
140
160
180
200
Time (seconds)

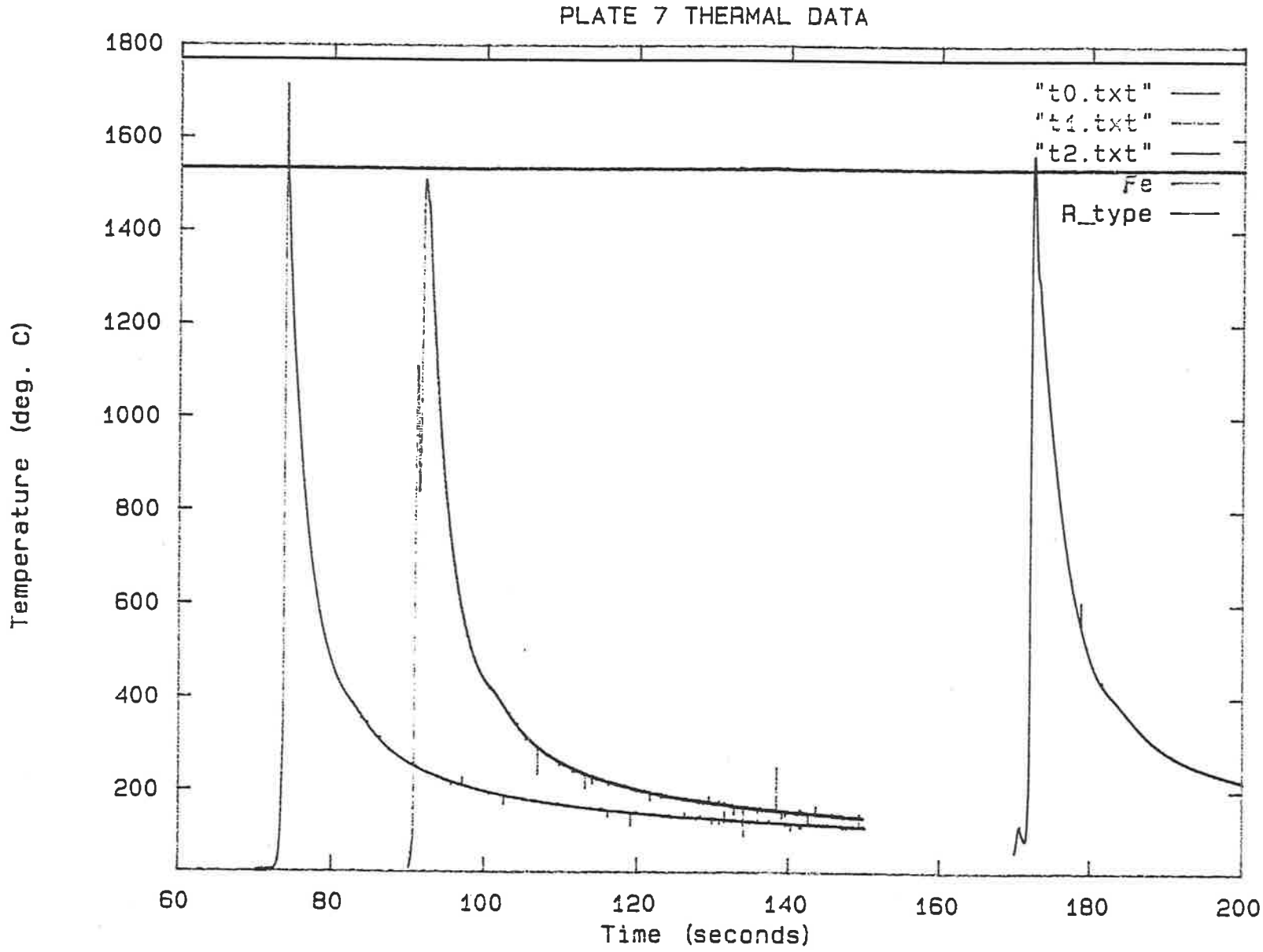
PLATE 7 THERMAL DATA
"t0.txt"
"t1.txt"
"t2.txt"
Fe
R_type
Temperature (deg. C)
1800
1600
1400
1200
1000
800
600
400
200
60
80
100
120
140
160
180
200
Time (seconds)

Appendix D Raw Hardness Data

Heat Input 1.12 kJ/mm

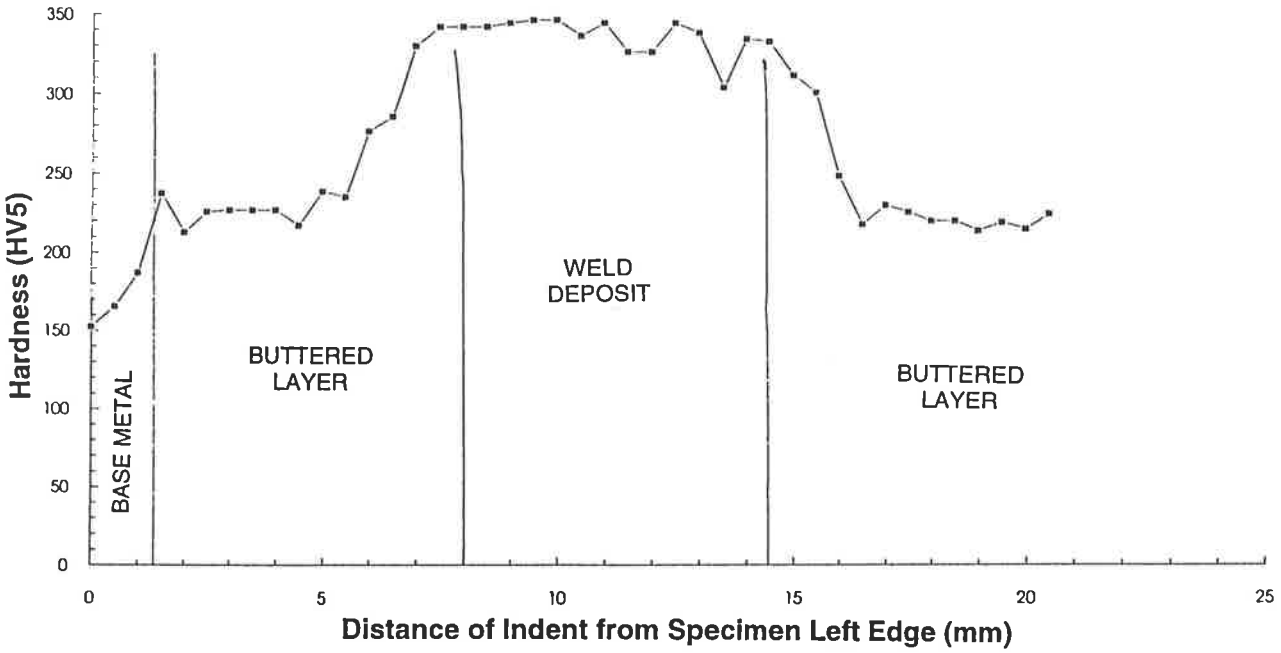

Heat Input 1.21 kJ/mm

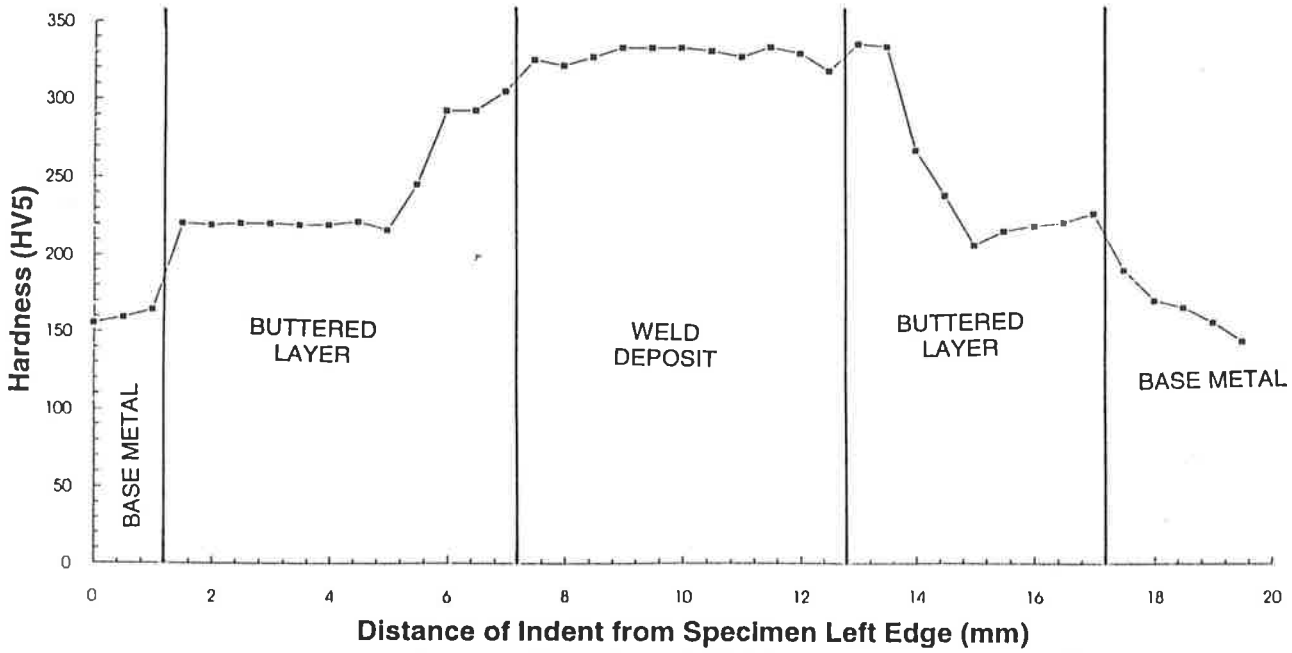

Heat Input 1.66 kJ/mm

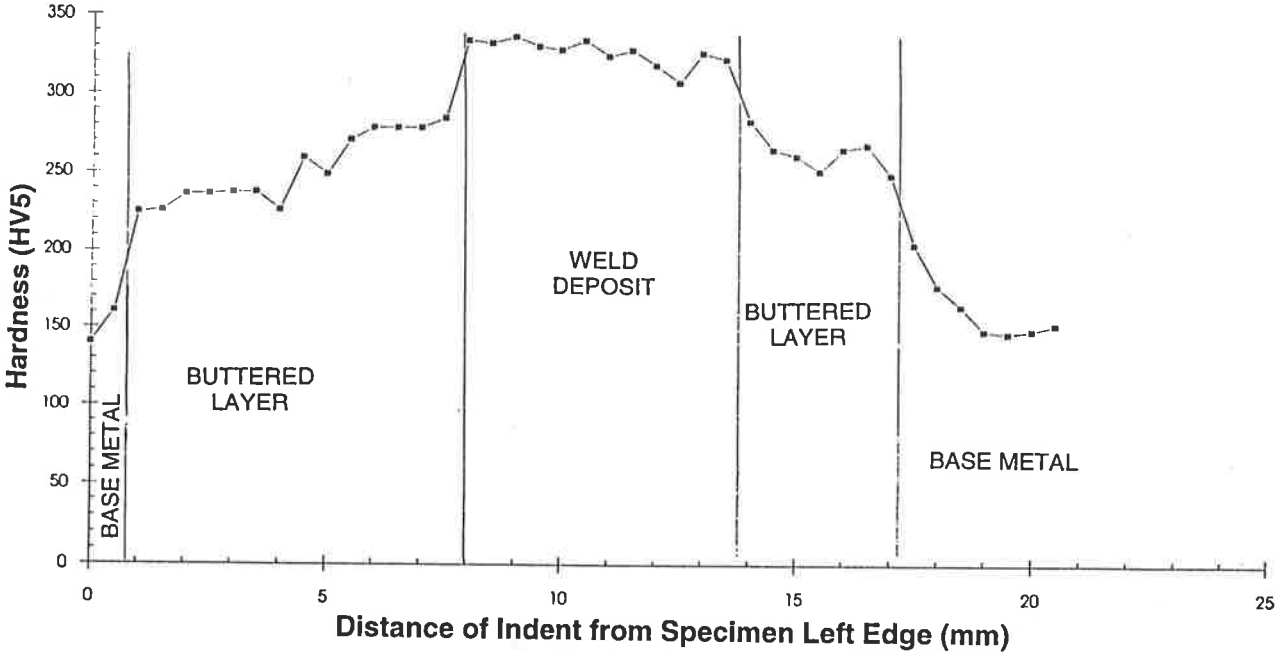

Heat Input 1.94 kJ/mm

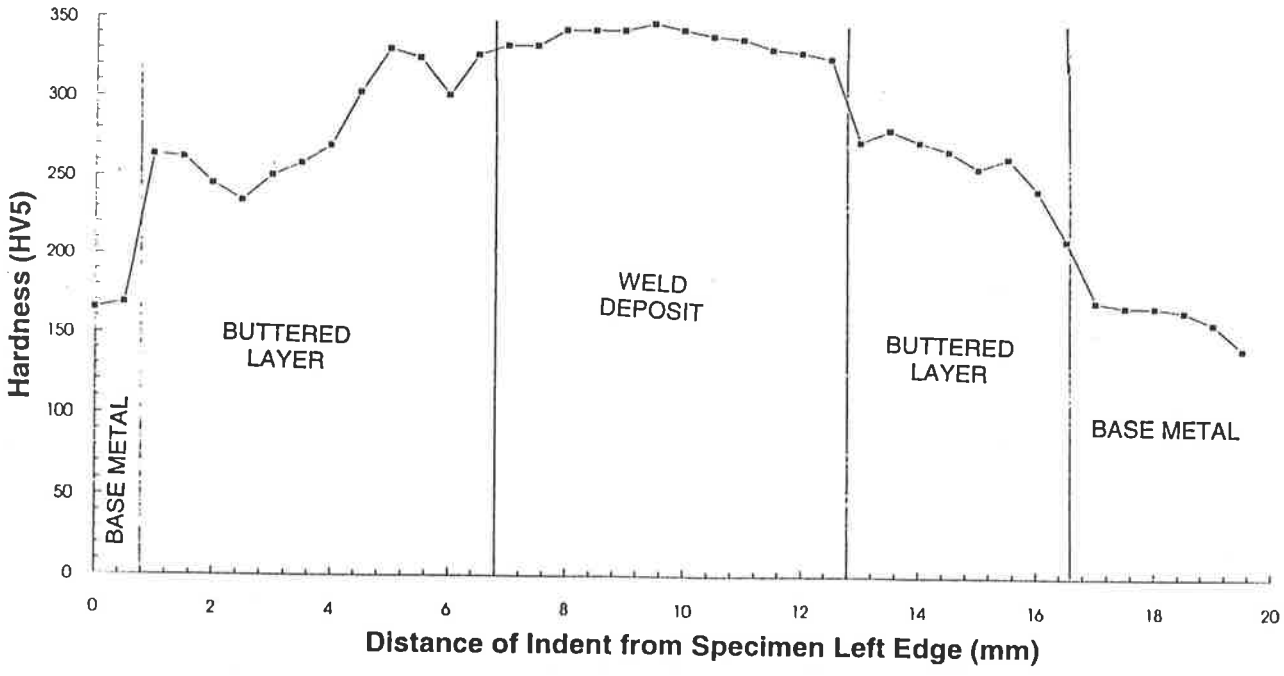

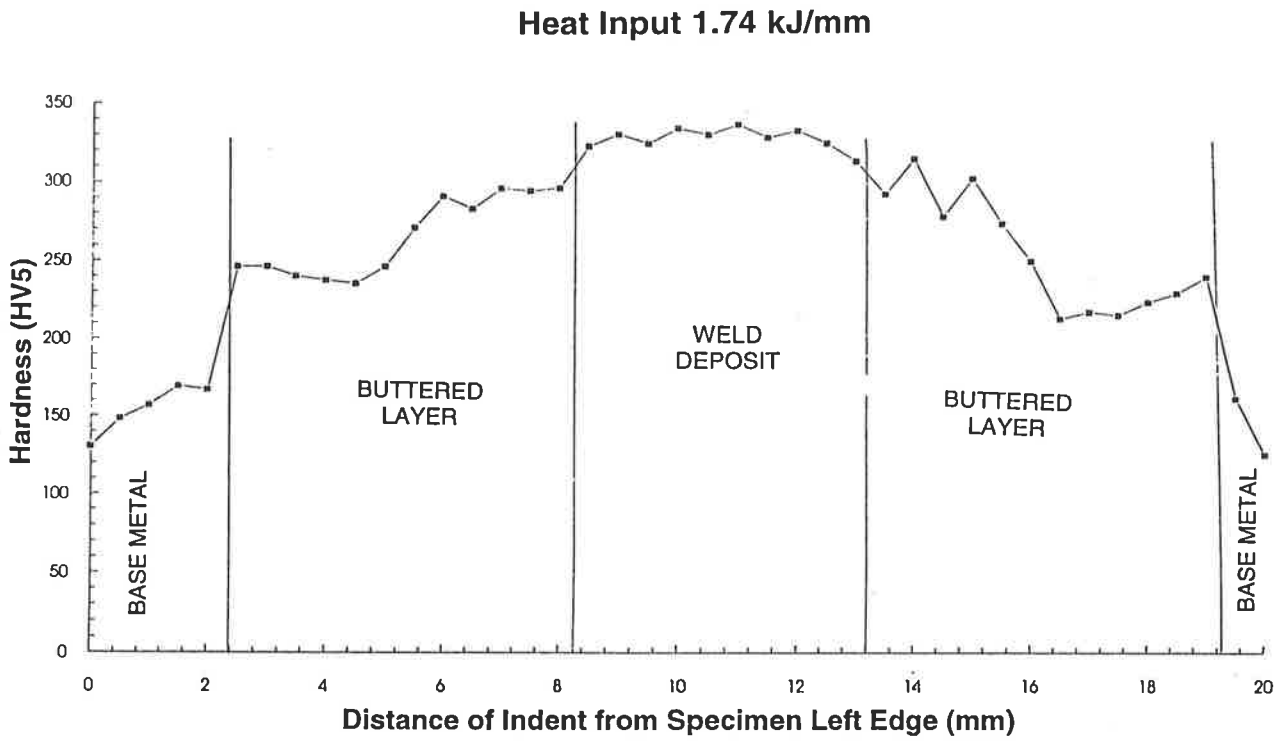
Heat Input 1.74 kJ/mm
Hardness (HV5)
350
300
250
200
150
100
50
0
BASE METAL
BUTTERED LAYER
WELD DEPOSIT
BUTTERED LAYER
BASE METAL
0
2
4
6
8
10
12
14
16
18
20
Distance of Indent from Specimen Left Edge (mm)

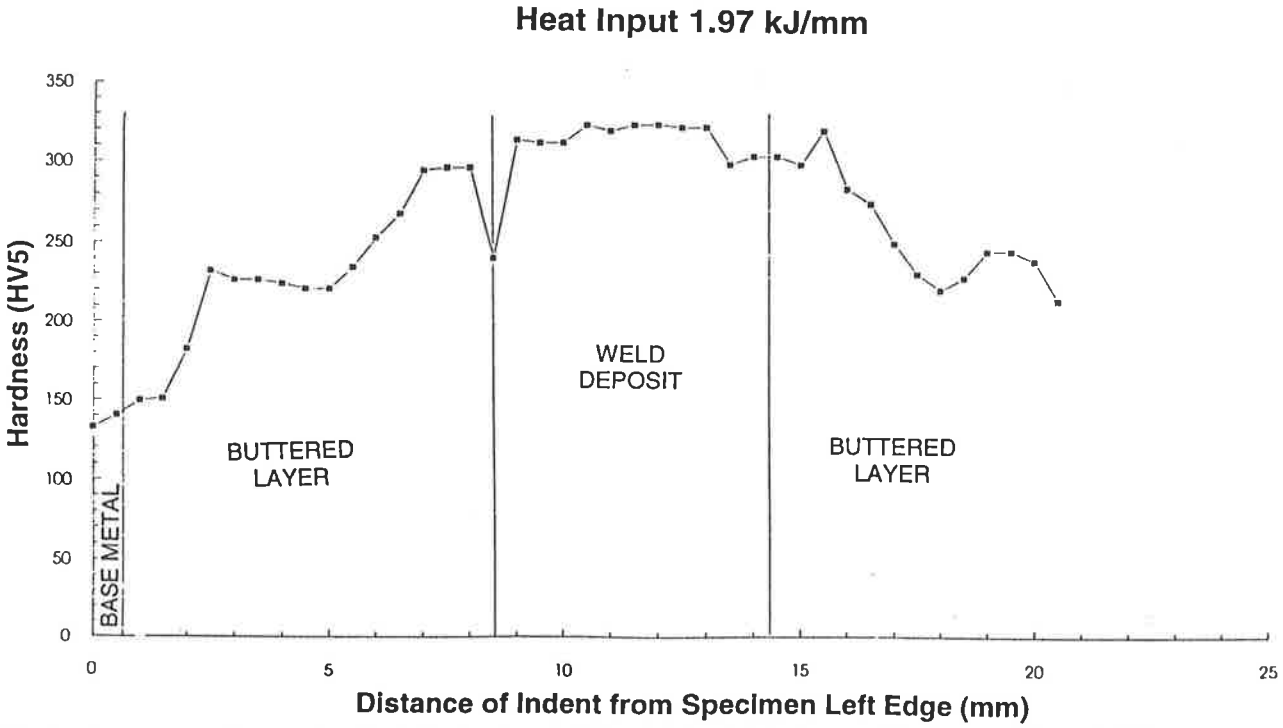
Heat Input 1.97 kJ/mm
Hardness (HV5)
350
300
250
200
150
100
50
0
BASE METAL
BUTTERED LAYER
WELD DEPOSIT
BUTTERED LAYER
0
5
10
15
20
25
Distance of Indent from Specimen Left Edge (mm)

Appendix E Drawings of Fracture Testing Rig

CTOD THREE POINT BENDING RIG ASSEMBLY

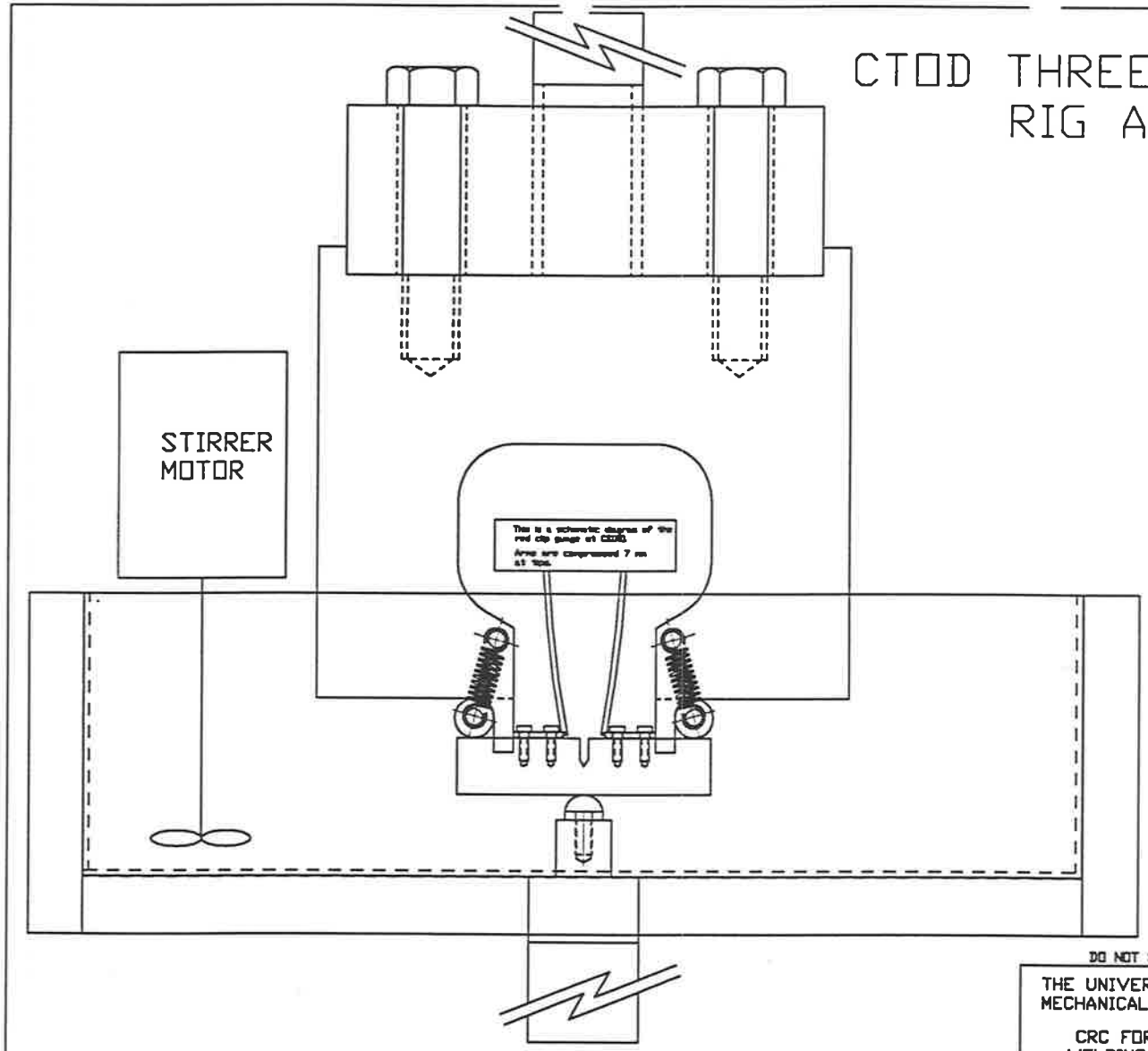

FRONT VIEW

DO NOT SCALE ALL DIMENSIONS IN MILLIMETRES

THE UNIVERSITY OF ADELAIDE MECHANICAL ENGINEERING DEPT CRC FOR MATERIALS, WELDING AND JOINING			TITLE FRACTURE RIG	
			PROJECT 93-05 MICROSTRUCTURE	
DRAWN BY GREG REDDEN	DATE 3 FEB 93	SCALE 1:1	DRAWING FRAC-01	A4

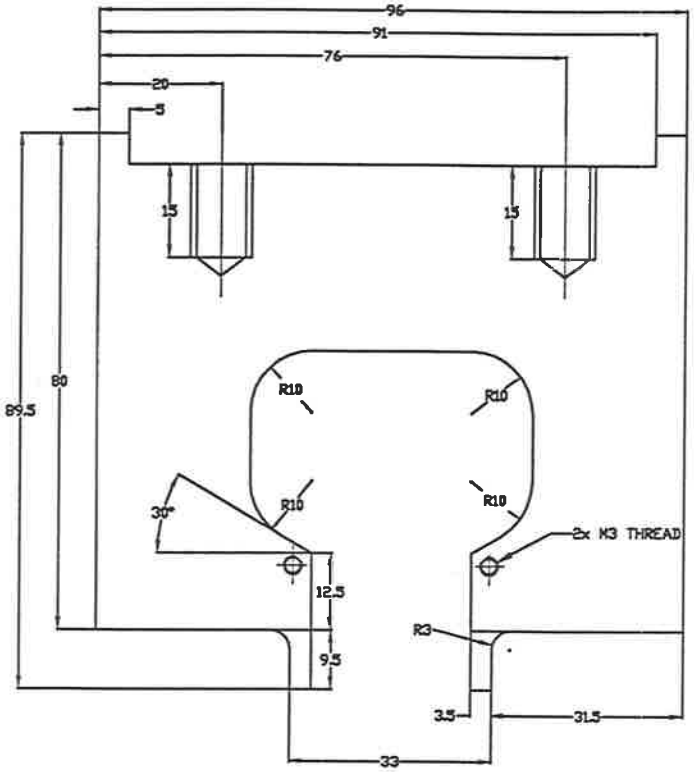

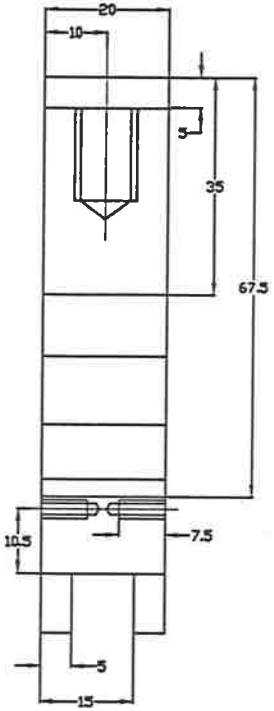

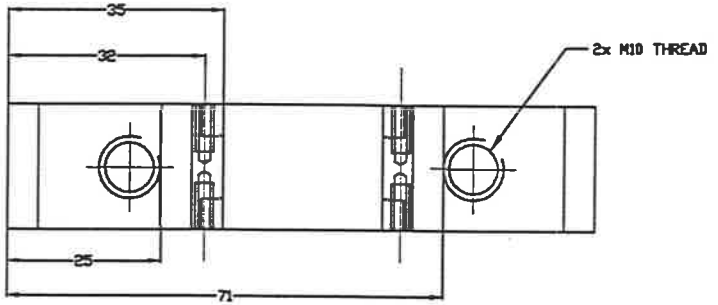

MATERIAL: MKS TOOL STEEL
NOTE: HEAT TREATMENT REQUIRED

3RD ANGLE PROJECTION

DO NOT SCALE ALL DIMENSIONS IN MILLIMETRES

THE UNIVERSITY OF ADELAIDE MECHANICAL ENGINEERING DEPT CRC FOR MATERIALS, WELDING AND JOINING			TITLE: LOAD FRAME PROJECT: 93-05 MICROSTRUCTURE	
DRAWN BY: GREG REDDEN	DATE: 3 FEB 93	SCALE: 1:1	DRAWING: FRAC-06	A4

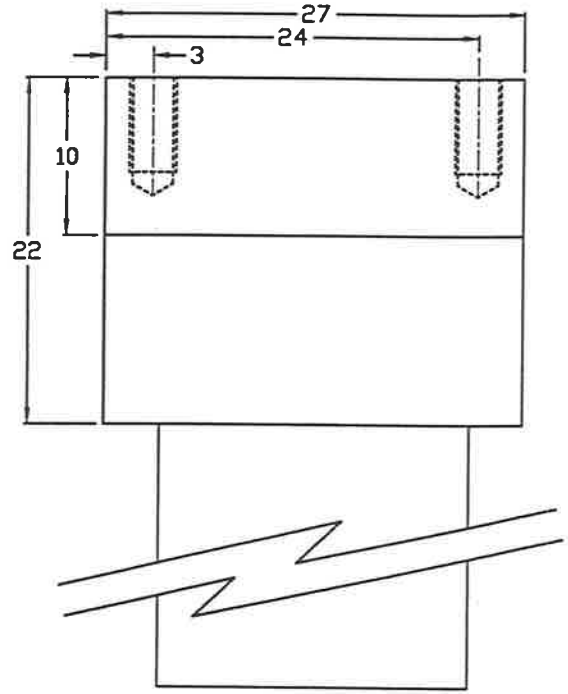

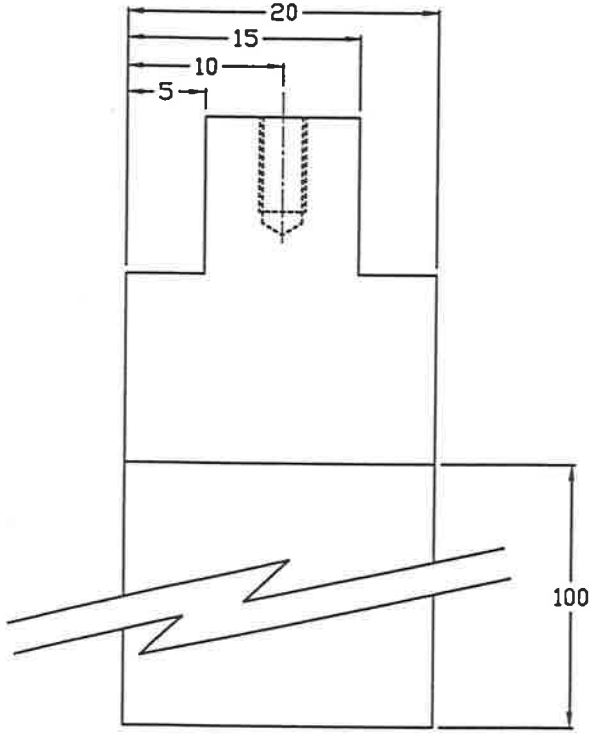

NOTES: Milled surface finish is satisfactory.

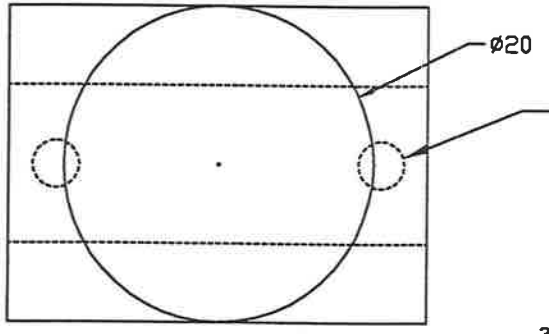

3RD ANGLE PROJECTION

DO NOT SCALE ALL DIMENSIONS IN MILLIMETRES

THE UNIVERSITY OF ADELAIDE MECHANICAL ENGINEERING DEPT CRC FOR MATERIALS, WELDING AND JOINING			TITLE: THREE POINT TIP HOLDER PROJECT: 93-05 MICROSTRUCTURE	
DRAWN BY: GREG REDDEN	DATE: 3 FEB 93	SCALE: 5:2	DRAWING: FRAC-05	A4

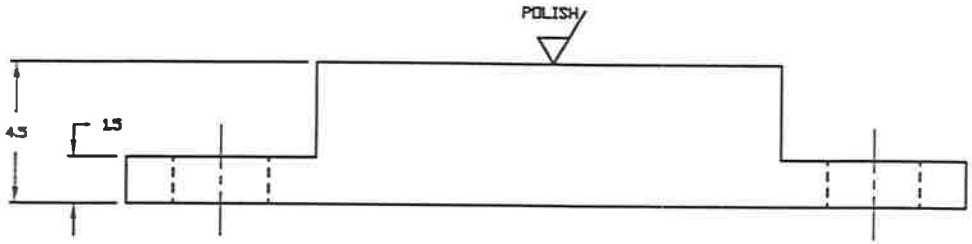

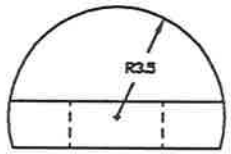

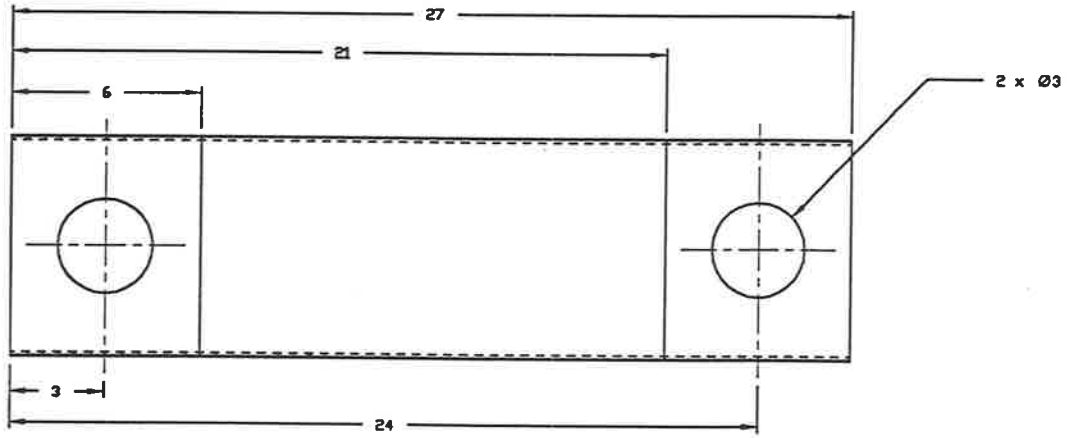

MATERIAL: Silver steel

3RD ANGLE PROJECTION

DO NOT SCALE ALL DIMENSIONS IN MILLIMETRES

THE UNIVERSITY OF ADELAIDE MECHANICAL ENGINEERING DEPT CRC FOR MATERIALS, WELDING AND JOINING			TITLE THREE POINT TIP	
			PROJECT 93-05 MICROSTRUCTURE	
DRAWN BY GREG REDDEN	DATE 3 FEB 93	SCALE 5:1	DRAWING FRAC-04	A4

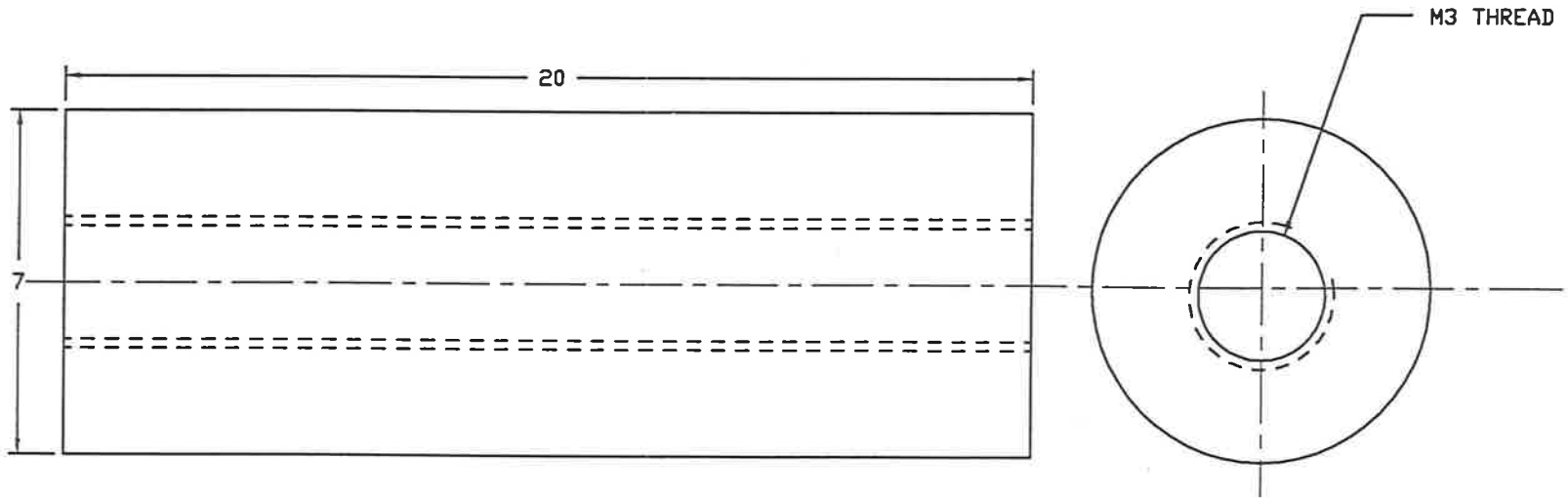

MATRIAL: Silver steel
NOTE: Surface must be polished

3RD ANGLE PROJECTION

DO NOT SCALE ALL DIMENSIONS IN MILLIMETRES

THE UNIVERSITY OF ADELAIDE MECHANICAL ENGINEERING DEPT CRC FOR MATERIALS, WELDING AND JOINING			TITLE: ROLLER PROJECT: 93-05 MICROSTRUCTURE	
DRAWN BY: GREG REDDEN	DATE: 3 FEB 93	SCALE: 8:1	DRAWING: FRAC-03	A4

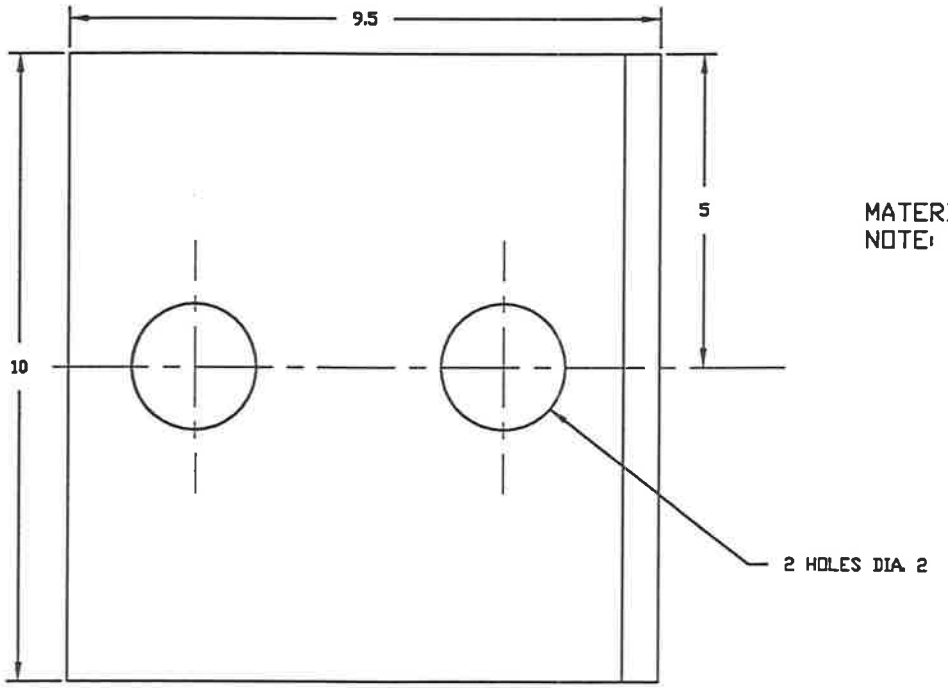

MATERIAL: Spring steel
NOTE: Surface finish must be ground.

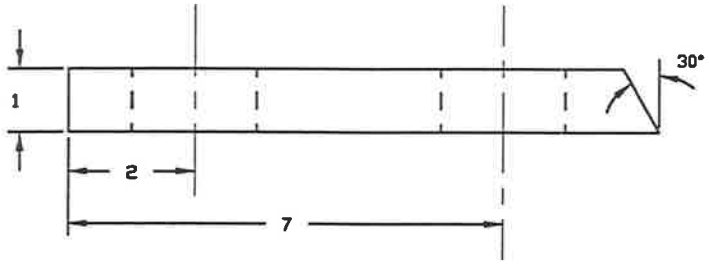

3RD ANGLE PROJECTION

DO NOT SCALE ALL DIMENSIONS IN MILLIMETRES

THE UNIVERSITY OF ADELAIDE MECHANICAL ENGINEERING DEPT CRC FOR MATERIALS, WELDING AND JOINING			TITLE KNIFE EDGE	
			PROJECT 93-05 MICROSTRUCTURE	
DRAWN BY GREG REDDEN	DATE 3 FEB 93	SCALE 1:10	DRAWING FRAC-02	A4

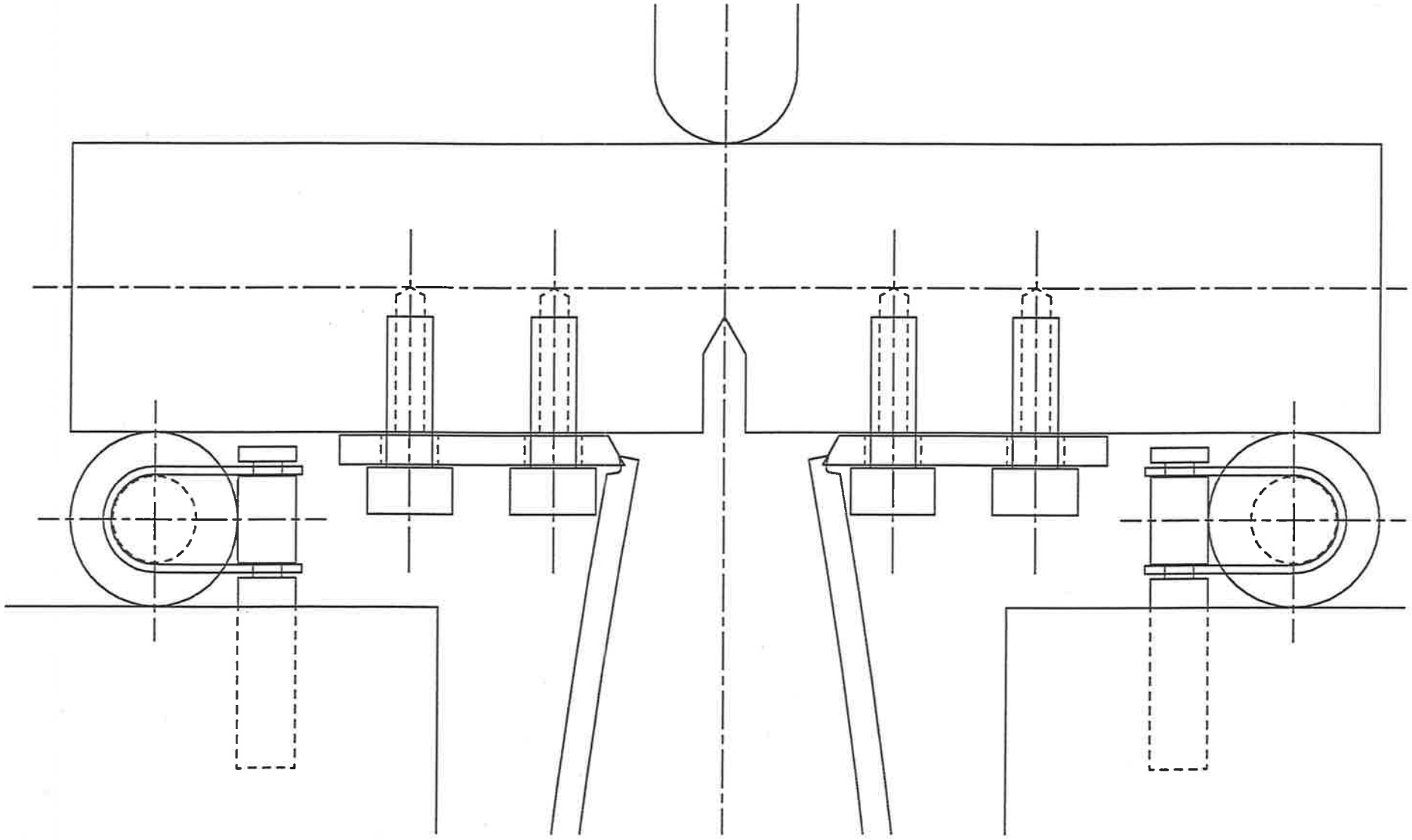

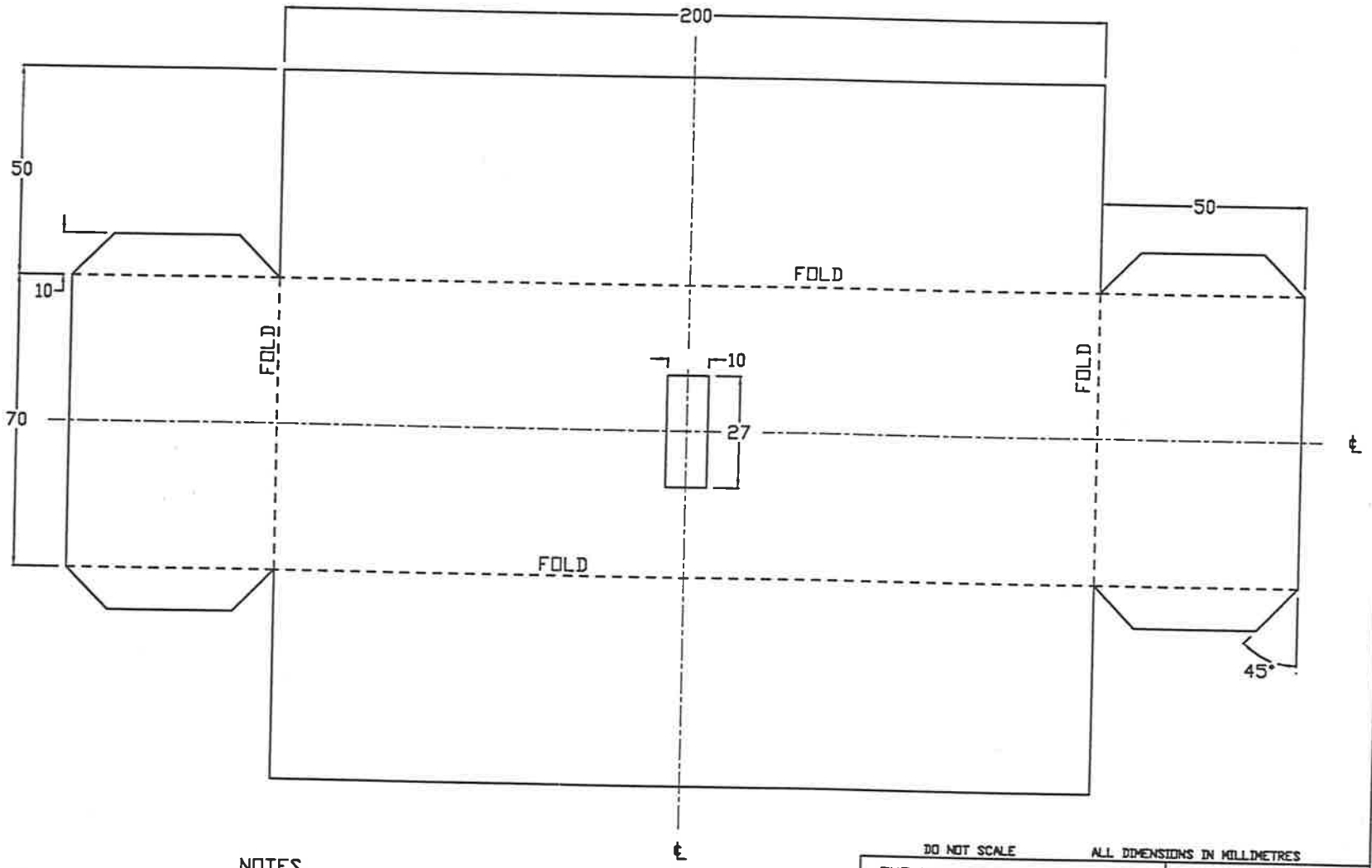

NOTES

1. Material thickness approx 1 mm
2. Fold dashed lines, cut solid lines.
3. Material must be able to be soldered or braised.
4. Workpiece is symetrical about centerlines.

DO NOT SCALE ALL DIMENSIONS IN MILLIMETRES

THE UNIVERSITY OF ADELAIDE MECHANICAL ENGINEERING DEPT CRC FOR MATERIALS, WELDING AND JOINING			TITLE: TANK CUTTING TEMPLATE PROJECT: 93-05 MICROSTRUCTURE	
DRAWN BY: GREG REDDEN	DATE: 3 FEB 93	SCALE: 5:4	DRAWING: FRAC-09	A4

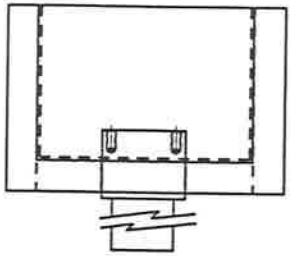

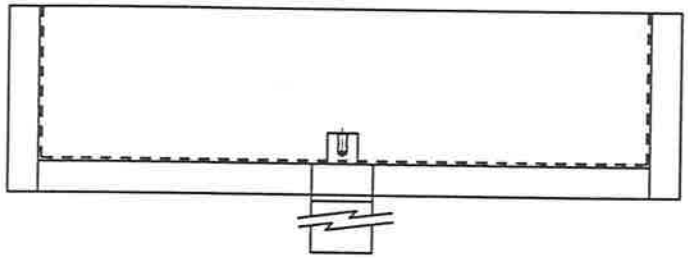

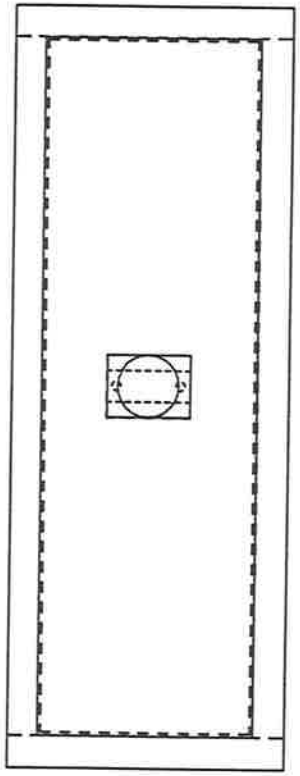

NOTE: Tank is to be attached to base
by braising or soldering
so as to achieve a leak proof seal.

3RD ANGLE PROJECTION

DO NOT SCALE ALL DIMENSIONS IN MILLIMETRES

THE UNIVERSITY OF ADELAIDE MECHANICAL ENGINEERING DEPT CRC FOR MATERIALS, WELDING AND JOINING			TITLE: TANK ATTACHMENT PROJECT: 93-05 MICROSTRUCTURE	
DRAWN BY: GREG REDDEN	DATE: 3 FEB 93	SCALE: 5:1	DRAWING: FRAC-08	A4

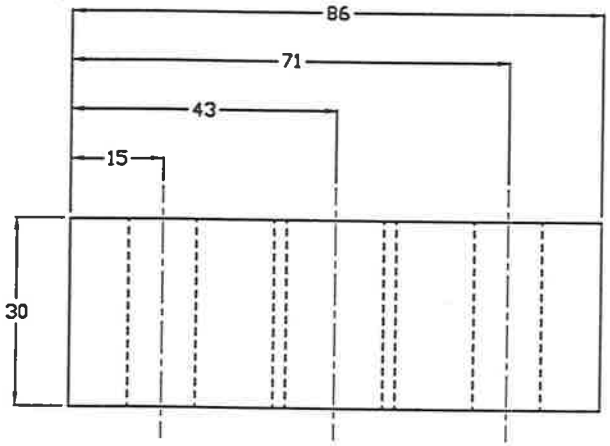

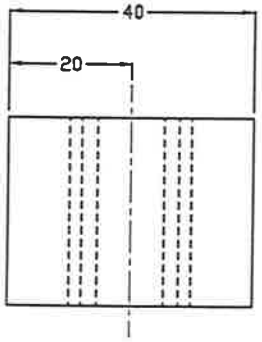

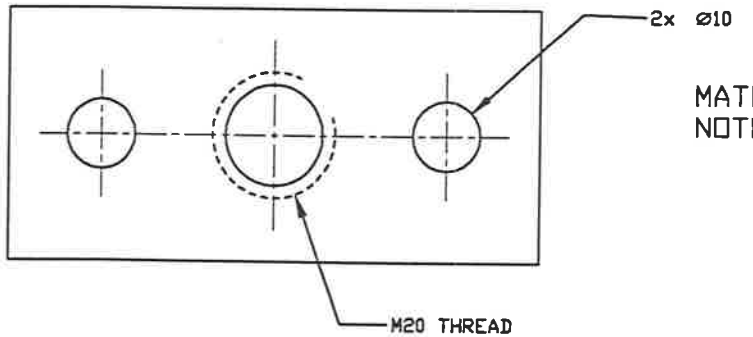

MATERIAL: Mild steel
NOTE: Milled surface finish is satisfactory

3RD ANGLE PROJECTION

DO NOT SCALE ALL DIMENSIONS IN MILLIMETRES

THE UNIVERSITY OF ADELAIDE MECHANICAL ENGINEERING DEPT CRC FOR MATERIALS, WELDING AND JOINING			TITLE: LOAD FRAME INTERFACE PROJECT: 93-05 MICROSTRUCTURE
DRAWN BY: GREG REDDEN	DATE: 3 FEB 93	SCALE: 1:1	DRAWING: FRAC-07 A4

Appendix F TEM Foil Preparation Procedure

Foils for TEM analysis were prepared using the following procedure:

1. Machine weld deposit to obtain a rod of weld metal of diameter 3.05mm (+0.00mm - 0.05mm) as shown in drawing over the page.
2. Cut wafers from machined material of thickens 0.5mm.
3. Grind wafers to 0.1mm thickness using firstly 600 then 1200 grit wet carbide paper.
4. Electropolish wafers until thinned to a foil and perforations appear. (Electropolishing fluid was a solution of 10% $HClO_4$ / 20% Glycerol / 70 % Ethyl Alcohol by volume. This mixture was cooled to between -10°C and 0°C by pouring liquid nitrogen into the mixture. The electropolisher was a twin jet unit).
5. Wash newly prepared foils in ethyl alcohol
6. Store dry foils in individual gelatine capsules.

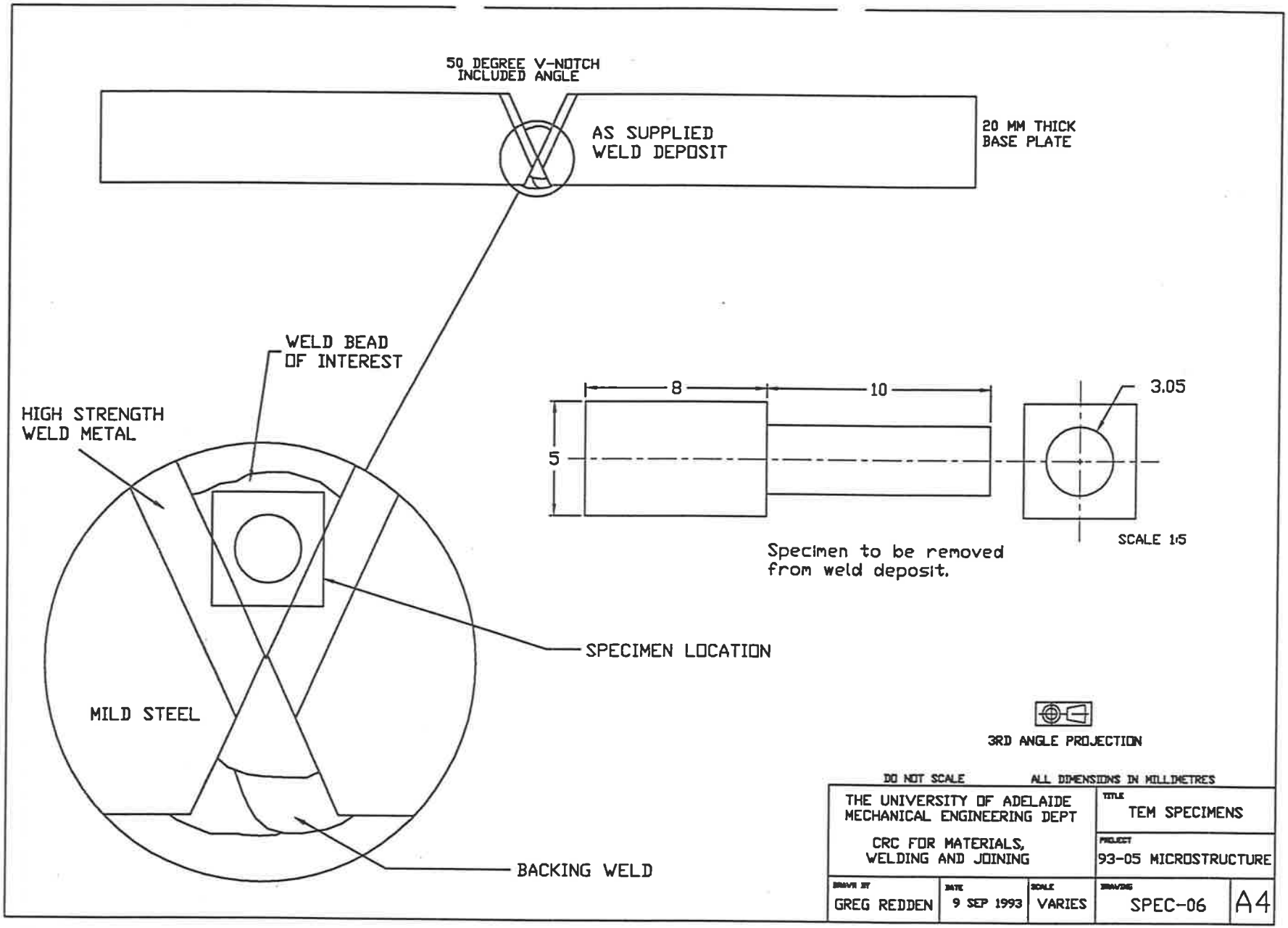
50 DEGREE V-NOTCH
INCLUDED ANGLE
AS SUPPLIED
WELD DEPOSIT
20 MM THICK
BASE PLATE
WELD BEAD
OF INTEREST
HIGH STRENGTH
WELD METAL
SPECIMEN LOCATION
MILD STEEL
BACKING WELD
8
10
5
3.05
SCALE 1:5
Specimen to be removed
from weld deposit.
3RD ANGLE PROJECTION
DO NOT SCALE
ALL DIMENSIONS IN MILLIMETRES
THE UNIVERSITY OF ADELAIDE
MECHANICAL ENGINEERING DEPT
CRC FOR MATERIALS,
WELDING AND JOINING
TITLE
TEM SPECIMENS
PROJECT
93-05 MICROSTRUCTURE
DRAWN BY
GREG REDDEN
DATE
9 SEP 1993
SCALE
VARIES
DRAWING
SPEC-06
A4

Appendix G Stress Intensity Factor Software Listing

```
/*
  This is a short program designed to assist in the determination of the
  correct parameters to use when performing a CTOD test on a three point
  bend test specimen.

  Greg Redden
  CRC Materials Welding and Joining
  April 1994

  Programmed using Borland Turbo C++ version 3.0
*/

#include <math.h>
#include <stdio.h>

const float B = 10e-3;  //Specimen breadth [meters]
const float S = 40e-3;  //Specimen span (S = 4W) [meters]
const float W = 10e-3;  //Specimen width or thickness [meters]

// The following constants of cod_function_slope and cod_function_const
// have been derived from experimental data collected from actual test
// specimens with notch lengths of 4mm and 5.5mm.


const float cod_function_slope = 6.9522; // [microns/(kN*mm)]
const float cod_function_const = -13.4798;


float ao_enter,a;
float bo,ao,Y;    // Y is the stress intensity coefficient.
float sigma_y,sigma_uts_enter,sigma_ys_enter,sigma_ys;
float ASTM_Pmax,BS_Pmax;
float Pmax, Pmin, Pmean;
float max_clip,clip_vs_load;


main()
{
printf("\nCTOD PARAMETER DETERMINATION");
printf("\nProgrammed by Greg Redden April 1994");
printf("\n\nEnter fatigue crack notch length (mm): ");
scanf("%f",&ao_enter);
ao = ao_enter/1000;
if ((ao>0.55*W) || (ao<0.45*W));
 printf("WARNING: Crack length not within recommended envelope.\n");
printf("Enter ultimate tensile strength (MPa): ");
scanf("%f",&sigma_uts_enter);
printf("Enter 0.2 percent offset yeild strength (MPa): ");
scanf("%f",&sigma_ys_enter);

sigma_ys = sigma_ys_enter*1e6;
```

```
sigma_y = (sigma_uts_enter + sigma_ys_enter)*1e6/2;
bo=W-ao;

a = ao/W; // The parameter "a" is used to simplify the following equation

Y=(6*pow(a,0.5)*(1.99-2.15*a+6.08*pow(a,2)-6.63*pow(a,3)+2.7*pow(a,4)))
 /((1+2*a)*pow((1-a),1.5));

ASTM_Pmax = 0.5*B*pow(bo,2)*sigma_y/S;
BS_Pmax = 0.63*sigma_ys*pow(B,1.5)*pow(W,0.5)/Y;

printf("\nSpecimen dimensions: B = %.2f mm, W = %.2f mm, S = %.2f mm"
      ,1000*B,1000*W,1000*S);


printf("\nStress intensity coefficient, Y = %.3f ",Y);
printf("\nMax fatigue precracking force = %.3f kN (ASTM E1290)"
     ,ASTM_Pmax/1000);
printf("\nMax fatigue precracking force = %.3f kN (BS 5762:1979)"
     ,BS_Pmax/1000);

Pmax = ASTM_Pmax;
Pmin = Pmax*0.1;
Pmean = Pmin + (Pmax - Pmin)/2;

printf("\nFATIGUE LOADING PARAMETERS BASED ON ASTM E1290");
printf("\nPmax = %.3f kN Pmin = %.3f kN Pmean = %.3f kN"
      ,Pmax/1000,Pmin/1000,Pmean/1000);

printf("\nEXPECTED CLIP GUAGE OPENING");


/*

The following procedure used to determine the expected clip
guage opening for a given crack length when using the recommended
fatigue loading parameters assumes (incorrectly) a linear
relationship between the clip guage opening for a given force
and the crack length.  This linear approximation of the real case
(which is in fact a cubic relationship) is expected to be
satisfactory.

*/


clip_vs_load = cod_function_slope*ao_enter + cod_function_const;
printf("\nClip guage displacement = %f microns/kN",clip_vs_load);
max_clip = clip_vs_load*Pmax/1000;
printf("\nMax guage displacement = %.2f microns",max_clip);

return 0;
}
```